UNSW SYDNEY

Anthracyclines used in the treatment of cancer: their harmful effects on the Reno-cardiovascular connection

Author:
Bedja, Djahida

Publication Date:
2008

DOI:
https://doi.org/10.26190/unsworks/17924

License:
https://creativecommons.org/licenses/by-nc-nd/3.0/au/
Link to license to see what you are allowed to do with this resource.

Downloaded from http://hdl.handle.net/1959.4/41501 in https://unsworks.unsw.edu.au on 2024-04-20

THE UNIVERSITY OF NEW SOUTH WALES

Anthracyclines Used in the Treatment of Cancer: Their Harmful Effects on the Reno-Cardiovascular Connection

by

Djahida Bedja

Academic dissertation submitted to
The University of New South Wales
for the degree of

Master of Biomedical Engineering

Supervision ; *Prof. Alberto P Avolio,* BE, PhD

Australian School of Advanced Medicine. Macquarie University, Sydney Australia
(Formerly: Graduate School of Biomedical Engineering, University of New South Wales)

Co-Supervision: *Assistant Professor Kathleen L. Gabrielson*, DVM, PhD

Dip, ACVP Department of Molecular and Comparative Pathobiology, Johns Hopkins University, 855 Broadway Research Building, Baltimore, MD 21205 USA

Copyright 2008 Djahida Bedja
All rights reserved

LIST OF ORIGINAL PUBLICATIONS

1. Moens AL, Champion HC, Claeys MJ, Tavazzi B, Kaminski PM, Wolin MS, Borgonjon DJ, Van Nassauw L, Haile A, Zviman M, **Bedja D**, Wuyts FL, Elsaesser RS, Cos P, Gabrielson KL, Lazzarino G, Paolocci N, Timmermans JP, Vrints CJ, and Kass DA. High-Dose Folic Acid Pretreatment Blunts Cardiac Dysfunction During Ischemia Coupled to Maintenance of High-Energy Phosphates and Reduces Postreperfusion Injury. Circulation, 2008.

*2. An L. Moens, Eiki Takimoto, Carlo G. Tocchetti, Khalid Chakir, **Djahida Bedja**, Gianfranco Cormaci, Elizabeth A. Ketner, Maulik Majmudar, Kathleen Gabrielson, Marc K. Halushka, James B. Mitchell, Shyam Biswal, Keith M. Channon, Michael S. Wolin, Nicholas J. Alp, Nazareno Paolocci, Hunter C. Champion, David A. Kass. Reversal of Cardiac Hypertrophy and Fibrosis From Pressure Overload by Tetrahydrobiopterin Reversal of Cardiac Hypertrophy and Fibrosis From Pressure Overload by Tetrahydrobiopterin-Efficacy of Recoupling Nitric Oxide Synthase as a Therapeutic Strategy. Circulation. 2008, 117(20):2626-36.*

3. Clarke G. Tankersley, Hunter C. Champion, Eiki Takimoto3, Kathleen Gabrielson,**Djahida Bedja**, Vikas Misra, Hazim El-Haddad, Richard Rabold, Wayne Mitzner. Exposure to Inhaled Particulate Matter Impairs Cardiac Function in Senescent Mice. AJP. 2008, Apr 30.

*4. Daniela Cihakova, Jobert G. Barin, Marina Afanasyeva, Miho Kimura, DeLisa Fairweather, Michael Berg, Monica V. Talor, G. Christian Baldeviano, Sylvia Frisancho, Kathleen Gabrielson, **Djahida Bedja** and Noel R. Rose. Interleukin-13 Protects Against Experimental Autoimmune Myocarditis by Regulating Macrophage Differentiation. American Journal of Pathology. 2008;172:1195-1208*

5. Georg Feldmann, Surajit Dhara, Volker Fendrich, **Djahida Bedja**, Robert Beaty, Michael Mullendore, Collins Karikari, Hector Alvarez, Christine Iacobuzio-Donahue, Antonio Jimeno, Kathleen L. Gabrielson, William Matsui and Anirban Maitra**.** Blockade of Hedgehog Signaling Inhibits Pancreatic Cancer Invasion and Metastases: A New Paradigm for Combination Therapy in Solid Cancers. Cancer Research 67, 2187-2196, March 1, 2007.

6. Feldmann G, Dhara S, Fendrich V, **Bedja D**, Beaty R, Mullendore M, Karikari C, Alvarez H, Iacobuzio-Donahue C, Jimeno A, Gabrielson KL, Matsui W, and Maitra A. Blockade of hedgehog signaling inhibits pancreatic cancer invasion and metastases: a new paradigm for combination therapy in solid cancers. *Cancer Res* 67: 2187-2196, 2007.

7. Gabrielson K, **Bedja D**, Pin S, Tsao A, Gama L, Yuan B, and Muratore N. Heat shock protein 90 and ErbB2 in the cardiac response to doxorubicin injury. *Cancer Res* 67: 1436-1441, 2007.

8. Habashi JP, Judge DP, Holm TM, Cohn RD, Loeys BL, Cooper TK, Myers L, Klein EC, Liu G, Calvi C, Podowski M, Neptune ER, Halushka MK, **Bedja D**, Gabrielson K, Rifkin DB, Carta L, Ramirez F, Huso DL, and Dietz HC. Losartan, an AT1 antagonist,

prevents aortic aneurysm in a mouse model of Marfan syndrome. *Science* 312: 117-121, 2006.

9. Lehrke S, Mazhari R, Durand DJ, Zheng M, **Bedja D**, Zimmet JM, Schuleri KH, Chi AS, Gabrielson KL, and Hare JM. Aging impairs the beneficial effect of granulocyte colony-stimulating factor and stem cell factor on post-myocardial infarction remodeling. *Circ Res* 99: 553-560, 2006.

10. Raju SV, Zheng M, Schuleri KH, Phan AC, **Bedja D**, Saraiva RM, Yiginer O, Vandegaer K, Gabrielson KL, O'Donnell C P, Berkowitz DE, Barouch LA, and Hare JM. Activation of the cardiac ciliary neurotrophic factor receptor reverses left ventricular hypertrophy in leptin-deficient and leptin-resistant obesity. *Proc Natl Acad Sci U S A* 103: 4222-4227, 2006.

11. Wachtman LM, Browning MD, **Bedja D**, Pin S, and Gabrielson KL. Validation of the use of long-term indwelling jugular catheters in a rat model of cardiotoxicity. *J Am Assoc Lab Anim Sci* 45: 55-64, 2006.

ABSTRACT

Background: The molecular and cellular mechanisms corresponding to the compensatory and maladaptive hypertrophy and remodeling of the left ventricle with chronic doxorubicin (DOX) treatment are currently unclear. Non-invasive methods of determining these changes are still deficient. To investigate these changes, 8 groups of rats in 4 different studies including a control saline group of the same age, gender and strain were evaluated for cardiac morphology and function including: (1) DOX dose response using a cumulative dose of 7.5mg/kg, and 15mg/kg in 8-10 week old female Sprague-Dawley (SD) rats, (2) strain differences were investigated in response to a cumulative dose of 15mg/kg in 8-10 week old female Fisher (F344) rats compared to the SD rats treated with same dose, (3) the role of gender and aging were studied in response to DOX at a cumulative dose of 3mg/kg in male and female neonates, and (4) combined losartan and a cumulative dose of 15mg/kg of DOX in 8-10 week old female SD rats compared to controls of saline and 15mg/kg treated SD rats.

Method: Onset of cardiac toxicity was assessed by echocardiography and the rat model of heart failure was developed when the fractional shortening declined ≤ 40%. The mean arterial pressure and single-photon-emission computer tomography scanning and Tc-99m-HYNIC-Annexin V were performed at week 10 to analyze blood pressure and quantify apoptosis, respectively. All rats were euthanized at week 10 except for the neonates and two of the 7.5mg/kg-treated SD rats that were left alive for study of long - term cardiac side effects. The heart and kidney tissues were harvested for protein

isolation and histopathological studies. Blood samples were collected for hematological and lipid profile analysis in all the rats.

Results: A dose- and time-dependent increase in LVmass coincided with a parallel increase in MAP, kidney damage, expression of myocardial erbB2, heat shock protein 90 Akt, mTOR, GSK-3β, TGF-β, pSMAD2, and cardiomyocyte apoptosis in SD rats treated with 7.5mg/kg and 15mg/kg of DOX at week 10. The 7.5 kg/kg treatment showed adaptive hypertrophy whereas the 15mg/kg treatment group showed maladaptive hypertrophy. However decompensation was apparent by week 14 in other rats treated with 7.5mg/kg. LVmass, FS, MAP, kidney damage, red blood cells and blood lipid levels were not significantly altered in the F344 rats compared to the 15 mg/kg-treated SD rats. Losartan supplementation reduced the left ventricular hypertrophy, improved myocardial contractility, and reduced TGF-β expression compared to the DOX-treated SD rats. The 3mg/kg of DOX in neonates induced cardiac toxicity and deaths in about 60% of males 50 weeks after treatment; the females instead developed mammary tumors.

Conclusion: The results of this study suggest that age, gender, and strain differences are risks factors for doxorubicin-induced harmful reno-cardiovascular toxicity. The inhibition of TGF-β expression by losartan can be used in prevention of chronic doxorubicin-induced cardiac toxicity without interfering with its anti-tumor activities.

TABLE OF CONTENTS

Chapter 1
INTRODUCTION

1.1. Anthracyclines used in the treatment of cancer

Doxorubicin (Adriamycin) is an anthracycline and quinone-containing antitumor antibiotic [1] originally isolated in the early 1960s from the pigment-producing bacterium *Streptomyces peucetius* [2-5]. It is widely used as the most effective chemotherapeutic course of treatment for most hematopoietic malignancies and advanced solid tumors of the breast, ovary, thyroid, and bone [6-9]. Cardiac toxicity is a serious adverse effect of doxorubicin (DOX) and limits its therapeutic potential [10]. Irreversible myocardial damage may develop as a concentration-time dependent response [2, 10, 11], leading to cardiomyopathy and congestive heart failure [10, 12]. This adverse effect may occur 4 to 20 years after stopping the treatment [2, 10, 11] and is in most cases refractory to common prescribed medications [13]. To avoid cardiac adverse effects, the maximum recommended cumulative dose of DOX for adults was tentatively set at 450 to 600 mg/m^2 [13]. However, toxicity can be distinguished in adults receiving cumulative doses of less than 300 mg/m^2 [8], and a cumulative dose of more than 550 mg/m^2 further raises the risk of congestive heart failure and death, especially in aged and hypertensive patients [7, 14]. In children, cumulative doses of 210 mg/m^2 or more were reported to cause adverse cardiac side effects with advancing age leading to severely compromised cardiac function [15, 16].

1.1.2. Epidemiology

One in 900 young adults is a childhood cancer survivor, prompting recognition of the potential long-term side effects of cancer therapy [17, 18]. In several studies of long-term survivors with a median age range of 15 to 23 years, 58% to 69% had at least one late effect of therapy, and 25% to 30% experienced moderate to severe complications [16, 18-20].

In a demonstration analysis of 20,227 childhood cancer patients who had survived 5 years, Mertens et al. reported the increased risk for death was 1.26, 0.027, and 0.0015 per 1,000 persons per year for cancers, cardiac, and pulmonary causes, respectively [21]. Other risks of late-onset side effects include second malignant neoplasm of the breasts, thyroid and skin, altered bone metabolism and osteoporosis, dyslipidemia, hypertension, diabetes mellitus, cardiovascular disease, liver failure, endocrine dysfunction [22-35], and renal failure [20, 36, 37]. One third of 201 children treated with anthracyclines at 4 to 6 years had fractional shortening (systolic function) values of < 20%, and over half had < 25% (normal is 30-45%) 10 years after treatment [38]. Late onset of arrhythmias and sudden deaths have been reported to have resulted in patients 15 years and more after anthracycline treatment [39-41].

1.1.3. Other anthracycline drugs

Several other anthracyclines, such as epirubicin, a semi-synthetic derivative of DOX which is significantly metabolized and has a shorter life [13], have been developed and used in the treatment of cancers [13]. However congestive heart failure was observed at cumulative doses of 950 mg/m^2 of epirubicin in patients with advanced breast cancer

without any previous anthracycline treatment [13, 42, 43]. Substituting epirubicin with doxorubicin, therefore, does not prevent the risk of developing cardiac toxicity [13].

1.1.4. Combinations of treatments

Cardiac toxicity can be intensified when anthracyclines are used in combination with other agents such as cyclophosphamide, bleomycin, cisplatin, methotrexane, and mitomycin C in addition to thoracic irradiation [38, 44, 45].

1.1.5. Trastuzumab

Trastuzumab (Herceptin), a monoclonal antibody treatment, was recently (September 1998) approved by the U.S. Food and Drug Administration (FDA) for the treatment of metastatic cancers which over-express erbB2 [46, 47]. Trastuzumab is directed against HER2, a proto-oncogene (also called c-neu or erbB2) transmembrane receptor tyrosine, which is a member of the epidermal growth factors receptor family (erbB1, erbB2, erbB3, erbB4). ErbB2 forms heterodimers with these erbB receptors that can bind neuregulins, polypeptides growth factors that are known to promote survival, growth of cardiac myocytes [46, 48] and known to be cardio-protective in the presence of cardiac postnatal injuries [46, 48]. Thus, inhibiting ErbB2 with a monoclonal anti-body may inhibit the myocardial adaptation to physiological stress and injury, such as that result from chemoradiotherapy, eventually leading to heart failure in most susceptible individuals [49]. Trastuzumab has been reported to induce heart failure in 28% of patients with breast cancer over-expressing erbB2 when treated in combination with anthracyclines [46, 50], compared to 7% when receiving DOX treatment alone [50]. The combination of treatments was used because both agents aim at killing the tumor, and the outcome is

significantly improved and faster compared to DOX alone [50, 51]. The combination of Trastuzumab and a DOX therapy was reported (Oncology Drugs Committee meeting September 2, 1998. Bethesda, MD) to improve 1-year (12 months) survival in 16% of women with metastatic breast cancer, compared to 13% survival when chemotherapy was used alone, which was not obvious until 18 months later [50].

1.1.6. Lapatinib

The recently developed drug lapatinib, an oral receptor tyrosine kinase inhibitor, targets both the ErbB-1 and ErbB-2 receptors over-expressed in breast cancer [52]. Time to onset of the decline in left ventricular ejection fraction (EF) was similar in both breast cancer and non–breast cancer patients treated with lapatinib [53]. The decline in EF was observed within 9 weeks of treatment in 66% of patients, 10–16 weeks in 15% of patients, and 17–24 weeks in 12% of patients [53].

Only 0.1% of symptomatic patients with decreased EF presented with dyspnea, palpitations, and signs of congestive heart failure (CHF), and responded rapidly to standard cardiac management [53]. Previous studies reported that in 1.3% of patients, incidence of symptomatic and asymptomatic decreases in EF in patients treated with lapatinib was less than that of trastuzumab-treated breast cancer patients [53]. Cardiac toxicity with lapatinib treatment was rarely reported [53].

Current startling clinical findings support the theory that inhibiting, cardiac neuregulin-erbB signaling significantly increases the vulnerability of the heart to injury and heart failure [48, 54]. ErbB2-deficient mutant mice died during the embryogenesis stage, on day 10.5 due to abnormal development of ventricular trabeculae [48, 55]. Chronic DOX

treatment alone induced cardiac toxicity in vivo mice with heterozygous knockout of neuregulin -1 gene (NRG-1+/-) compared with wild-type [54]. Since little or nothing is known about the long-term adverse effects with lapatinib treatment alone or in combination with DOX on the cardiovascular system, further research studies on animal models may be required to understand mechanisms and prevent irreversible cardiovascular damage.

Characterization and prevention of doxorubicin-induced cardiac toxicity alone have been the subject of intense research for years, but no single intervention has been demonstrated to successfully reverse or ameliorate the damaging effect of this drug on the heart while conserving its antineoplastic efficacy [56]. This drug is still being used as an important cancer therapy.

1.2. Anthracycline-induced cardiovascular toxicity

1.2.1. Acute cardiovascular side effects

The acute cardiovascular side effects of anthracyclines include various type of arrhythmias [57]; hypotension and a mild decline in cardiac contractile function [13] may occur within 24 hours to a week after administration [13]. Acute doses exceeding the threshold of 900-1000 mg/m^2 of epirubicin, 550mg/m^2 of donorubicin or doxorubicin, and 160 mg/m^2 of mitoxantrone [58] may alter myocardial calcium homeostasis and may lead to heart failure [57, 58]. These acute cardiovascular changes are reported as manageable and may respond to inotropic agents such as digitalis, isoproterenol, and high perfusion of calcium (Ca^{2+}) [13]. On rare occasions, acute complications may be

associated with myocarditis and pericardial effusion several weeks after initiation of treatment [59].

1.2.2. Chronic cardiovascular side effects

The greatest limiting factor of anthracycline treatment is the cardiac toxicity associated with chronic treatment leading to cardiomyopathy and, in severe cases, congestive heart failure [7, 10, 58, 60]. This cardiomyopathy and congestive heart failure is due to depressed myocardial contractility, which can be manifest months, years, or even decades after relatively low levels of treatment [2, 11]. This problem is especially apparent in individuals with additional risk factors such as increased age, hypertension, pre-existing and/or a family history of heart disease [60].

1.2.3. Inter-individual doxorubicin-induced cardiac toxicity

The reasons for variations in inter-individual susceptibility to doxorubicin-induced cardiac toxicity are unclear. The genetic component in humans is supported by the broad variation in the individual vulnerability to this drug [61]. DOX doses of more than 1000 mg/m^2 are endured by some patients [62], whereas after a cumulative dose of only 200 mg/m^2, other patients develop cardiac toxicity [61, 62].

1.2.4. Gender difference and doxorubicin toxicity

Gender differences and incidences of cardiovascular disorders have been reported to be more prevalent in males than females [63]. Epidemiological studies on postmenopausal women over the age of 50 years, report 1 in 2 women die of heart disease or stroke, while only 1 in 25 women will die with breast cancer (Miller et al. 1997). A number of epidemiological and

animal experimental studies have suggested a cardioprotective role of estrogen [64]. The implication of an estrogen mechanism of cardioprotection and tumor growth is still unclear.

1.3. Methods for monitoring anthracycline-induced cardiovascular toxicity

1.3.1. Endomyocardial biopsy

Endomyocardial biopsy analysis was among the first and most sensitive approaches monitored in the detection of myocardial damage, and is used as a guide to establish safety for further therapy [65-69]. Based on a prior light microscopy study, 35% of patients with indication of anthracycline-induced cardiac toxicity did not have any specific histological lesions on biopsy assessment, highlighting the meager sensitivity of this method [70]. In contrast, transmission electron microscopy was regarded as more sensitive and able to identify sarcotubular dilation, vacuolization, myofibril loss of actin and myosin, elongated mitochondria, and peripheral Z band remnants [71]. This technique provides vital information on setting up further therapeutic strategies depending on the time course and extent of damage [71]; however, both methods are invasive and expensive requiring a small sample of the myocardium to be taken for diagnostic analysis and are without the risk of complications, especially in a debilitated oncologic patient [72].

1.3.2. Systolic function

DOX dose-dependant myocardial toxicity is characterized by impairment of the left ventricular diastolic dysfunction, followed by reduced systolic function with progressive left ventricular wall thinning and chamber dilatation [38]. The recommendation for monitoring, dosage modification, and discontinuation of anthracycline treatment is based on the results of serial follow-up non-invasive echocardiographic and radionuclide ventriculography evaluation. Left ventricular systolic dysfunction, estimated by the decline in the percent of left ventricular ejection fraction (EF) in humans and/or fractional shortening (FS) in small experimental animals, are the parameters that are monitored. A value of $\leq 45\%$ in ejection fraction (50-70% is normal range for human adults) was the threshold set for termination of DOX treatment [38, 73]. This value was considered abnormal and could lead to an increase in left ventricular end diastolic pressure and pulmonary congestion [74]. These patients were automatically disqualified from chemotherapy on the basis of their systolic function [75]. In the prevention of anthracycline-induced cardiac toxicity, The Cardiology Committee of the Children's Cancer Study Group recommended regular echocardiography and radionuclide ventriculography during treatment. If the initial examination remains normal, long-term echocardiography follow-up should be performed every 3 to 6 months, 12 months, and then in alternate years after stopping the treatment [71]. Ideally, methods need to be developed for identifying patients at risk of cardiac toxicity or identifying cardiac toxicity before it causes irreversible depression of myocardial function in time and DOX concentration dependent response [38].

1.3.3. Diastolic dysfunction

Diastolic dysfunction results from impaired left ventricular relaxation [76], occurring in response to fibrosis accumulation and cell death while systolic function (ejection fraction or fractional shortening) is preserved [77]. Diastolic dysfunction precedes systolic dysfunction and predicts the development of heart failure and risk of mortality [78]. Diastolic function or myocardial relaxation is assessed via simple and inexpensive non-invasive echocardiography methods using mitral flow and tissue-derived Doppler parameters such as isovolumetric relaxation time (IVTR), Tei Index, or the myocardial performance index (MPI) and others [74, 79]. Documenting changes in the regional wall motion while the systolic ejection is preserved is developing into the most inexpensive method for assessing various cardiovascular diseases [80]. If detected earlier, it may define mechanism of DOX toxicity and the application of therapeutic strategies to reverse the progress to heart failure.

1.4 Mechanisms of myocardial dysfunction and doxorubicin-induced cardiomyopathy

1.4.1. Major hypotheses

The mechanism(s) responsible for myocardial injury and dysfunction leading to cardiomyopathy and congestive heart failure after chronic DOX toxicity continues to be debated. Several major hypotheses have been proposed:

a) generation of reactive oxygen species (ROS) [81-84], and lipid peroxidation [81, 85, 86]

b) reduction in activity of myocardial antioxidant enzymes [87, 88]

c) release of vasoactive amines such as catecholamine, histamine, and prostaglandins [89-92]

d) changes in myocardial adrenergic function [93, 94], and alterations of sarcoplasmic reticulum (RS) calcium transport, and homeostasis [3, 95]

e) changes in activity of adenylate cyclase, sodium-potassium ATPase and calcium-ATPase [96, 97] and,

f) deterioration of energetic response [98], prevention of DNA repair and replication [3, 99].

1.4.2 Reactive oxygen and apoptosis

Doxorubicin-induced cardiac toxicity appears to be complex, and no single mechanism entirely explains the pathogenesis of the myocardial damage [98]. However, most pathological changes may involve free radical production and lipid peroxidation (see hypothesis above), which could be partly responsible for apoptosis (programmed cell death) of cardiomyocytes [82, 90, 98, 100]. Reactive oxygen species are also implicated in a variety of heart diseases and supported by various studies performed over the past two decades, including: myocardial ischemia/reperfusion injury [101], hypertrophic cardiomyopathy [102], atherosclerosis [103], and heart failure as the end stage results of excess cardiomyocytes apoptotosis [104]. However, the mechanism of ROS and apoptosis stimulation in doxorubicin-induced cardiac toxicity is unclear.

1.4.3 Reactive oxygen species in cardiovascular disease and antioxidant defense mechanisms in the cardiovascular disease and toxicity

Reactive oxygen species (ROS) include free radicals such as superoxide (O_2^-) and hydroxyl radicals (HO^-) and compounds such hydrogen peroxide (H_2O_2) which are highly reactive molecules [90, 105]. They act as oxidizers or reducing agents [90]. They participate in both normal aerobic metabolism [106] and in pathologic biochemical reactions [105, 107] and are produced endogenously as a byproduct of normal cellular metabolism [108].

1.4.3.1. Superoxide

Superoxide (O_2^-), a free radical with an unpaired electron, is highly reactive [109] and water soluble and can diffuse through cell membranes via anion channels [109]. It is produced intra-cellularly through the activation of nicotinamide-adenenine dinucleotide phosphate (NAD(P)H oxidase, xantine oxidase (XO), uncoupling of nitric oxide synthase (NOS), electron transport and leakage during oxidative phosphorylation in the mitochondria [105].

1.4.3.2. Hydrogen peroxide

Under normal physiological states, hydrogen peroxide (H_2O_2) is generated from dismutation of low levels of O_2^- and catalyzed by high levels of superoxide dismutase (SOD) [109]. H_2O_2 is lipid soluble and its reduction generates a highly reactive hydroxyl radical (OH^-) in the presence of iron [105] which can induce local damage [109].

1.4.3.3. Nitric oxide

Nitric oxide (NO), previously known as endothelium-derived relaxing factor (EDRF), is a vasodilator and reactive molecule discovered by Ignarro LJ and Furchgott RF et al. around the 1980s for its role as a signaling molecule in the cardiovascular system [110-112] and for which they won the Nobel Prize in Physiology in the 1998. In normal physiological conditions, NO release is stimulated by agents such as acetylcholine [113], bradykinin [114], and also by shear stress [109]. NO in turn, activates intracellular soluble granulate cyclase (sCG) and stimulates the synthesis of cyclic guanosine monophosphate (cGMP) [105, 115]. The cGMP controls cellular function by stimulating protein kinase G (PKG) [105, 115]. PKG, in turn modulates vascular tone and myocardial contractility [115]. NO interacts with proteins via S-nitrosylation which is initiated by normal levels of O_2^- and inhibited by O_2 overload [105, 107]. Excess O_2^- production results in the conversion of NO into peroxynitrite ($ONOO^-$) [116, 117].

1.4.3.4. Peroxynitrite

Surplus of $ONOO^-$ may become oxidative and cytotoxic, leading to lipid peroxidation, protein oxidation and the alteration of excitation and contraction coupling [105, 107, 116] manifested as systolic and diastolic dysfunction that may lead to chronic heart failure [117].

1.4.3.5. Reactive oxygen and antioxidant system

The toxic effects of O_2^-, H_2O_2, NO, $OONO^-$ and OH^- are known as reactive oxygen species or ROS and occur when they are generated in excess and when antioxidant

defenses are inundated or deficient, leading to cellular and organ damage [118]. ROS is controlled by antioxidants such as superoxide dismutase (SOD), catalase, thioredoxin, glutathione peroxidase, and non-enzymatic antioxidants such as vitamin E, vitamin C, beta carotene, ubiquinone, and lipotic acid [105, 109, 118].

1.4.3.6. Doxorubicin and reactive oxygen generation

Doxorubicin exposure can significantly increase formation of intracellular reactive oxygen species (ROS) [119]. ROS may react with membrane proteins and may cause oxidative damage to the nuclear and mitochondrial DNA [119]. Acute doxorubicin-induced cardiac toxicity is generally thought to be attributed to the damaging effects of ROS arising from 1-electron reduction of anthracyclines [61]. In contrast, chronic toxicity has been proposed to result, partly, from the effects of anthracycline alcohols, which are generated by 2-electron reduction such as aldo-keto reductase and carbonylreductases [120].

The increase in available DOX further participates in reduction/oxidation cycles, as a result generating more superoxide [121]. Increased levels of ROS due to DOX has been detected indirectly by electron spin resonance spectroscopy [90, 122, 123], and indirectly by an increase in malondialdehyde formation which is the end product of lipid peroxidation [81, 86, 90].

1.4.3.7 Doxorubicin-induced superoxide radicals and hydrogen peroxide toxicity

In the presence of oxygen, redox cycling of DOX-derived quinone-semiquinone forms superoxide radicals (O_2^-) [13, 90]. The O_2^- is then transformed to hydrogen peroxide

(H_2O_2) by superoxide dismutase, producing hydroxyl radicals that can react with polyunsaturated fatty acids to yield lipid hydroperoxide [2, 90]. Surplus of reactive oxygen species or O_2^- compounds above the physiological levels leads to the commencement of lipid chain reaction and oxidative damage to cell membranes [2, 90].

The reduction of DOX in cardiac tissue is known to be (complex I) due to NAD(P)H reductase such as cytochrome P450, mitochondrial NAD dehydrogenase, xanthine dehydrogenase, and endothelial nitric oxide synthase (eNOS) present in cardiac and endothelial sarcoplasm and mitochondria [1, 82, 86, 121, 124, 125].

1.4.3.8. Doxorubicin-iron complex

ROS may also be produced after the formation of a DOX-iron complex, which reduces oxygen to hydrogen peroxide (H_2O_2) and cleaves the peroxide to give way to a powerful oxidant such as the hydroxyl radical (OH^-). This DOX-iron complex was found to play a central role in lipid peroxidation [126-128].

1.4.3.9. Doxorubicin and nitric oxide synthase expression

Anthracycline-induced cardiac toxicity is mediated by the stimulation of nitric oxide synthase (NOS) expression, NO release in the heart, and the capacity of NOS to promote anthracycline redox cycling to produce reactive oxygen species such as O_2^-, and H_2O_2 [2]. Excess generation of these ROS, may interact with NO to form peroxynitrite ($ONOO^-$) [2, 105]. This in turn may generate cytotoxic effects including lipid peroxidation, protein oxidation, leading to myocardial injury, dysfunction, and eventually to heart failure [2, 105, 117, 129].

1.4.10. Reactive oxygen and molecular signal transduction

A large amount of evidence suggests that ROS plays an important function in cellular signaling mechanisms that transmit transcriptional and translational cellular growth, differentiation and apoptosis [130, 131] in cardiovascular diseases and toxicity.

O_2^- and H_2O_2 were reported to stimulate the tyrosine kinase Src, GTP-binding protein Ras, protein kinase C (PKC), mitogen-activated protein kinases (MAPKs) including the extracellular signal–regulated kinase (ERK1/2), Jun-nuclear kinase (JNK), and the p38 kinase [105, 132, 133]. During the adaptive hypertrophic myocardial remodeling, with preserved systolic function (myocardial contractility), low levels of O_2^-, and H_2O_2 are associated with phosphoinositol-3-kinase (PI3K), Akt and ERK1/2, activation and protein synthesis [105, 134, 135], whereas high of O_2^- and H_2O_2 levels stimulate JNK and the p38 MAPK to induce apoptosis [105, 134, 136]. A high level of apoptosis is associated with left ventricular dilation and wall thinning with marked decline in myocardial contractility which are features of maladaptive hypertrophy and leads to heart failure and deaths [135].

Several potential sources of ROS generation were suggested to be involved in cardiovascular disease including: angiotensin II, α-adrenergic agonists, endothelin-1, tumor necrosis factor-α, and cyclic stretch [137]. Regardless of the presence of these multiple ROS sources, several latest studies indicate that a major source of ROS production involves the redox cycling of NAD(P)H oxidase [102, 137]. Targeting all these sources may thus bring about potential therapeutic interventions in treatment of cardiovascular diseases and toxicities [102].

1.5 Apoptosis and necrosis

1.5.1. Types of cell death

Apoptosis and necrosis are two types of cell death which are different both biochemically and morphologically [138]. Apoptosis was discovered by Kerr et al. in 1971-1972 as a programmed cell death [139, 140]. These biochemical and morphological changes in dying cells are a direct basis of organ dysfunction [3]. Apoptosis is normally an energy (or ATP) requiring a process that involves active intracellular signaling pathways [141]. It plays a role in the development and morphogenesis of normal cell turnover, hormone-dependant organ atrophy, and immune system function [142, 143]. The ultra-structural alterations of apoptosis are characterized by cellular shrinkage, cytoplasmic blebbing, nuclear chromatin condensation, DNA fragmentation and decomposition into numerous membrane bound vesicles known as apoptotic bodies, which are cleared by phagocytosis, either by neighboring cells or phagocytes such as macrophages [143, 144].

In contrast, necrosis is characterized by the depletion of energy or ATP [141, 145]. The ultra-structural alterations include: cell swelling, damage to intracellular organelles, rupture of cell membrane, and the extrusion of intracellular contents into the surrounding tissue, resulting in an inflammatory reaction and damage to neighboring cells with scare tissue development [141, 144-146].

1.5.2. Apoptosis and necrosis in cardiovascular disease and toxicity

Apoptosis has been reported in various cardiac diseases, particularly in ischemia-reperfusion and non-ischemic heart failure, myocardial infarction and arrhythmias [147], [148], end stage heart failure [149], left ventricular remodeling and hypertrophy [150], diabetes [151], atherosclerosis, and DOX-induced cardiac toxicity [152]. There is also copious evidence that myocytes die by apoptosis in response to various stressors of experimental models such as hypoxia/reoxygenation [153-157], acidosis [157-159], ischemia-reperfusion injury [160], oxidative stress [161], serum and glucose depletion and metabolic inhibition [162], administration of β-adrenergic agonists [163], angiotensin II stimulation [152, 164], viral infections, work load and mechanical stretch [146, 154, 160, 165, 166].

The distinctions between apoptosis and necrosis have been proposed in animal models and on human tissues after myocardial infarction studies whereby cardiomyocyte death primarily occurs through apoptotic pathways, whereas necrosis occurs afterward following the ischemic insult [158, 159, 167].

The vital mechanism by which anthracyclines cause both tumor cell killing and cardiomyocyte damage remains still undetermined [4]. Several hypotheses that lead to such synergism has been proposed to involve the following events:
a) the generation of free radicals through the redox cycling of oxygen, leading directly to lipid peroxidation and DNA damage, or
b) through indirect trigger of apoptosis by alteration of the mitochondrial membranes, kinase signaling molecules, apoptotic regulatory proteins and transcriptional proteins, and

c) the release of iron from the alcohol derivative of anthracyclines, generating more free radical and causing further cell damage,
d) anthracyclines was also suggested to stabilize a reaction of topoisomerase II and DNA strands and p53-mediated genotoxicity and apoptosis [4].

1.5.3. Signaling transduction pathways of apoptosis

The two major signal transduction pathways have been suggested necessary in the initiation of apoptosis program including: (i) surface death receptor-mediated "extrinsic" pathways which are members of the TNF family and (ii) mitochondria-mediated "intrinsic" pathways—both of which result in the activation of cellular protease such as the caspases [168, 169].

The intrinsic mitochondrial death pathway is regulated by proteins that belong to the Bcl-2 family, including the pro-apoptotic Bid, Bax, Bad, Noxa, Puma, Bnip3, and the anti-apoptotic family members such as the Bcl2 and Bcl-xl [170, 171] which control the permeability of the outer and inner mitochondrial membranes [172, 173]. The final stage of apoptosis involves the activation of caspases associated with signal transduction via cell-surface death receptors [174]. These caspases, which reside in the cytosol [175], are believed to play a part in DNA fragmentation, chromatin condensation, membrane blebbing, cell shrinkage, and development of apoptotic cells [176].

As previously discussed, three major mitogen activator protein kinases (MAPKs) signaling pathways have been identified in the cardiomyocytes [177]. MAPKs are a family of serine/threonine protein kinases known to play a part in the transmission of extracellular signals to cytoplasm and nuclear pathways when activated by various

extracellular stimuli [178, 179]. These MAPKs include (i) extracellular signal-regulated kinases (ERK1/2) known to induce cell growth and survival [171], (ii) the c-Jun N-terminal kinase (JNK), and (iii) the p38-MAPKs which are stress activated protein kinases (SAPK) and contributors to apoptosis [171]. The role of regulation of apoptotic cell death by JNK and the p38-MAPKs are still unclear and may be cell and stimuli type-specific [177]. Experimental studies indicate that JNK and the p38-MAPKs may represent the primary intermediates in the stimulation of apoptosis when phosphorylated in response to cellular stress such as (i) H_2O_2 in ischemia/reperfusion (R/I) of isolated cardiomyocytes [136, 180-182], by (ii) O^-_2 and H_2O_2 in chronic DOX-induced cardiomyopathy [152], in (iii) hypoxia-induced activation of JNKs in isolated cardiomyocytes [152, 180], and (vi) ultraviolet radiation and cytokines [171].
It was suggested that through "cross talk" occurring between these various apoptotic and pro-apoptotic signaling pathways and regulatory mechanisms, the loss of cardiomyocytes reactivates hypertrophy of the remaining myocytes to preserve cardiac function in adaptation to increased mechanical workload and myocardial stretch [147].

Based on in vitro cardiomyocyte studies of apoptosis in animal models with cardiovascular disease, several potent stimuli of cardiomyocyte apoptosis were suggested including: free radicals such as superoxide (O_2^-) which interact with NO to form peroxynitrite ($ONOO^-$), others are cytokines such as tumor necrosis-α (TNFα) and G protein-coupled receptors that mediate stimuli induced by agonists/ligands such as norepinephrine (NE), angiotensin (AII) and endothelin-1 (ET-1), [147], mechanical stress, and stretch that leads to the increase in wall tension and remodeling [183, 184]. The source of stimulation, initiation, and mechanism of anthracycline-induced

cardiomyocytes apoptosis are mainly reported with in vitro studies and less in the in vivo cardiomyocytes studies [4]

Understanding the source of the stimulation and mechanism of apoptosis using in vivo non-invasive physiological assessment in animal models treated chronically with DOX would help understand the process of apoptosis stimulation, molecular signaling, and the histopathological basis of cardiac toxicity. This will help develop new therapeutic strategies and prevention of anthracycline-induced cardiac toxicity.

1.6. Myocardial hypertrophy and remodeling

1.6.1. Cardiac remodeling

Cardiac remodeling involves changes associated with progressive heart failure of all etiologies that include hypertrophy, ischemia, interstitial fibrosis, cardiomyocyte apoptosis, and necrosis [144]. All of these pathological lesions result in depressed myocardial function [144].

1.6.2. Historic perspective

Understanding of adaptive and maladaptive hypertrophy (from Greek *hyper* + *trophy*, growth) started in 1745, when the Italian Lancisi Giovanni Maria made a distinction between heart chamber dilatation and thickening of its walls. This finding correlated with the French Nicholas Jean's observation in 1801 that hypertrophy ("active aneurysm") strengthens the heart, whereas dilatation ("passive aneurysm") diminishes the energy of cardiac contractility [185]. In 1892, Osler first described this cardiac hypertrophy as adaptive and maladaptive, following three stages of development [185-189]:

1) the phase when hypertrophy develops step-by-step and counterbalances the impairment of the valve,

2) the phase of full compensation through which the heart vigor meets the conditions of the circulation, and

3) the phase of "broken compensation," when death arises from weakening of the heart.

By the 19th century German Leopold Schroetter and the French Paul Constantine hypothesized that hypertrophy, although it offers an adaptive response that augments the heart's capacity to pump blood, is also maladaptive, because cardiac enlargement seems to reduce survival [185]. Felix Meerso further demonstrated that myocyte death in animals subject to transaortic constriction is the causal factor for shortened survival in a process of "cardiomyopathy of overload" [185, 190]. On the other hand, in 1982, Hochman and Bulkley described the myocardial alterations observed at the periphery of rat myocardial infarcts as part of the cardiac remodeling process [144].

Between the 18th and 19th century, the in vitro distinction between concentric and dilated hypertrophy was found largely due to cardiomyocyte thickening and elongation mediated by signal transduction pathways [185, 191].

Myocytes thickening was suggested to be attributed to accumulation of new sarcomeres in parallel, whereas elongation occurs when new sarcomeres are added at the end of the muscle fiber [185, 191].

In 1992, remodeling was finally characterized by an international forum on cardiac remodeling held in Atlanta, Georgia, as the suite of molecular, cellular, interstitial, and genomic alterations manifested clinically as changes in size, shape, and function of the heart following cardiac injury [144].

These changes may occur following myocardial infarction (MI), pressure or volume overload as seen with hypertension, dilated cardiomyopathy, and other inflammatory heart diseases such as myocarditis [144]. The only difference in these pathologies is the etiologies, the time course, and the nature of the initiating insult [144].

The inhibition of the signal transduction pathways that leads to the accumulation of new sarcomeres in chains of apoptotic cell death was suggested to delay or probably reverse the maladaptive growth response that may progress to dilatation of the failing heart [185, 191]. In fact, inhibition of cardiac hypertrophy and remodeling is currently emerging as a therapeutic target for the prevention of cardiac disease and heart failure [144, 192-195].

1.6.3. Mechanisms of hypertrophy

Despite a decade of research, the stimuli for hypertrophy have not been clearly described all known [196]. Furthermore, the precise mechanisms responsible for the transition of cardiac hypertrophy to cardiac failure are still being debated [197]. Left ventricular hypertrophy may be “physiological” in high performance elite athletes, and also arises in pathological conditions, such as hypertension, myocardial infarction, cardiomyopathies, valvular heart disease, and others [196]. The hypertrophy may be initiated by factors extrinsic and intrinsic to the cardiomyocyte [196]. The extrinsic stimuli include peptides such as angiotensin II and endothelin-1, adrenergic agonists such as norepinephrine, epinephrine, and phenylephrine, activators of protein kinase , peptide growth factors such as insulin-like growth factors (IGF-II), transforming growth factors-β (TGF-β), cytokines and mechanical and stretch factors [196]. Intrinsic stimuli include increased $Ca^{2+,}$ heterotrimeric G protein Gq, as well as activated small G proteins, kinase, phosphatase, and transcriptional factors [198]. These extrinsic and intrinsic factors elicit multiple

cascades of intracellular pathways, termed the “hypertrophic response” which leads in increased muscle hypertrophy and increase in muscle mass, reprogramming of myocardial gene expression, and cardiomyocytes apoptosis [196]. Hypertrophy is thought to control myocytes apoptosis in support of cardiomyocytes survival [199]. The phenotype result, either maintenance of adaptive hypertrophy or transition into heart failure, depends on the balance between the hypertrophic and apoptosis processes [199].

1.6.4. Hemodynamic overload and cardiac hypertrophy

Strain, pressure, and shear stress, in time, can induce pathological hypertrophy and remodeling of the vascular and myocardial wall [200]. This may provide functional benefits or adaptation by increasing the number of contractile elements (sarcomers) per cardiac myocytes and by lowering the ventricular wall stress through an increase in wall thickness [197] required to sustain cardiac output in response to stress [201]. The beneficial effects of this hypertrophy can be expressed through the application of physical principles showing that increased myocardial wall thickness preserves cardiac ejection performance by normalizing wall stress [202]. This process is demonstrated by the Law of LaPlace ($\sigma=pr/2h$): where wall stress (**σ)** of a sphere (or ellipsoid form as in the heart chamber or the ventricle) is determined by intramural pressure (**p**), cavity or ventricular dimension (**r**), and wall thickness (**h**) of the cavity [202]. Therefore, in hypertension, where the augmentation in pressure results in increased myocardial wall stress, a reactive increase in wall thickness can normalize wall stress and preserve systolic function (myocardial contractility) [202, 203]. Prolonged hypertrophy, however, leads to irreversible myocardial damage and heart failure characterized by myocardial wall

thinning, ventricular dilatation, decline in myocardial contractility, and heart failure [201]. This may be a result of sustained pressure overload (hypertension) from myocardial ischemia or infarction, volume overloads, or inherited and acquired cardiomyopathies such as result from chronic strenuous competitive sports (as in cardiomegaly), and chronic chemotherapeutic toxicity [201]. The progression of cardiac hypertrophy has been reported to be associated with a significant increase in the risk of heart failure and sudden death in human populations [201].

1.6.5. Pathophysiological and molecular mechanisms in cardiac hypertrophy and remodeling

There are situations where adaptive cardiac hypertrophy or growth can occur as a feature of normal postnatal cardiac eutrophy or as physiological hypertrophy (for example, in the heart of an athlete) resulting from regular endurance exercise routine [197, 204, 205]. It has been suggested that among the important differences in biomechanical signals in these circumstances, compared with pathological situations, is their transient duration of excess homodynamic load, as compared with persistent increases observed in pathological conditions [197]. Thus it is critical to define and distinguish between the pathways that regulate adaptive versus maladaptive hypertrophy in order to target the latter in human disease by using novel pharmacological or gene transfer approaches [204].

Structural remodeling of the heart is known to be related to various processes mediated by mechanical, neurohormonal, or growth hormone and cytokine pathways [206]. However, the dose-dependant anthracycline-mechanism of cardiac hypertrophy and

remodeling remains controversial and incompletely understood [207]. Furthermore, mechanisms that lead to the transition from adaptive left ventricle hypertrophy to dilated maladaptive hypertrophy is also not clearly understood, particularly with chronic DOX toxicity.

1.6.5.1. Phosphoinositide 3-kinase/Akt signaling pathways and cardiac hypertrophy

PI3K/PDK1/Akt signaling regulates growth and apoptosis, carbohydrate metabolism, protein synthesis, and glycogenesis [208]. PI3K is localized downstream of several receptor tyrosine kinases including IGF-1 and erbB2 receptors [199]. Akt mediate cell survival by controlling various apoptotic effectors such as Bad or procaspase-9 [209, 210]. Akt phosphorylates and activates endothelial nitric oxide synthase [211] which is important in regulation of cardiac function and is present in both cardiac myocytes and cardiac endothelial cells [208]. Akt was reported to be at a signaling cascade node, where its effects on cell death and survival is directly mediated via the forkhead box (FOXO) family of transcription factors and other regulators of apoptosis [212]. A number of FOXO target genes have been identified as controllers of numerous cellular functions including DNA repair, apoptosis, differentiation, and glucose metabolism [213].

The critical role of the PI3K/PDK1/Akt pathways in regulating normal heart growth is shown by the finding that cardiac-specific ablation of PKD1 leads to reduced cardiac growth and cardiomyopathy [214]. Furthermore, PI3K or Akt inhibition in human embryonic stem cell-derived cardiomyocytes, was associated with impaired cardiomyocyte proliferation, suggesting that PI3K/Akt signaling promotes embryonic

cardiomyocytes proliferation [215], and is a major kinase effector of PI3K signaling [216].

The effects on a given form of hypertrophic response are determined by signaling branch downstream of Akt [216]. These include the branch that leads to rapamycin (mTOR) protein and the protein synthetic machinery essential for all forms of hypertrophy [216]. The other branch leads to glycogen synthase kinase-3 (GSK-3), which is involved in metabolism, and protein translational machinery with transcription factor target linked in both normal and pathological hypertrophy [216, 217]. Both of these branches were also found to be controlled by stress-activated, Gq-dependent coupled receptor signaling mechanisms [218, 219] to promote cardiac-myocyte hypertrophy independent of Akt [216]. This partly explains the hypertrophy of the Akt1-/- mouse heart in response to pathological stress [216].

1.6.5.2. Rapamycin (mTOR)

The mTOR appears to coordinate inputs from hormones, mitogen and other stimuli, such as nutrients (branched-amino acids), and regulates protein synthesis, gene expression, cell size and proliferation [220-223]. Several studies implied that in cardiac hypertrophy, mTOR blocks cardiomyocyte hypertrophy induced by phenylephrine (PE) and/or endotholin-1 (ET-1)[224, 225], AII [226], and H_2O_2 [134]. The drug rapamycin was reported to significantly regress cardiac hypertrophy and decreased left ventricle end systolic diameter in mice subjected to transaortic constriction and decompensated hypertrophy, suggesting rapamycin as a possible therapeutic target in the prevention and/or reversal of cardiac remodeling [227].

1.6.5.3 Glycogen synthase kinase-3β (GSK-3β)

The role of GSK-3β as a negative regulator of cardiac hypertrophy is supported by the findings that persistent inhibition of GSK-3ß induced compensatory hypertrophy, inhibition apoptosis, and fibrosis, and increased myocardial contractility [228]. Transgenic mice overexpressing GSK-3β in the heart had a significant impairment of normal post-natal cardiomyocyte growth and myocardial dysfunction [229]. Transgenic mice overexpressing GSK-3 subject to pressure volume overload were reported to develop a significant amount of apoptosis and fibrosis with marked decline in myocardial function [217].

1.6.5.4. Epidermal growth factors (erbB2) and ligand neuregulin-1 (NRG-1)

The erbB2 protein is a tyrosine kinase receptor, also known as HER2, and is a member of the epidermal growth factor receptors (EGRF) family including erbB1, erbB3 and erbB4 [230]. ErbB2 is located in the transverse tubules within the cardiomyocytes [231] (Figure 15). Overexpression of erbB2 is found in 25-30% of breast and ovarian cancers [230]. ErbB2 function in muscle cells is still poorly understood [232]. ErbB2 receptor does not have a known ligand but signaling through its heterodimerization to erbB4 (after NRG-1β ligand stimulation) was reported to promote hypertrophic changes including changes in cell morphology, increases in protein synthesis, and expression of embryonic genes [233]. In postnatal and adult hearts, erbB2's role is an essential part in the myocardial adaptation to physiological stress, suggesting a primary role in cardiac growth and the cell survival mechanism against apoptosis [234], whereas its inhibition diminishes normal cardiac growth [48]. The decline in its expression is associated with the transition

from compensated myocardial hypertrophy to maladaptive hypertrophy and remodeling in aortic banding models [54]. Mice with knockouts of erbB2, erbB4, or its ligand neuregulin -1(NRG-1) died in utero due to cardiac development impairment [231, 235]. Furthermore, heterozygous NRG-1 mutant mice were found to be more susceptible to doxorubicin-induced heart failure than normal wild type mice [236]. NRG-1 receptors erbB2 and erbB4 are down-regulated in the early stage of heart failure in animals with chronic hypertrophy secondary to aortic stenosis, suggesting a role for disabled erbB2 signaling in the transition from compensatory to maladaptive heart failure [54].

ErbB2 activation may be associated with a secondary stress or activator of pro-inflammatory pathways such as ischemia, increased cardiac load, and cardiac agents [50]. Stimulation of angiotensin II receptor type 1 (AT1) by oxidative stress for example, induces transactivation of erbB2 and other epidermal growth factor receptors (EGFR) [237]. Of the four members of the EGFR/erbB2 family, erbB2 is the preferred and potent heterodimerization partner for all the erbB receptors to elicit signaling pathways [237, 238] including the MAPKs, ERK/Akt, and JNK pathways that lead to DNA synthesis and cell proliferation [239].

1.6.5.5. Heat shock proteins

Over the past decades, a series of studies have shown that heat shock proteins (hsp) such as the hsp 70 and the hsp 90 are able to protect cardiomyocytes against oxidative stress induced by exercise and in response to myocardial ischemia/reperfusion [194, 238-241], high temperature, apoptosis, and necrosis [240-243]. Heat shock proteins function as molecular chaperones [231] to prevent protein aggregation in response to stress by

binding to denatured and malfolded proteins and by assisting in the translocation of newly synthesized proteins to their proper cellular compartment [244]. Heat shock proteins may protect mitochondria against the damaging effect of reactive oxygen species and preserve cardiomyocytes protein structure and function [245, 246]. Several natural products, including radicicol and annamycin, and antibiotics geldanamycin and herbimycin -A, were reported to inhibit heat shock protein 90 by binding tightly to its highly conserved ATP/ADP pocket in its amino-terminal domain that is required for its function [247-250].

1.6.5.6. MAPKs: p38, c-Jun N-terminal kinases, and the extracellular signal-regulated kinase (ERK).

Once activated by phosphorylation, ERKs, JNKs, and P38 may translate to the nucleus where they phosphorylate mitogenic- or stress-responsive transcription factors [251]. As discussed previously, these MAPKs have been implicated in survival and apoptotic signaling pathways in response to ischemia/reperfusion, oxidative stress, hypoxia, β-adrenergic stimulation, and chemotherapeutic treatments [252]. ERK1/2 regulates cardiac hypertrophy [253] and is cardiac-protective during erbB2 signaling in DOX treatment [251]. Anti-erbB2 (Herceptin2) is used to treat human breast cancer with erbB2 overexpression [236] and the ERK1/2 pathway is thus blocked in breast cancer and most likely in the heart of the cancer patient. ERK1/2 is activated by cell stretching in cultured cardiac myocytes and by acute pressure overload stimulation in mice subject to transaortic constriction [252, 254].

DOX treatment results in decreased levels of phosphorylated ERK1/2 in the heart of NRG1 (NRG1-/-) mice compared to control mice [236, 255]. The inhibition of ERK signaling was also observed to increase doxorubicin-induced apoptosis in cardiomyocytes cultures [256]. In addition, DOX administration to β_2-adrenergic receptor (β_2-AR) mutant mice results in altered ERK1/2 activation and decreased contractile function [257]. Mice overexpressing MEK1, an upstream activator of ERK1/2, display enhanced cardiac contractility [258]. Insulin-like growth factor-1 (IGF-1), cardiotrophin-1 (CT-1), and catecholamine were shown to exert their anti-apoptotic effects, in part, by ERK signaling [251, 259, 260].

The level of activated ERKs in cardiac tissue sample of a failing heart was unaffected, whereas levels of JNKs and P38 kinase activation were considerably higher, suggesting that the MAPKs are differentially regulated during cardiac disease [251]. The outlook that pharmacological modulation of these signaling pathways in heart failure may re-establish the balance existing among the MAPKs is worth further animal studies [251].

1.6.5.7. Angiotensin receptor type 1 and TGF-β pathways

Transforming growth factor-β (TGF-β) plays a vital role in the regulation of growth and development, differentiation, tissue maintenance and repair in a large range of cells and tissues [261-263]. In the heart, TGF-β is expressed significantly during cardiac development and pathology [261-263]. Gene ablation of TGF-1 has demonstrated function of TGF-1 β in lymphocyte function [264-266], genetic stability [267], platelet activation [268], and cancer [269-271]. TGF-1 β has been implicated in myocardial hypertrophy [272], the stimulation of collagen production by fibroblasts [273, 274], and fibrosis [274-276] [277]. Other studies suggest that TGF-β is induced in the

hypertrophied myocardium following myocardial infarction [263, 278], pressure overload [279], and the infusion of norepinephrine (NE) [280].

Recent studies (2006) demonstrat that the AT1 receptor antagonist, losartan, prevented vascular remodeling and aortic aneurysm in a mouse model of Marfan syndrome by reducing the levels of TGF-β and this beneficial effect was associated with reduced interstitial collagen accumulation [273].

1.7. AIMS OF THE THESIS

The present study was planned to investigate the following hypothesis:

Hypothesis: In vivo non-invasive echocardiography using 2D, M-mode, and tissue Doppler, MAP and SPECT/CT Tc-99m-HYNIC-Annexin V show that chronic DOX is dose, age, strain, and gender dependent correlating with in vitro cellular and molecular signaling pathways as well as ex vivo histopathological, TUNEL staining, and pSMA2 immunohistochemestry findings:

Dose response:

Question:

Determine the process of adaptive and maladaptive left ventricular remodeling in response to low and high dose of doxorubicin?

i) Adaptive hypertrophy: A small amount of cardiomyocytes apoptosis will be associated with a significant increase in relative wall thickness and the preservation of myocardial contractility in the 7.5mg/kg treatment.

ii) Maladaptive hypertrophy: A larger amount of cell death will result in regression of RWT, ventricular dilation, increase in LVmass, and increase in MAP and

marked decline in myocardial contractility in the 15 mg/kg treatment as compared to the 7.5 mg/g treatment. Both adaptive and maladaptive left ventricular hypertrophy and remodeling will occur at the same point of time (Week 10) at the 2 dose 7.5 and 15 mg/kg, respectively.

iii) Prolonged adaptive left ventricular hypertrophy with 7.5 mg/kg dose of DOX will inevitably lead to maladaptive hypertrophy.

iv) Severe kidney damage and sustained hypertension would accelerate the transition of adaptive to maladaptive hypertrophy and remodeling in the 15 mg/kg treatment at week 10.

v) Vascular wall thickening and damage, increase in blood viscosity, would contribute to hypertension, thrombosis formation and reno-cardiovascular failure.

vi) Anemia would contribute to the decline in oxygen consumption, tissue damage, and dysfunction.

vii) SPECT/CT with Tc-99m-HYNIC-Annexin V imaging, guided with echocardiography follow-up methods, would provide better understanding of hypertrophy and remodeling mechanism, and would correlate to cardiac apoptosis formation in rats treated with doxorubicin.

viii) The increase in MAP and LVmass would parallel the increase in erbB2, NRG-1, Akt, mTOR, GSK-3, heat shock proteins (70-90), TGF-β pathway activation, and cardiomyocytes apoptosis.

ix) Persistent expression of erbB2, NRG-1, Akt/ERK1/2, mTOR, GSK-3, heat shock proteins (70-90), and TGF-β expression would be associated with continuous increase in cardiomyocytes apoptosis and marked decline in left ventricular

contractility. Excess cardiomyocytes apoptotosis would contribute to the conversion of adaptive hypertrophy to maladaptive hypertrophy and myocardial dysfunction.

x) Excess phosphorylated pSMAD2 would further confirm that excess TGF-β expression may be pro-apoptotic and the causal factor of toxicity in both kidney and heart of the DOX-treated SD rats.

Losartan:

Hypothesis 2: Losartan, angiotensin II receptor type 1 antagonist treatment would reverse left ventricular and vascular hypertrophy and remodeling, reduce blood pressure, and improve myocardial contractility.

Question 1:

Define in vivo and in vitro physiological and molecular mechanism by which losartan inhibits left ventricular hypertrophy and remodeling?

i) Non-invasive echocardiography follow-up would show reduction of RWT, reduction of LVmass, and normalization of myocardial contractility which will correlate to decline in blood pressure, a decline in blood platelet levels, and a decline in TGF-β expression.

Strain differences:

Question 2:

Is there any phenotypic difference in the kidney of Sprague-Dawley rats?

x) The Sprague-Dawley rats are more susceptible to DOX induced kidney damage than the F344 rats and this would be the contributing factor to earlier development of hypertension and heart failure.

xi) Risk of mortality is higher in SD than F344 rats treated with the same cumulative dose of 15 mg/kg doxorubicin at week 10 and may be due to a significant decline in myocardial contractility, increase in left ventricular mass, hypertension, hyperlipidemia, platelet aggregation, thrombogenesis, and nephrotoxicity.

xii) The significant increase in LVmass, body weight and kidney weight, and low level of red blood cell in the control saline SD as compared to the control saline-treated SD F344 rats may be predisposing factors to an unfavorable reno-cardiovascular connection to early hypertension and heart failure after 15 mg/kg of DOX at week 10. The F344 rats would show resistance to this same dose of DOX in the same point of time.

xiii) F344 rat treated with 15 mg/kg of DOX would exhibit a less significant amount of pSMAD2 phosphorylation in the kidney and the heart than the SD rat strain treated with the same dose of DOX at the same point of time (week 10).

xiv) The F344 rats are less susceptible to DOX-induced hypertension and left ventricular hypertrophy because they have less damage to the kidney than the SD rat strain treated with the same dose (15 mg/kg) of DOX. The F344 rats may also be irresponsive to angiotensin effect on the reno-cardiovascular system.

Gender differences:

Hypothesis: Males are more susceptible to DOX toxicity than females.

Question: What are the long-term side effects associated with DOX toxicity in males and females?

xv) Males would die with cardiac toxicity whereas females would develop mammary tumor.

CHAPTER 2

MATERIALS AND METHODS

2.1. Animals

Female Sprague-Dawley rats, 8–10 weeks old and weighing approximately 200g were used for most of the experiments. Male and female Sprague Dawley rats, neonatal rat pups 7 days old were also used in the experiments for dose response; female Fisher rats, 8-10 weeks old, were also used in the experiments on strain differences (as detailed in Table 1). The rats, purchased from Zivic Miller (Pittsburgh, PA), were acclimated for 1 week prior to the start of the experiments.

All procedures associated with this study were reviewed and approved by the Institutional Animal Care and Use Committee (IACUC) of the Johns Hopkins University School of Medicine. These procedures were performed in a facility accredited by the Association for the Assessment and Accreditation of Laboratory Animal Care International.

2.2. Overview of experimental protocol

The experimental approaches used to investigate the three aims of this study, namely DOX dose response, effects of losartan, and strain differences, are summarized in Table 1.

Table 1: Experimental design and methods used for doxorubicin dose response, combined losartan and doxorubicin, and rat strain differences

Aim and type of rat studied	In vivo TTE	In vivo Blood Pressure	In vivo SPEC/CT	In vitro Bio-distribution	Necropsy Histopathology Ultrastructure Blood profile	In vitro Western blotting
1. Dose response SD, 8-10 wks + neonate	+	+	+	+	+	+
2. Losartan SD, 8-10 wks	+	+	-	-	+	+
3. Strain differences SD + F344, 8-10 wks	+	+	-	-	+	+

Abbreviations:

F344: Fisher

SD: Sprague-Dawley

SPECT/CT: Single-photon-emission computer tomography/computed tomography scanning and 99mTc-annexin V

TTE: transthoracic echocardiography

Symbol + mean performed and – was not performed

2.3. Treatment method and schedule, data collection

2.3.1. Treatment method and schedule

Rats were randomly assigned to one of the treatment groups and to the control group; there were a total of 110 SD female rats and 30 female F344 rats aged 8-10 weeks. The neonatal study (part of aim 1) had a total of 24 rats: 12 males and 12 females. All experiments/treatments (except the neonates and 2 other SD rats treated with 7.5 mg/kg

DOX) lasted 10 weeks, after which time the animals were euthanized with sedation (ketamine/zylazine) when myocardial contractility was markedly reduced ≤ 40%.

For the treatments, DOX (Novaplus, Bedford Laboratories, USA) was administered intravenously via the jugular vein under anesthesia (ketamine/zylazine) in the 8-10 weeks rats, and via intraperitoneal in the neonates at the age of 7 days. Losartan dose of 0.6g/liter was administered in a drinking water after titration to reach comparable hemodynamic effects in vivo, including 15 to 20% decline in heart rate and a 10 to 20% decline in blood pressure[273]. The treatment groups were as follows:

Aim 1: Doxorubicin dose response

Sprague Dawley rats, age 8–10 weeks, female

Group 1: 2.5 mg/kg DOX weekly for 6 weeks, cumulative final dose of 15 mg/kg (n=40).

Group 2: 2.5mg/kg DOX weekly for 3 weeks, cumulative final dose of 7.5 mg/kg (n=10). Two of these rats were kept for long-term follow-up for DOX side effects on the cardiovascular response.

Control: Comparative dose of saline weekly for 6 weeks (n=30).

Sprague Dawley rats, neonates, males and females

Group 1: 1 mg/kg in volume of 25-50 μL every other week in 1, 2 and 3 doses, cumulative final dose of 1, 2, 3 mg/kg (n=3 for each group of treatment) in both male and female neonates.

Control 2: Comparative dose of saline (n=3).

Aim 2: Losartan

Sprague Dawley rats, age 8–10 weeks, females.

Group 1: 2.5 mg/kg of DOX weekly for 6 weeks, cumulative final dose of 15 mg/kg, supplemented with losartan in drinking water from the first DOX injection daily until week 10 (n=30).

Aim 3: Strain differences

Fisher rats, 8–10 weeks, females

Group 1: 2.5 mg/kg doxorubicin weekly for 6 weeks, cumulative final dose of 15 mg/kg (n=20)

Group 2: Comparative dose of saline administered once a week for 6 weeks (n=10).

2.3.2. Data collection

For all groups of 8–10 week old rats, data for in vivo, in vitro, and ex vivo at necropsy (see Table 1) is presented for the 10-week time point.

For the neonatal rats, from Aim 1, TTE data is presented for the 50 weeks time point.

For Aim 1, Dose Reponses, 8–10 week old rats, in vivo data was also collected at week 10. Week 10 data is presented because the 15 mg/kg treated SD rats had marked decline in cardiac function and thrombosis associated with unpredictable deaths. Two SD rats treated with 7.5 mg/kg of DOX were not euthanized at week 10 because the 7.5mg/kg treatment was associated with adaptive myocardial hypertrophy. These rats were kept alive for long-term observation and follow-up cardiac hypertrophy and remodeling to determine the changes associated with adaptive and maladaptive hypertrophic response over time. The quantification of fibrosis and collagen in the myocardium and vascular wall and damage to the kidneys were estimated visually using the scale of small, moderate, and severe extent of damage of tissue section.

2.4. Transthoracic echocardiography

2.4.1. Ultrasound equipment

Transthoracic echocardiography was performed using Sequoia Acuson C256 (Malvern, PA) or the 660 Vevo Visualsonics (Toronto, Ontario, Canada) ultrasound machine, equipped with 15MHz and 40MHz linear transducer, respectively [194, 281].

2.4.2. Maintenance of rats during echocardiography

To perform echocardiography without sedation, rats were habituated to immobilization inside a modified disposable rodent restrainer (Decapicone, Braintree Scientific, Inc.). Multiple air holes were cut in the plastic restrainer to allow for air circulation. The rat's chest was shaved and maintained in the restrainer for 1-3 minutes until normal resting heart rate was reached and rat was relaxed before an imaging session. While inside the restrainer, the rat was gently held in the left lateral dicubitus position. Pre-warmed hypoallergenic ultrasonic transmission gel (Parker Laboratories, Fairfield, New Jersey) was applied through an opening cut to obtain better ultrasonic penetration and better images. Care was taken to minimize the slightest chest compression which could cause bradycardia.

To prevent repetitive strain injuries to the handler arising from improper body mechanics during imaging, the handler rested her forearm on a flat platform, from elbow to wrist, while keeping her neck and lower back straight and maintaining the normal curvature using an ergonomic chair.

2.4.3. Image acquisition

2.4.4. M-mode and 2-Dimensional echocardiogram

The heart was first imaged in the two-dimensional (2-D) mode in the parasternal short and long axis view of the left ventricle (LV) at sweep speed of 200 mm/sec. From this view the M-mode echocardiogram was obtained by positioning the cursor perpendicularly to the interventricular septum and the left ventricular posterior wall at the level of the papillary muscles.

From the M-mode echocardiogram image, four parameters were measured: (i) left ventricular posterior wall thickness at end of diastole (PWTED), (ii) interventricular septal thickness at end of diastole (IVSD), (iii) left ventricle (LV) chamber diameter at end of diastole (LVEDD), and (iv) left ventricle chamber diameter at end of systole (LVESD). All measurements were performed according to the guidelines set by the American Echocardiography Society. For each rat, three to five values for each measurement were obtained and averaged for evaluation.

Using the LVEDD and LVESD, we derived the fractional shortening (FS) which represented the percent change in left ventricular (LV) chamber dimension with systolic contraction. We used the FS in the estimation of the LV wall contractility or the systolic function based on the following equation:

$$\mathbf{FS\ (\%) = [(LVEDD - LVESD)/LVEDD]\ X\ 100}$$

The left ventricular mass (LVmass) was derived and used in the assessment of left ventricular hypertrophy and enlargement, using the following equation [282]:

$$\textbf{LV mass (mg): } 1.055\ [(IVSD + LVEDD + PWTED)^3 - (LVEDD)^3]$$

where 1.055 is the specific gravity of the myocardium.

2.4.5. Tissue Doppler Imaging

Tissue Doppler Imaging (TDI) was used for evaluation of regional wall motion (Figure 1).

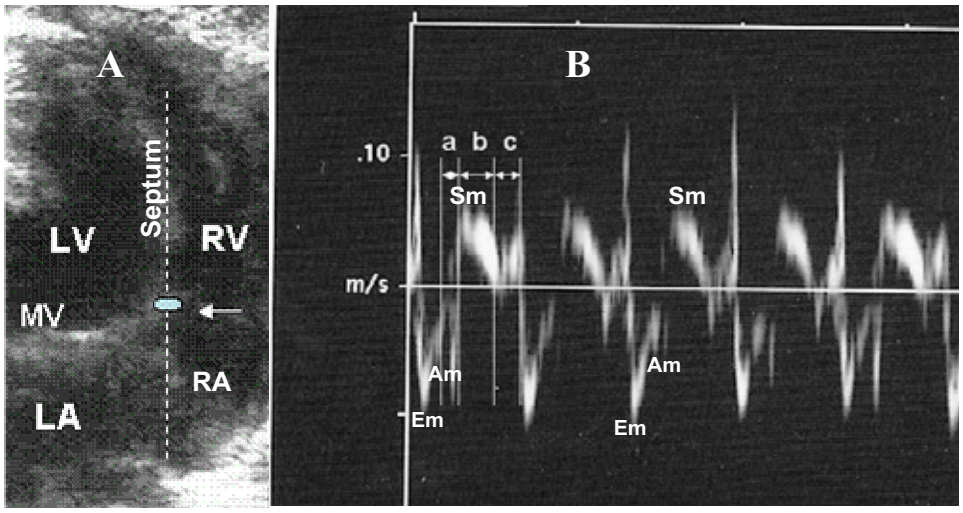

Figure 1 *Shows for the first time the four chamber view of the heart in two-dimensional echocardiogram (A) and the derived (B) tissue pulsed wave Doppler spectrum of conscious adapted rat. The four chamber view shows the left ventricle (LV), the right ventricle (RV), the left atrium (LA), the right ventricle, the mitral valve (MV). The arrow in this Figure (A) shows the sample volume placement at septal base of the mitral valve annulus were tissue pulsed wave velocity is recorded. In Figure B, interval* ***a*** *represents the isovolumetric contraction time* (*IVCT) measured from the cessation of the peak velocity of atrial diastolic filling (Am wave) to the onset of the mitral annular peak systolic velocity (Sm),* ***b*** *represents the left ventricular ejection time (ET), or the systolic ejection, measured as the duration of the mitral annular peak systolic velocity (Sm) and the* ***c*** *representing the isovolumetric relaxation time (IVRT) or the diastolic function, measured from the cessation of the peak systolic velocity (Sm) to the onset of peak early diastolic mitral*

Myocardial relaxation (or diastolic) and contraction (systolic) velocities of the left ventricle were measured using the four chamber view. The sample volume was positioned at the basal level of the interventricular septum. The septal ejection time (ET), isovolumetric contraction time (IVCT), and isovolumetric relaxation time (IVRT) were measured and used in the calculation of Tei index (TEI), also known as the myocardial performance index. The Tei index was used in the assessment of both systolic and diastolic function [283, 284]:

$$\mathbf{TEI = (IVC+IVRT)/ET}$$

All measurements were performed according to the guidelines set by the American Society of Echocardiography. For each rat, three to five values for each measurement were obtained and averaged for evaluation.

The rats were euthanized under anesthesia (Ketamine/zylazine) when FS ≤40%, the diastolic (IVRT) and/or the Tei index were significantly prolonged indicating dysfunction as compared to control saline group and according to physical symptoms associated with the level of activity, weight loss, and other manifestations relating to toxicity.

2.5. Risk of death and administration of euthanasia

Echocardiography weekly between 7 to 10 weeks helped us define the onset of adaptive myocardial hypertrophy/remodeling and its transition to maladaptive myocardial hypertrophy. The data presented in this study is of week 10 because a severe cardiac dysfunction associated with FS ≤ 40% occurred about 10 weeks after treatment. The rats were euthanized under anesthesia (ketamine/zylazine) when this target threshold (FS ≤40%) was reached and according to physical symptoms associated with the level of activity, weight loss, diarrhea, thrombosis, and manifestations relating to toxicity which commonly occurred at week 10.

Left ventricular function and morphology was assessed first to estimate the risk of mortality in the most susceptible subjects and to develop a rat model of heart failure. The tissue Doppler analysis of diastolic and systolic function was used to determine diastolic dysfunction in subjects with left ventricular hypertrophy and preserved systolic function and compared to rats affected with both systolic and diastolic function as well as the control group.

2.6. Tail-cuff blood pressure

MAP was recorded non-invasively after the last echocardiography study (week 10) by the tail-cuff method using the CODA 2 system (Kent Scientific Corp, USA) while the animal was anesthetized in closed chamber with isoflurane exposure. The flow of anesthesia was maintained by mask ventilation of 1.5% isoflurane in 100% O_2, using scavenging system. The rat was positioned ventrally on temperature-controlled circuit board (Indus Instruments, Houston, TX). The body temperature was maintained at constant normal 37^{o}C. Averages of 10 measurements were recorded per rats.

2.7. SPECT/CT imaging

2.7.1. SPECT imaging

In vivo SPECT quantification of cardiac cell death (apoptosis) in DOX dose dependent response was performed as follows:

(i) Rats injected with 7-8mCi Tc-99m-HYNIC-Annexin V

(ii) Images acquired 1 hour post-injection

(iii) High resolution dual-head single pinhole imaging

(iv) Planar – 15 min (n=2)

(v) Tomography – 90 views, 30s/view (n=9)

(vi) High detection efficiency 5-pinhole imaging

(vii) Tomography – 90 views, 30s/view (n=8)

(viii) Data reconstructed with OS-EM based 3D pinhole reconstruction algorithm

Two regions of interest (ROIs) were drawn in the mediastinal and the axillary soft tissue regions on SPECT images to calculate the cardiac uptake ratio (CUR) as a semi-quantitative index of cell death, using the following equation:

$$\text{CUR} = \frac{\text{Myocardium-soft tissue}}{\text{soft tissue}}$$

2.7.2. CT imaging

CT data were acquired sequentially after SPECT and fused with SPECT images to provide anatomical information. The images were acquired at settings of 75 kVp, 0.24mA, 512 projections, and 0.1s/projection.

2.8. Biodistribution of cell death

After euthanasia, 10-20 mg portions of left ventricle, right ventricle, blood, muscle, and fat were harvested and the biodistribution of annexin label was determined. Data were reported as standardized % ID/g.

2.9. Histopathology and ultrastructure of heart and kidney tissue

After euthanasia (ketamine/zylazine), the heart and both kidneys were weighed (both as total weight) and the small portions (5-10mg) of left ventricle (papillary level) was

sectioned and frozen in -80ºF for molecular studies (see 2.9 below). The remainder of the heart and kidneys were fixed in 10% formalin for H&E histopathology, pSMAD2 immunohistochemistry staining, and terminal deoxynucleotidyl transferase–mediated dUTP nick-end labeling (TUNEL) evaluation (for the hearts only). 3-6 micron sections were used for these studies.

Other rats' hearts were perfused via aortic cannulation with 0.2% glutaraldehyde and 4% paraformaldahyde fixative for immunoelectron microscopy.

2.10. Western blotting analysis for proteins

Frozen left ventricle (40mg) was rapidly homogenized in lysis buffer as described [231] and standard gel electrophoresis and immunoblotting were done.

The following 9 antibodies were used: ErbB2 (sc-285; 1:500; Santa Cruz Biotechnology, Inc., Santa Cruz, CA), ErbB4 (sc-283; 1:500; Santa Cruz Biotechnology), NRG-1β (sc-1792; 1:500; Santa Cruz Biotechnology), phospho–mammalian target of rapamycin (mTOR; 1:1,000; Cell Signaling, Boston, MA), phospho-p70s6k (1:1,000; Cell Signaling), phospho-Akt (1:1,000; Cell Signaling), total Akt (1:1,000; Cell Signaling), HSP90 (1:1,000; BD Transduction Laboratories, San Diego, CA), and HSP70 (1:5,000; Stressgen, San Diego, CA).

After incubation in anti-rabbit or anti-mouse horseradish peroxidase secondary antibody (1:2500; Amersham, Piscataway, NJ), blots were exposed to chemiluminescent substrate (Pierce, Rockford, IL) and exposed to CL-XPosure film (Pierce, Rockford, IL). Protein levels were normalized to total Akt or actin.

2.11. Real time-PCR (qPCR) and mRNA quantification

RNA (1 μg) was isolated from 20-30 mg of the left ventricle tissue (mid-papillary level) using a Trizol Neasy protocol (Qiagen), with an in-column Dnase treatment (RNase-Free DNase Set, Qiagen). Quality and concentration of the samples were assessed using a NanoDrop ND-1000 and 2100 Bioanalyzer, respectively. In vitro transcribed RNA (T7 Megascript, Ambion) was quantified by spectrometry and used as standard for the real-time PCR assay. A total of 1 μg RNA was transcribed into cDNA using random hexamere primers and Superscript II reverse transcriptase (Applied Biosystems, Foster City, CA) according to the manufacturer's protocol in an i-Cycler (thermal cycler, Bio-Rad Laboratories, CA). mRNA expression was determined using SYBR green (Applied Biosystems, Foster City, CA) on a BioRad i-Cycler. An amount of 0.41 ng of cDNA per reaction was used for determining 18S-rRNA and 12.5 ng for all the other genes. All measurements were performed as duplicates.

For each gene, intron-spanning primer pairs were used in a final concentration of 0.2 μM (see Table 2, 3 for details).

Table 2. List of gene used in the qPCR analysis

Gene primers	Function	Gene description
CTGF	.++	Rattus novegicus mRNA for connective tissue growth factor
PAI-1	.++	Rattus novegicus plasminogen activator inhibitor 1 (PAI-1)
HSP90a	.++	Rattus novegicus heat shock protein 1, alpha (Hspca)
VDAC1	.++	Rattus novegicus voltage-dependent anion channel 1 (VDAC1) mRNA
VDAC2	.++	Rattus novegicusoltage-dependent anion channel 2 (VDAC2) mRNA
S28	.++	Rattus novegicus mitochondrial ribosomal protein S28
HSP90b	.+	Rattus novegicusheat shock 90kDa protein 1, beta (Hspcb)
Adra1d	.+	Rattus novegicus adrenergic receptor, alpha 1d (Adra1d)
Adrb1	.-	Rattus novegicusadrenergic receptor, beta 1 (Adrb1)
BCL2	.-	Rattus novegicus similar to Apoptosis facilitator Bcl-2-like

++ shows high gene expression, + shows low gene expression, and – shows negative gene expression.

Table 3. Primer for q-PCR using SYBR green

Gene symbol	Primer	Sequence (5'-3')	Polimer	TeC
R-BCL2-F	Forward	5'-CTGGTCCAGATCCCTGTCCA-3'	20mer	59oC
R-BCL2-R	Reverse	5'-GGCCTTGCAATTCAAAGTGC-3'	20mer	59oC
VDAC-1F	Forward	5'-AACGGCAGTCTGGAAACCAA-3'	20mer	60oC
VDAC-1R	Reverse	5'-TTTCCCAGTGTTAGGCGAGAA-3'	20mer	60oC
VDAC-2F	Forward	5'-ATGCCAACGGCCAATTTGT-3'	19mer	60oC
VDAC-2R	Reverse	5'-TTGGTCTCCAAGGTCCCACT-3'	20mer	60oC
R-HS90a-F	Forward	5'-CATTTCCAACTCCTCAGACG-3'	20mer	60oC
R-HS90a-R	Reverse	5'-TTCCAATGCCAGTATCCACAA-3'	21mer	60oC
R-HS90b-F	Forward	5'-TGACTGACCCTTCCAAGTTG-3'	20mer	60oC
R-HS90b-R	Reverse	5'-CAGACTTAGCAATGGTTCCC-3'	20mer	60oC
R-28S-F	Forward	5'-GGAATTGTTCGTGTTGACCG-3'	20mer	60oC
R-28S-R	Reverse	5'-TCTCTGATGGCCTCTTGCG-3'	19mer	60oC
R-CTGF-F	Forward	5'-TCTTCGGTGGGTCCGTGTAC-3'	20mer	59oC
R-CTGF-R	Reverse	5'-TCTTCCAGTCGGTAGGCAGC-3'	20mer	59oC
R-HSP90b-F	Forward	new 5'-CAAGTTGGACAGCGGGAAA-3'	20mer	60oC
R-HSP90b-R	Reverse	new 5'-CCATGAACGCCTTTGTACC-3'	20mer	60oC
mGAPDH-F	Forward	5'-TGACGTGCCGCCTGGAGAA-3'	20mer	60oC
mGAPDH-R	Reverse	5'-AGTGTAGCCCAAGATGCCCT-3'	20mer	60oC
R-TGFb-2F	Forward	5-CCGGAGGTGTGATTTCCATCTA-3'	20mer	59oC
R-TGFb-2R	Reverse	5-CCGACGATTCTGAAGTAGG-3'	20mer	59oC

Q-PCR cycling conditions were as follows: in an initial step, reverse transcription was carried out at 50 °C for 30 minutes, taq-polymerase was activated at a temperatureof 95 °C for 10 minutes. Subsequently, amplification cycle conditions were 94 °C for 30 s, 60 °C for 30 s, 72 °C for 30 s (28S-rRNA) and 94 °C for 30 s, 60 °C for 30 s, and 72 °C for 30 s (for all other genes), respectively. Amplification cycles were repeated 40 times. After each run a melting curve analysis was performed to ensure amplification of correct products. mRNA expression was normalized for levels of cardiac 28S-rRNA as a housekeeping gene, which do not change during neonatal development. RT-PCR and expression level of erBb2 gene in heart in DOX-treated and non-treated heart are described in the our recently published data [231].

2.12. Blood lipid and hematological profile

Blood lipid and hematological profiles were performed using the ACE clinical chemistry system and reagents (Alfa Wassermann, Inc,). Blood was collected at week 10 in non-fasted state via the jugular veins while rats were sedated with ketamine and xylazine anesthesia injected the intraperitoneal route.

2.13. Statistical analysis

The results were expressed as mean and standard deviation (mean ± SD). One-way analysis of *ANOVA* and the Bonferroni multiple-comparison tests were used for comparing all groups and pairs of groups respectively. A $P < 0.05$ was considered significantly different. All analyses were carried out using Prism and Excel statistical analysis software.

CHAPTER 3

RESULTS

Follow-up echocardiography of the left ventricular morphology and function began at week 7 until target fractional shortening (indices of myocardial contractility) was ≤ 40% and dilated hypertrophic cardiomyopathy model developed by week 10 in the majority of the Sprague Dawley rats, exposed to 15 mg/kg of doxorubicin (DOX). Thrombus formation and unpredictable deaths were commonly observed in these rats at this dose and time point.

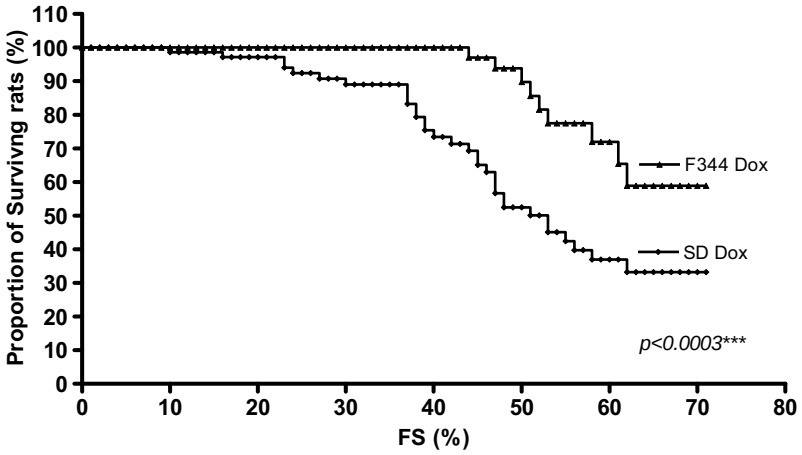

Figure 1: *The Kaplan-Meier survival curve by fractional shortening (FS) in Fisher (F344) and Sprague-Dawley rats (SD), 10 weeks after treatment with 15mg/kg of doxorubicin.*

There was a considerably significant risk for sudden death among the SD rats compared to F344 rats. Thrombus growth was commonly observed during the end stage cardiac toxicity in the majority of the female Sprague-Dawley and may have also been the leading cause of mortality. Some of the F344 rats that were not euthanize, and not presented in this present study were not euthanized until week 18 and had to be euthanized for other studies.

Non-invasive studiesincluding blood pressure, SPECT/CT Tc-99m-hydrazinonicotinic Annexin V (Tc-99m-HYNIC-Annexin V) were used after echocardiography analysis at about week 10 to evaluate the mean arterial pressure and quantify myocytes apoptosis. All rats at this time point, except the two rats treated with 7.5mg/kg of DOX and the neonates, were euthanized under sedation (ketamine/xylazine) at week 10 when the target FS ≤ 40% was reached. Blood was collected from the jugular veins for hematology and lipid profile while the rats were sedated. The right and left portion of ventricles were used in the biodistribution study for in vitro cardiomyocytes deaths and the remainder tissue was frozen for Western blotting and qPCR analysis. The kidneys and the rest of the heart were collected and harvested for histopathology, including TUNEL staining for apoptosis and pSMA2 immunohistochemistry.

All rats were euthanized mainly due to atrial thrombus development associated with significant decline in myocardial systolic function (FS) and mortality rates among the 15 mg/kg-treated SD rats as compared to Fisher rats (Figure 1). The two other rats treated with 7.5 mg/kg of DOX were euthanized 14 weeks after a marked decline in FS. The majority of male neonates died with cardiac toxicity and the females developed mammary tumors 50 weeks after treatment.

The 7.5 mg/kg of DOX-treated SD rats, left for the long-term side effects associated with DOX were at risk of death during week 14 because FS was lower than expected (28%). Some of the Fisher rats' cardiovascular changes seemed to plateau up to 18 weeks (results are not shown). Those that were euthanized were used in the study of strain differences and the reno-cardiovascular response to 15 mg/kg of DOX in comparison to the SD rats treated with the same dose of DOX and studied at week 10 after treatment.

3.1. Doxorubicin dose response, gender and strain differences with and without losartan treatment

3.1.2 Body, organ weight, and necropsy results

Body, heart weight, heart weight and body weight ratio, kidney weight, lipid, hematological and cardiovascular profile are outlined in Table 1. Body weight showed a mean percent difference of 35.03%, with the control saline-treated SD rats being significantly ($p<0.001$**) higher than the control saline-treated F344 rats (325.4±36.58 vs. 211.4±29.06), indicating phenotypic or strain differences in body weight (Table 1).

Parameters	SD Saline	F344 Saline	F344 15mg/kg DOX	SD 15mg/kg DOX+LOS	SD 7.5mg/kg DOX	SD 15mg/kg DOX
BW (g)	325.4±36.58 (20)	211.4±29.06(10)	169.2±12.65 (17)	210.7±20.02(14)	225.4±33.6 (8)	230.9±23.99 (12)
HW (g)	0.99±0.08(20)	0.49±0.03(10)	0.46±0.05 (17)	0.53±0.06 (14)	0.67±0.1 (8)	0.57±0.07 (12)
HW/BW(mg/g)	3.07±0.24(20)	2.34±0.41(10)	2.74±0.34(17)	2.52±0.31 (14)	2.95±0.15(8)	2.46±0.13(12)
KW (g)	1.47±0.06 (10)	1.1±0.06 (10)	1.02±0.08 (21)	1.67±0.4 (14)	1.81±0.19 (5)	1.73±0.31 (16)
LVmass (mg)	776.6±73.67 (16)	627.6±58.29 (10)	616.4±74.06 (16)	821.8±78.08 (10)	781.2±86 (5)	1024±85.72 (18)
RWT (%)	73.6±4.79 (8)	70.38±3.82 (8)	67.36±5.45 (11)	28.49±1.1 (10)	72.59±5.54 (5)	31.27±1.23 (6)
MAP (mmHg)	93.6±4.6 (5)	87.5±3.1 (4)	88±4.5 (3)	88±8.7 (10)	111.1±4.07 (2)	117.2±10.33 (5)
FS (%)	70.92±1.45 (31)	71.32±2.09 (10)	53.97±7.5 9 (16)	59.84±4.5 (27)	66.49±6.89 (10)	37.1±11.17 (24)
HR (b/min)	510.3±10.93 (15)	531.9±16.41 (5)	479.7±27.2 (10)	435.2±39.93 (23)	480±14.14 (5)	447.3±26.71 (22)
RBC(M/µL)	7.08±1.2 (9)	9.1±0.13 (4)	7.87±0.5 (15)	4.85±0.58 (10)	5.22±0.16 (2)	4.67±0.65 (9)
BUN(mg/dl)	17.56±2.65 (9)	14.75±1.5 (4)	15.78±4.75 (18)	61.78±25.02 (9)	32.5±12.02 (2)	40±4.32 (4)
Cre(mg/dl)	0.45±0.05 (10)	0.48±0.05(4)	0.47±0.13 (13)	1.44±0.88 (11)	0.55±0.78 (2)	0.79±0.23 (7)
Plat(k/µ/L)	344.4±109.8 (7)	301.3±104.2 (4)	346.6±82.79 (7)	573.8±248.3 (10)	970.5±263.8 (2)	758.1±337.2 (8)
CHOL(mg/dl)	116.4±15.28 (10)	125.3±23.56 (7)	313.4±90.61 (17)	1506±276.1 (10)	1078±17.68 (2)	877.4±396.6 (18)
TG(mg/dl)	50.58±16.01 (12)	106.2±56.04 (6)	341.4±201.3 (16)	3645±2951 (8)	1167±0.00 (1)	2261±2033 (17)
HDL(mg/dl)	54.92±8.59 (12)	56.83±18.05 (n=6)	110.1±25.86 (13)	173.3±25.6 (13)	177±57.98 (2)	160.2±49.5 (17)

Data expressed in mean±standard deviation (sample size). Body weight (BW), heart weight (HW), heart weight and body weight ratio (W/BW), kidney weight (KW), left ventricle mass (LVmass), relative wall thickness (RWT), mean arterial pressure (MAP), fractional shortening (FS), heart rate (HR), red blood cell (RBC), blood urea nitrogen (BUN), creatinine (Cre), platelet (PLAT), cholesterol (CHOL), Fisher (F344), Sprague-Dawley (SD), doxorubicin (DOX), 15mg/kg DOX+losartan (15mg/kg DOX+LOS).

Both the losartan and 15 mg/kg of DOX treatment combination (DOX+LOS) and the 15 mg/kg of DOX-only-treated SD rats had a significantly ($p<0.001$**) lower body weight than the control group of the same strain and was 210.7±20.02 (DOX+LOS) and 230.9±23.99 (DOX), respectively versus 325.4±36.58 (control SD).

Differences between these two groups include low levels of activity and frequency of diarrhea observed in SD rats treated with 15 mg/kg of DOX alone as compared to those treated with losartan and DOX combination. Body weight (225.4±33.6) in the 7.5 mg/kg DOX treated SD rats (Table 1) was significantly different ($P<0.001$**) from the controls of the same strain (SD rats).

The 15 mg/kg DOX-treated F344 rats had an average body weight of 169.2±12.65 representing a drop of 19.96% in mean percent difference from the control saline treated F344 rats (211.4±29.06) with a slight statistical difference ($p<0.01$*) than the other treated groups. These strains of rats were also physically more active than the SD strain-treated with the same dose of DOX as observed at the same time point, suggesting their resistance to DOX treatment. The SD rats treated with the same 15 mg/kg of DOX showed a drop of body weight of 29.04% lower than the controls of the same strain. This suggests greater body weight loss may be a risk factor for chronic doxorubicin-induced cardiovascular toxicity. Weight loss in the 15 mg/kg DOX alone treated SD rats was also associated with a significant amount of ascites and cardiac pleural effusion not observed in the LOX+LOS treated SD rats, nor the F344 treated with 15 mg/kg of DOX, and neither the SD rats treated with 7.5 mg/k of DOX at week 10.

Although the kidneys were pale and enlarged, their weight (total weight of both kidneys) were 1.73±0.31 and 1.81±0.19 in the 15mg/kg and 7.5mg/kg DOX treated SD rats, respectively, and 1.67±0.4 in the DOX+LOS treatment group as compared to their

control saline treated rats (1.47±0.06) with normal color. These differences were not statistically significant between these groups.

The F344 control (saline) treated rats showed a significantly ($p<0.01$*) lower kidney weight than the control saline treated SD strain. They showed a kidney weight of 1.02±0.08, representing a less significant drop after DOX treatment as compared to its saline control group (1.1±0.06). In addition, the DOX-treated F344 rats' kidneys appeared normal during necropsy. Histological finding of a small to an insignificant damage was observed whereas, the SD rats treated with the same 15 mg/kg of DOX showed moderate to severe kidney damage.

Heart weight were significantly lower ($p<0.001$**) in the 15mg/kg (0.57±0.07), in the DOX+LOS (0.53±0.06) and in the 7.5 mg/kg (0.67±0.1) treated SD rats ($p<0.001$**) than 0.99±0.08 in the control saline treated SD rats of the same strain respectively.

The mean percent difference drop in heart weight of the 7.5mg/kg was 32.32% lower than 42.42% in the 15mg/kg and 46.46% in the DOX+LOS treated SD rats.

In DOX+LOS treated rats, the decline in heart weight corresponded to the regression of left ventricular hypertrophy as indicated by the decline in RWT and LVmass, and which resulted in normalization of systolic function and blood pressure (Table 1). In the 7.5 mg/kg of DOX alone treated SD rats, the heart weight declined but not as significant as the DOX+LOS and the DOX treated SD rats and may have resulted from a significant increase in RWT, a slight increase in LVmass and preserved systolic function in response to a small amount of cardiomyocyte deaths. These changes occurred in adaptation to increase in workload and in support of more cardiac output.

In the 15mg/kg DOX alone treated SD rats heart weight, however, might be attributed to the significant amount of cardiomyocytes death (Figure 4A3) that lead to a significant decline in relative wall thickness (RWT), a significant increase in LVmass, a marked decline in myocardial contractility and increase blood pressure (Figure 5, 6, 7,8 and Table 1).

Changes observed in the LVmass in the 7.5mg/kg and the DOX+LOS might be attributable to a decrease in chamber size, normalization of wall thickness, lower MAP contrary to the 15mg/kg treated SD rats. Increase in LVmass and wall thinning was associated with increase in ventricular dilation, higher MAP and apoptosis in the 15mg/kg of DOX alone treated SD rats. The 7.5mg/kg showed smaller amount of cardiomyocytes apoptosis with similar characteristics of normalization of RWT, LVmass, MAP and the preservation of systolic function to the LOS+DOX treated rats, suggesting also that LOS+DOX may be also be associated with less apoptosis and that apoptosis may play part in heart weight and HW/BW decline.

Heart weight in the F344 rats was not significantly altered with 15 mg/kg of DOX treatment and was about 0.46±0.05 as compared to 0.49±0.03 in the control (Saline) of the same strain, suggesting their resistance to the treatment; whereas the control saline-treated SD heart weight was 51.51% greater than the control saline-treated F344 rats, suggesting their susceptibility to the development of hypertension, LVH and subsequently to heart and renal failure. Ascites, pleural effusion, pale kidneys and decline in heart weight from wall thinning, cell death, and ventricular dilation in the 15 mg/kg DOX-treated SD suggests connection of hypertension, nephropathy, and heart failure.

Heart weight/body weight (HW/BW) was 23.78% significantly higher (P<0.001**) in the control saline SD rats (3.07±0.24) than the control (Saline) F344 rats (2.34±0.41) confirming further the strain differences between the 2 groups may exist. The decline in HW/BW was significantly (p<0.001**) lower in the SD rats treated with 15mg/kg DOX alone (2.46±0.13) as compared to the F344 rats treated with same dose of DOX at same time point (2.74±0.34). DOX in the F344 rats, instead, showed a slight increase in HW/BW than their respective control group and could attributed to an increase in RWT, and decline in LV chamber size. The 7.5mg/kg DOX treated SD rats HW/BW showed not significant change and could be due to adaptive hypertrophy that is characterized by increase in RWT, decline in ventricular chamber size and preserved myocardial systolic function. The LOS+DOX treated SD rats showed a significantly lower (p<0.001) HW/BW (2.54±0.31) than normal control (saline) treated SD rats but not significantly different from the 15mg/kg DOX treated SD rats. This is partly due normalization of RWT, LVmass, MAP and systolic function in the LOS+DOX. In the 15mg/kg DOX treated SD rat's HW/BW may be due to significant decline in RWT, increase in LVmass, apoptosis and MAP.

3.1.3 Blood profile

3.1.3.1. Blood BUN and creatinine levels

Blood urea nitrogen (BUN) level in saline (Control) F344 was 14.75±1.5 lower than 17.56±2.65 in saline (Control) SD-treated rats showing a mean percent difference of 15.95% which was not statistically significant (Table 1).

SD rats showed a rise to 32.5±12.02 with 7.5 mg/kg DOX, 40±4.32 with 15mg/kg DOX and 61.78±25.02 with DOX+OX treatment (Table 1). The results of the DOX+LOS group showed the most significant ($p<0.001$**) increase in blood BUN levels as compared to saline (Control) treated SD rats which was not statistically different from the 15 mg/kg of DOX-treated SD alone.

The rise in BUN in both the 7.5mg/kg and the 15 mg/kg DOX treatment group increased in dose-dependent response but were also not statistically significantly different from the saline-treated SD rats.

There was a significant ($p<0.001$**) increase in blood creatinine levels of 1.44±0.88 with the DOX+LOS treatment group as compared to 0.45±0.05 in the control saline-treated SD rats of the same strain. The levels of creatinine in the 15 mg/kg DOX-treated SD rats were 0.79±0.23 higher than 0.55±0.78 in the 7.5 mg/kg DOX-treated SD rats, but were not statistically significant.

The significant increase in BUN and creatinine levels in the DOX+LOS suggests that renal dysfunction may be significantly higher than the DOX-alone treated SD rats. However, the MAP, cardiac morphology, and function in this group of rats appeared normal, suggesting that glomerular filtration of BUN and creatinine should also be normalized and should result in much less damage to the kidneys than the DOX-alone treated group. The increase in BUN and creatinine may have resulted from measurement variations, dosage, and other factors. It may also be due to the fact that the kidneys of this strain of rats may not have tolerated the treatment dosaged use in this study.

Thrombus formation with 15 mg/kg of DOX in SD rats was commonly observed in the left atrium by 2-dimensional echocardiogram mode and confirmed by histology around

week 10, suggesting vascular occlusion at the renal level may also be the causal factor for renal dysfunction. Thrombosis-induced renal damage may be the contributing factor to renal dysfunction, demonstrated by the rise in BUN and creatinine levels in the DOX+LOS group. Smaller size thrombi were also observed by histology in the DOX+LOS, suggesting that losartan may have an anti-thrombotic effect. Losartan may also have reduced the size of thrombus into smaller thrombi which can more displaceable and occlusive to the peripheral vascular system. Death with the LOS+DOX treatment did occur in other studies around 14 to 15 weeks after treatment and may have been the result of vascular occlusion leading to sudden death by stroke, MI, and renal failure. The long-term effect of losartan in experimental models may merit further investigation, particularly in the most susceptible strain of rats, such as SD rats. There were no significant differences in blood BUN or creatinine in control saline F344 and SD rats. The F344 rats showed no significant changes with either BUN or creatinine level, indicating a resistance to this drug.

Defects within kidney morphology or function may exist in the SD strain of rats because the F344 strain of rats also showed less significant damage to the kidneys compared to treated SD rats. SD control rats showed greater kidney weight than control F344 rats; this alone could be the predisposing risk factor for DOX-induced nephropathy. As a result, the losartan effect on improving kidney function would be less effective.

3.1.3.2. Blood Lipid profile

Blood lipid analysis showed a significantly higher levels of cholesterol (CHOL) and triglycerides (TG) in the DOX+LOS-treated SD rats than the DOX alone treated group (Table 1).

The CHOL rise in the DOX+LOS of 92.27% was significantly ($p<0.001$**) greater than the 89.2% increase in the 7.5 mg/kg-treated SD rats, and 86.73% increase in the 15 mg/kg DOX-treated SD rats. Both the 7.5 mg/kg and the 15 mg/kg of DOX-treated rats showed a significantly ($p<0.001$**) higher CHOL level as compared to the control saline-treated SD rats (Table 1).

The F344 rats treated with 15 mg/kg of DOX showed no significant changes in CHOL level relative to its control saline-treated F344 group.

The triglyceride levels in the DOX+LOS treatment group showed a significantly ($p<0.001$**) higher level of 98.63% than the control group. There was a difference of 37.97% in blood TG levels between the DOX+LOS and the 15mg/kg DOX-alone treatment groups but was not statistically significant (Table 1).

Although the F344 rats showed a 68.89% increase in TG, there was not significant alteration in TG levels compared to its control saline-treated F344 rats; however, this increase was significantly lower ($p<0.01$*) than the 15 mg/kg DOX-treated SD group, and significantly lower ($p<0.001$**) than the DOX+LOS-treated SD rats (Table 1).

HDL levels rose up to 65.72% in the 15 mg/kg DOX dose, 68.97% in the 7.5 mg/kg DOX dose and 68.31% in the DOX+LOS-treated rats; each was significantly ($p<0.001$**) higher than the control saline-treated group, respectively (Table 1).

The F344 rats showed a 48.38% rise in HDL which was significantly ($p<0.05$*) higher than their normal saline-treated F344 rats (Table 1). Since there was no statistically significant rise in the blood CHOL and TG level in the 15 mg/kg-treated F344 rats, this increase in HDL seemed to be functional in lowering lipids in the blood compared to the DOX-alone treated and the Los + Dox-treated SD rats.

The red blood cell counts dropped by 26.27% in the 7.5 mg/kg DOX-treated SD rats, 31.5% in the Los + Dox-treated SD rats, and 34.04% in the 15 mg/kg DOX-treated SD rats (Table 1). All of these groups showed a significantly ($p<0.05$*, $p<0.001$**, $p<0.001$**) lower RBC respectively compared to the control salin- treated SD rats, suggesting iron deficiency and anemia in dos- dependent response.

The normal saline-treated F344 rats showed a 22.2% significantly higher RBC than the normal saline-treated SD rats (Table 1). The decline in RBC in the F344 rats treated with the same 15 mg/kg DOX as the SD rats showed no significant differences relative to the normal saline-treated F344 rats, suggesting higher oxygen consumption, higher metabolic rate, and less cell death and tissue damage than the SD rats.

Physical inactivity and lack of food intake was observed in the 15 mg/kg DOX-treated SD rats; fatty liver was also evident in this strain, further substantiating metabolic disorder as demonstrated by the significant increase in blood lipid profile. Bone degeneration was also evident in the 15 mg/kg DOX-treated SD, suggesting a possible abnormality with production of RBC by bone marrow.

Higher levels of RBC and low levels of lipids in the blood, and higher levels of physical activity was most likely due to higher oxygen consumption in the DOX F344 strain than these treated SD rats. In these cases, hyperlipidemia and anemia in the SD rats treated with DOX alone or in combination with losartan may benefit from treatment with lipid-lowering agent and folic acid supplement.

3.1.3.3. Blood platelet levels and thrombogenesis

The most significant increase in blood platelet (PLAT) levels was 64.5% ($p<0.05$*) in the 7.5 mg/kg DOX-treated SD rats, followed by a 54.57% ($p<0.05$*) increase in the 15

mg/kg of DOX-treated SD rats, and 39.98% increase in the Los + Dox-treated SD rats compared to their control saline-treated SD rats (Table 1, Figure 2).

The 15 mg/kg DOX-treated rats showed a slight decline in PLAT counts which might have been due to their aggregation into thrombus. Thrombosis was a common occurrence in this group of SD rat. Atrial thrombi were observed to occupy 30% to 90% of the atrium cavity, evidenced by two-dimensional echocardiography and histology as shown in Figure 3.

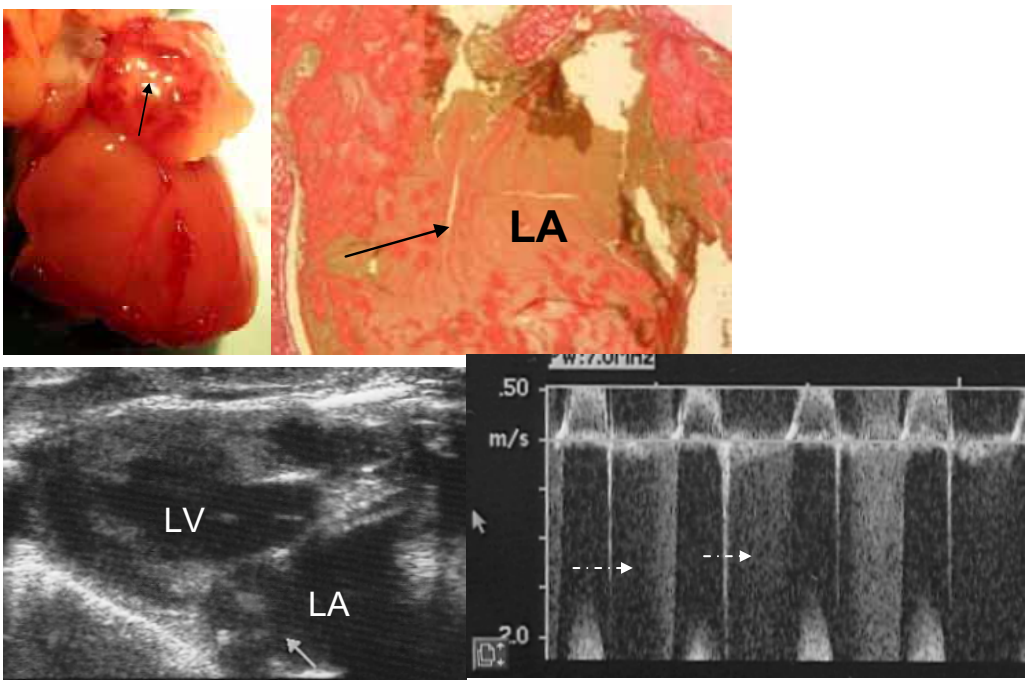

Figure 3 *Representing, a gross picture (A), histological (B) and 2-dimentional echocardiogram showing the left atria thrombi (Arrow head in A, B, C). The Doppler spectrum on (D) shows a moderate to severe valve regurgitation (3 dotted arrow head). These changes are frequently observed in rat treated with cumulative dose of 15mg/kg around week 10 in the Sprague-Dawley rats. Left atrium (LA), left ventricle (LV).*

Death among the 15 mg/kg DOX-treated SD strain of rats may have been attributable to thrombi rupture resulting from increase in blood pressure and leading to vascular

obstruction. The greater increase in PLATS in the 7.5 mg/kg DOX group, on the other hand, may be due to less PLAT aggregation. The increase and decline in PLAT counts in 7.5 mg/kg and 15 mg/kg of DOX-treated SD rats, respectively, may be a dose- and time-dependent response.

DOX+LOS-treated SD rats showed a significantly lower decline in PLAT count than the DOX-treated SD rats but not significantly different from the normal saline-treated SD rats. Thrombosis was smaller in size and less frequently detected compared to the 15 mg/kg of DOX group. Smaller size thrombi were observed by two-dimensional echocardiography and histology in the 7.5 mg/kg DOX group that related to lower dose of DOX used, treatment frequency, and the duration for their development.

A relationship may exist between low blood RBC, hyperlipidemia, and high blood platelet levels in the development of thrombosis commonly observed around week 10 in all the SD DOX-treated groups, particularly with the dose of 15mg/kg.

The F344 rats showed a slight increase in PLAT of 13.07% which was not significantly different than their normal saline-treated F344 rats, suggesting resistance to 15 mg/kg of DOX treatment. These strains of rats did not develop thrombosis at week 10 and survived longer with less reno-cardiovascular side effects.

Blood platelet level in saline treated SD, saline treated F344 were not significantly different from the F344 treated with 15mg/kg at week 10, and suggesting low response to Dox-induced increase blood platelet level, aggregation and thrombus formation may ended exist in the F344 strain. This study demonstrates that there is a considerable phenotypic difference in platelet aggregation which is reflected by thrombus formation in the SD strain and not in the F344 rat's strain 10 week after DOX treatment.

3.1.7 In vivo cardiovascular assessment--the Left ventricular hypertrophy and myocardial contractility

3.1.7.1. In vivo non-invasive M-mode echocardiographic-left ventricular hypertrophy and remodeling

The 7.5 mg/kg DOX-treated rats (Figure 4 B2) showed increases in RWT indicating left ventricular hypertrophy with a preserved systolic function.

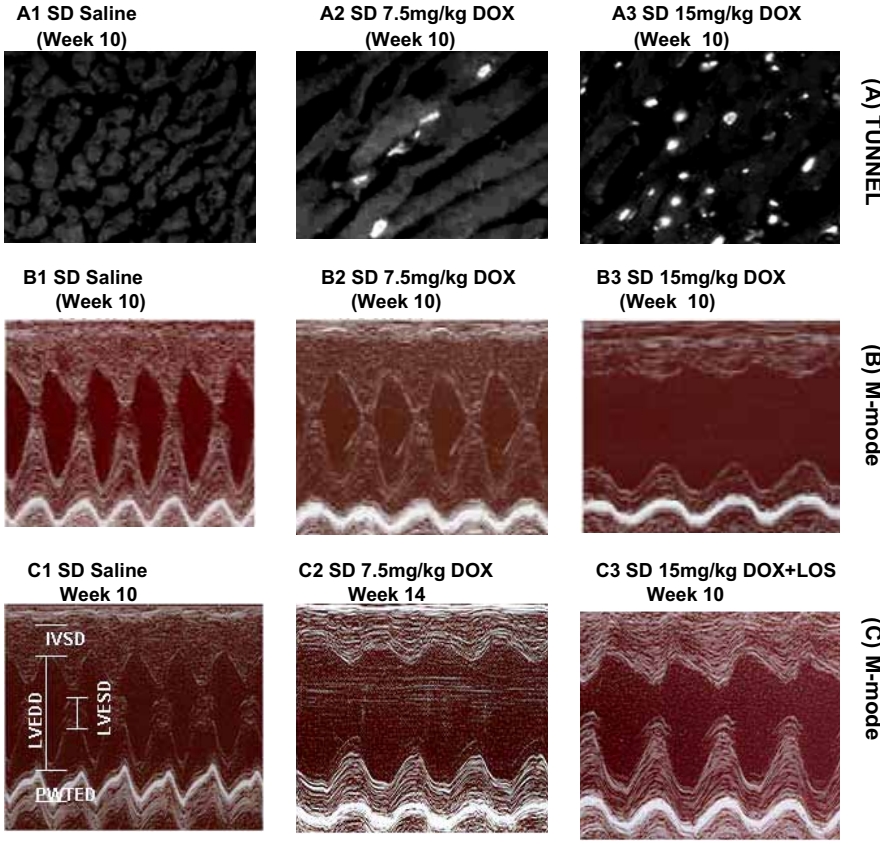

Figure 4*TUNEL Nuclei representation of saline, 7.5 mg/kg and 15mg/kg of cumulative dose of DOX 10 week after treatment (A1, A2, A3) with the corresponding M-mode echocardiogram of the left ventricle (B1,B2, B3). The third M-mode echocardiogram trace is of saline treated rat's left ventricle (C1), demonstrate the left ventricular diameter at end diastolic (LVDED) and at end systolic (LVESD), left ventricular inter-ventricular septum diameter at end diastolic (IVSD) and left ventricular posterior wall thickness at end diastolic (PWTED) phase. LV M-mode of 7.5mg/kg DOX in*

The increase in relative wall thickness was proportional to the increase in blood pressure (MAP), volume overloads from mild kidney damage, and increase in myocardial wall stress. Also observed in the TUNEL (Figure 4A2) and histopatho-logical images were hypertrophied myocytes in this group of rats (7.5mg/kg DOX-treated group) and a small amount of cell death (White nuclei) at week 10. This suggests these cardiomyocyte deaths may be the causal factor to the increase in myocyte hypertrophy and the increase in RWT (Table 1).

A small amount of cardiomyocyte deaths in this group resulted in the preservation of systolic function (Figure 4 B2). The rats treated with 15mg/kg of DOX showed left ventricular dilation and wall thinning, a decline in myocardial contractility featuring maladaptive hypertrophy and remodeling at week 10 (Figure 4B3). This could have been the result of further increases in the amount of cardiomyocyte deaths (Figure 4A3) and increases in blood pressure or MAP and volume overload (Table 1). This group of rat showed myocytes degeneration and disarray with an extensive amount of cell deaths (Figure 4A3) and fibrosis at week 10, contrary to the 7.5 mg/kg DOX-treated SD rats (Figure 4A2) The DOX+LOS-treated rats (Figure 4C3) showed a regression in RWT, decline in LVmass, and normalized FS and MAP (Table 1) which was beneficial.

3.1.7.2. Hemodynamic response to doxorubicin- LVmass vs. MAP and LVmass vs. apoptosis

Mean arterial pressure (MAP) is the average arterial pressure (Figure 5) in a single cardiac cycle and is considered the perfusion pressure by organs in the body [285]. MAP is a function of systolic and diastolic pressure or left ventricular contractility, heart rate, vascular resistance, and elasticity averaged over time [286, 287]. MAP in this present

study was used with other cardiovascular parameters to predict risk of mortality with DOX-induced cardiovascular toxicity.

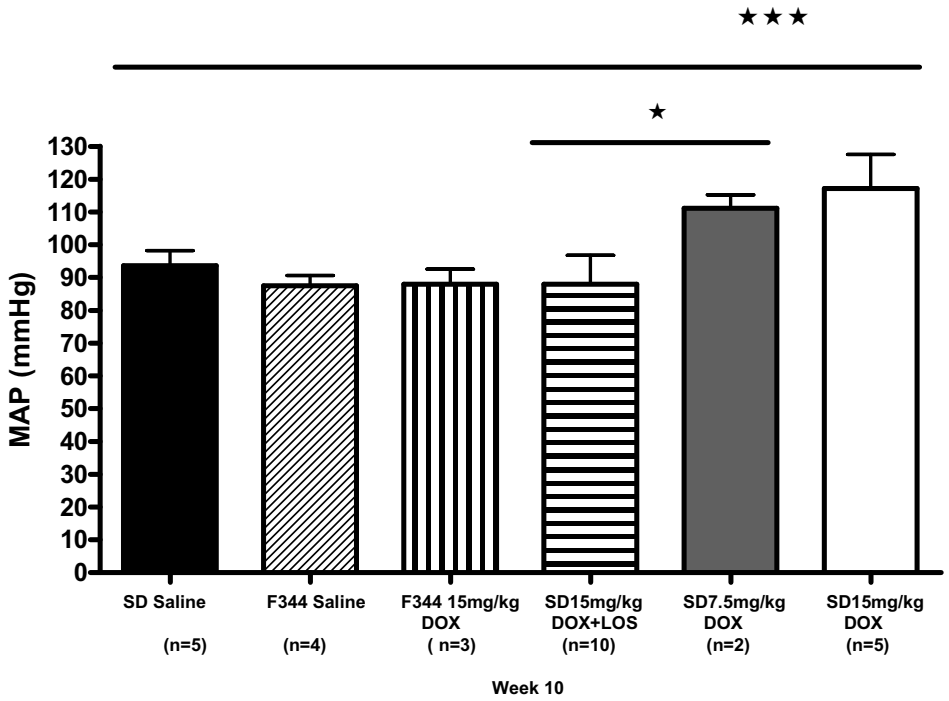

Figure 5 *Mean arterial pressure (MAP) of saline treated Sprague-Dawley (Saline SD) and Fisher (Saline F344) rats, 15mg/kg of doxorubicin treated F344 rats (F344 15mg/kg), combined 15mg/kg of doxorubicin with losartan supplement in the SD rats (SD15mg/kg+Los), 7.5 mg/kg of doxorubicin treated SD rats (SD 7.5mg/kg), and 15mg/kg doxorubicin treated rats (SD 15mg/kg). One-way analysis of variance*

The most significant ($p<0.001$**) increase in MAP affected the SD treated with 15mg/kg of DOX alone and was about 117.2±10.33 compared to 111.1±4.07 in the 7.5mg/kg DOX-treated SD, 88±8.7 in the F344 treated with 15 mg/kg of DOX alone, and 88±4.5 in DOX+LOS-treated rats (Figure 5).

There was a 6.52% difference in MAP between the saline-treated F344 rats with MAP of 87.5±3.1 and the saline-treated SD rats with MAP 93.6±4.6. Although the increase in the SD rats was not significantly different from the F344 rats, it could still have been the predisposing factor that lead to a significant increase in LVmass and marked decline in

systolic function with the cumulative dose of 15 mg/kg of DOX treatment. The significant increase in MAP suggests that 15 mg/kg of DOX may induce hypertension, a risk factor for heart failure in the SD rat strain (Table 1).Even though an 18.7% rise in MAP in the 7.5 mg/kg DOX-treated SD rats seemed higher than the saline and the DOX+LOS-treated rats, this was considered statistically insignificant. The main results here suggest that the SD rats were much more prone to development of hypertension in dose-dependent response than the F344 strain which showed not significant changes. The MAP in the DOX+LOS treatment group, on the other hand, was significantly ($p<0.001$**) lower than the saline-SD treated and 15mg/kg DOX alone treated SD. It was also slightly lower ($p<0.01$*) than the 7.5 mg/kg of DOX-alone treated SD rats. The lowering effect of losartan on blood pressure was associated with regression of left ventricular hypertrophy, demonstrated by a decline in the LVmass through change in LV size, RWT and improvement of left ventricular contractility.

Increase in MAP was also manifested by the increase in amount of pleural fluid retention, ascites, and renal insufficiency determined by the increase (but not statistically significant) in urea nitrogen (BUN) and creatinine levels (Table 1) in blood, enlargement and pale color of the kidneys among the 15 mg/kg DOX-treated SD rats.

The saline treated SD and the saline treated F344 rats were not significantly different from the F344 treated with 15mg/kg of DOX at same time point (Week 10) and suggesting resistance to DOX-induced hypertension. This study demonstrates that there is a considerable phenotypic difference in blood pressure regulation which is reflected by hypertension in the SD strain and not in the F344 rat's strain 10 week after DOX treatment.

LVmass in this present study shows a significant correlation with increase in MAP, marked decline in left ventricular wall contractility, and predicts risk of mortality in the 15 mg/kg DOX-treated SD rats (Figure 6).

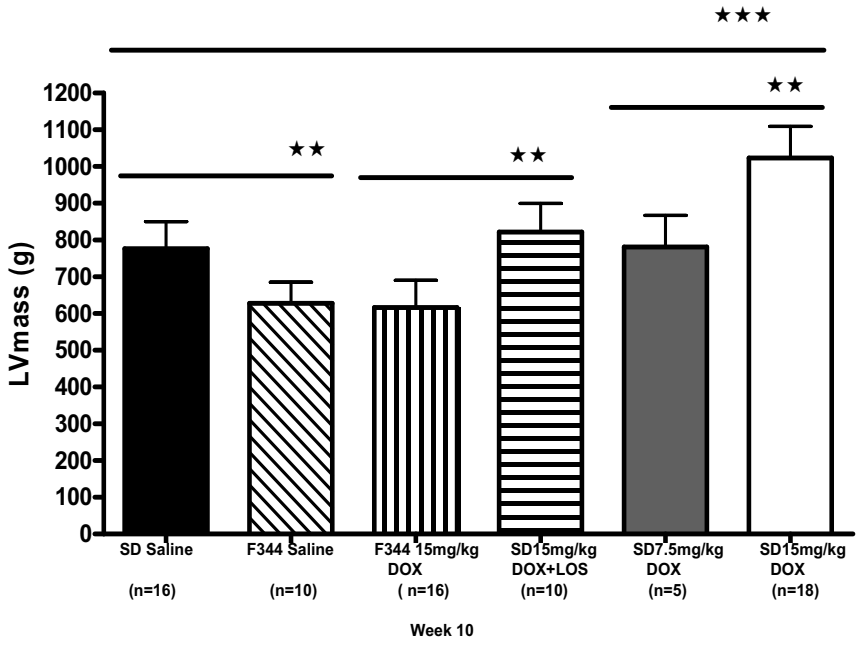

Figure 6 *Left ventricular mass (LVmass) used in the estimation of left ventricular hypertrophy as represented in of saline treated Sprague-Dawley (Saline SD) and Fisher (Saline F344) rats, 15mg/kg doxorubicin treated F344 rats (F344 15mg/kg), 7.5mg/kg treated SD rats (SD 7.5mg/kg), combined 15mg/kg doxorubicin and losartan (SD 15mg/kg+Los) treated SD rats, and 15mg/kg doxorubicin treated rats SD (SD 15mg/kg). One-way analysis of variance shows a p<0.0001***significant differences between groups.*

The increase in MAP in this group of rats (15 mg/kg DOX-treated SD rats) was associated with a significantly ($p<0.0001$***) higher LVmass (Table 1, Figure 6) of 1024±85.72 which is about 24% more than the control saline (776.6±73.67) and the 7.5mg/kg DOX (781.2±86) treated SD rats of the same strain, indicating enlarged heart. The difference in LVmass between the 15mg/kg and the 7.5mg/kg of DOX-treated rats was associated with changes in the left ventricular diameter (LVEDD and LVESD) and

wall thickness. The 15 mg/kg DOX-treated rats had ventricular chamber dilation, wall thinning and dysfunction resulting from significantly higher amounts of myocyte death than hypertrophied cardiomyocytes and volume overload due to hypertension. In the 7.5 mg/kg treatment, less cell death and more myocytes were continually growing, giving rise to an increase in RWT, a slight increase in LVmass which resulted in the preservation of the left ventricular chambers diameter and systolic function. The M-mode echocardiogram (Figure 4B2) of the 7.5mg/kg treated rats at week 10 showed a smaller LVESD, also indicating a better myocardial contractility than the 15mg/kg of DOX-treated rats. This was mainly due to larger amount of cardiomyocytes that have hypertrophied to compensate for the smaller amount of cardiomyocytes lost by oxidative stress. The 15 mg/kg DOX-treated SD rats instead showed an increase in LVESD, representing a marked decline in myocardial contractility at week 10 due to an increase in cardiomyocytes death that encompassed the number of hypertrophied cardiomyocytes.

The LOS+DOX-treated SD rats showed a significantly ($p<0.001$**) lower LVmass of 821.8±78.08 followed by a significantly lower MAP and improved myocardial contractility than with 15mg/kg of DOX alone (Table 1, Figure 4C3, 5, 6). This indicates that losartan has an effect on both the regression of LVH and blood pressure. The LVmass of 781.2±86 in the 7.5mg/kg of DOX-treated SD rats compared to their control saline-treated rats (776.6±73.67) showed no significant differences even though there was a slight increase in MAP of about 15.75%. Left ventricular hypertrophy in this group (7.5mg/kg DOX-treated SD rats) as previously mentioned was adaptive and was associated with a preserved myocardial contractility (Figure 4B2, 7, Table 1), a slight but not statistically significant increase in LVmass in response to the small amount of

cardiomyocytes death (Fig 4A2, 6) as compared to the 15mg/kg treated SD rats and a possible slight increase in volume overload resulting from mild to moderate kidney damage. The left ventricular diameter in this group was maintained, whereas the thickness of the myocardium was slightly increased (Table 1) giving rise to a more or less concentric hypertrophy than dilated hypertrophy in the 15 mg/kg DOX-treated SD-treated rats of the same strain.

LVmass in the 15 mg/kg DOX-treated F344 strain was not significantly different to its control saline-treated F344 rats of the same strain, showing 616.4±74.06 vs. 627.6±58.29, respectively, correlating with a normal MAP and suggesting compensated myocardial morphology and function.

The LVmass in the control saline-treated F344 rats (Figure 5) was also significantly ($p<0.001$**) lower than the control saline-treated SD rats of different strain with 19.19% difference, correlating to a significantly ($p<0.001$**) lower body weight, lower heart weigh and body weight ratio (Table1) and significantly lower kidney ($p<0.01$*) weight than the normal SD rat.

The heart weights, body weight, heart weight and body weight ratio, kidney weight and LVmass were all statistically different between the two control saline- treated groups of different strain (F344 and SD rats). The percent difference of 50.51% higher heart weight, 35.03% higher body weight, 25.1% higher kidney weight, and 19.19% higher LVmass in the control SD group as compared to control F344 rats suggest strain differences that could represent a risk factor for DOX-induced hypertension and LVH in the SD strain.

As previously indicated, the heart weight in the 15 mg/kg DOX-treated F344 rats was not significantly different from their control saline-treated F344 rats and was 0.49±0.03 vs. 0.46±0.05, respectively. Kidney weight on the other hand was not significantly altered in the F344 rats after treatment with 15 mg/kg of Dox and was 1.02±0.08 vs. 1.1±0.06 compared to their control saline-treated F344 rats (Table 1).

In the SD rats, DOX treatment induced an 18.78% and 15.03% increase in kidney weight (Table 1) with 7.5 mg/kg and 15 mg/kg dose in the treated SD rats, respectively. During necropsy, the kidneys in this group of rats were pale and appeared engorged with fluid, suggesting renal damage, whereas the DOX F344 rats appeared normal. This was further evidenced with histology, showing moderate to severe kidney damage in the 15 mg/kg of DOX-treated SD rats compared with mild to moderate in the 7.5 mg/kg of DOX-treated rats of the same strain (SD) as compared to the saline treated SD rats. The F344 rats treated with the same dose instead showed small to no significant kidney damage. Severe kidney damage was associated with a significant increase in MAP, a significant increase in LVmass, apoptosis and a marked decline in myocardial contractility contrary to the F344 strain of rats. In experimental animal model, the rennin-angiotensin – aldosterone system (RAAS) activation have been implicated as a deleterious component in both renal and cardiac disorders and could strain dependent [288].

A large amount of cell death of 30±6.7% correlated with a drop of 57.51% in relative wall thickness (RWT) and 24.16% increase in the LVmass in the 15 mg/kg treated SD rats compared to a drop of 15±1.2% in cell death and 1.37% drop in RWT (Table 1) and a 0.59% in LV mass in the 7.5 mg/kg DOX-treated SD rats of the same strain at week 10.

This was demonstrated by M-mode echocardiography, TUNEL and SPECT/CT, and Annexin V findings.

The excess of cell (Figure 4A3) death in the 15 mg/kg of DOX-treated SD rats caused a more significant ($p<0.001$**) drop in FS of 37.1±11.17 vs. 70.92±1.45, myocardial dilatation, and wall thinning compared to control saline of the same strain, the SD rats (Figure 4A1, 7). As discussed earlier, the decline in %FS may also have been the result of increased MAP (Figure 5, table 1) and volume overload from renal dysfunction and possible damage to the arterial wall.

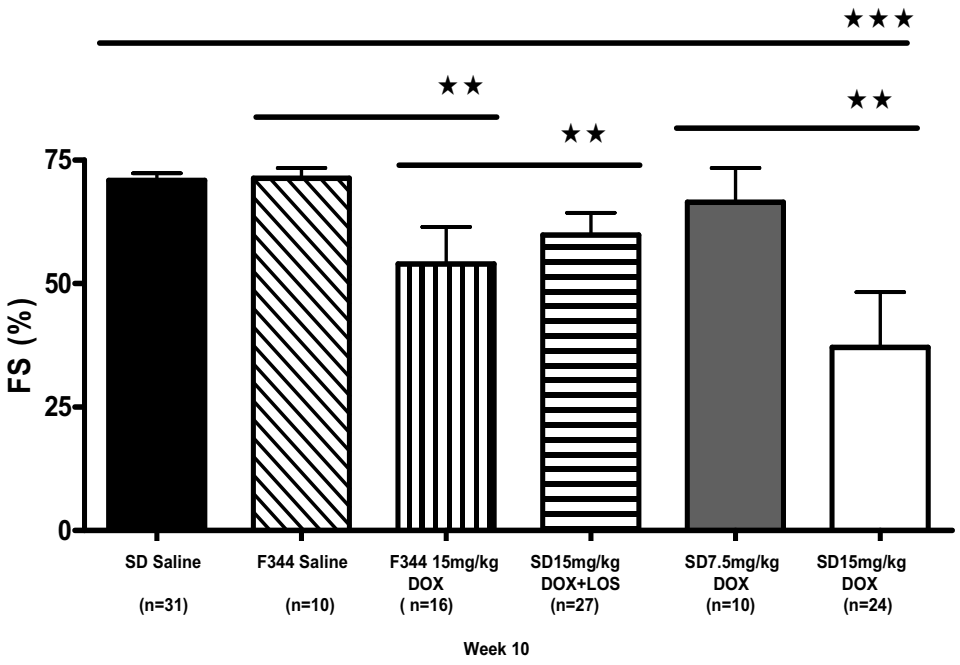

Figure 7*: Fractional shortening (FS), estimate myocardial contractility of left ventricle as represented in saline treated Sprague-Dawley (Saline SD) and Fisher (Saline F344) rats, 7.5mg/kg treated SD rats (SD 7.5mg/kg), combined 15mg/kg doxorubicin and losartan (SD Los+15mg/kg) treated SD rats, 15mg/kg doxorubicin treated F344 rats (F344 15mg/kg), and 15mg/kg doxorubicin treated rats SD (SD 15mg/kg DOX). One-way analysis of variance shows a P<0.0001** significant differences between group.*

The % in FS in the 7.5mg/kg DOX SD (Figure 7, Table 1) was not significantly different from LOS+DOX treated SD rats and the F344 rats treated with 15mg/kg of DOX at week 10 suggesting normalization of MAP, LVmass, wall thickness and apoptosis.

The small decline in RWT (Figure 8, Table 1) in the 7.5 mg/kg may have been due to the hypertrophy of the remaining surviving cardiomyocytes in response to the slight increase in workload or the MAP in adaptation to wall stressand in support of more cardiac output and tissue oxygen consumption.

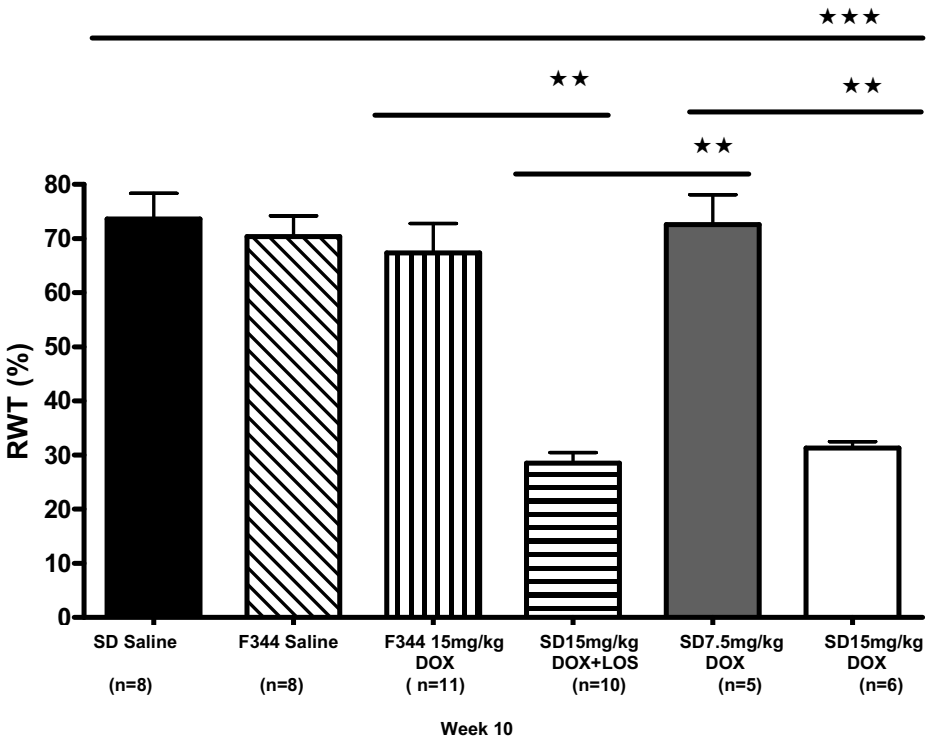

Figure 8 *Relative wall thickness (RWT), estimate the geometrical changes of left ventricle wall (PWTED) relative to its chamber diameter (LVEDD) at end diastolic phase, in response to increase in pressure and volume overload as represented in saline treated Sprague-Dawley (Saline SD) and Fisher (Saline F344) rats, 7.5mg/kg treated SD rats (SD 7.5mg/kg), 15mg/kg doxorubicin treated F344 rats (F344 15mg/kg), combined 15mg/kg doxorubicin and losartan (SD Los+15mg/kg) treated SD rats, and 15mg/kg doxorubicin treated rats SD (SD 15mg/kg). One-way analysis of variance shows $p<0.0001$*** significant differences between groups.*

The RWT of this group (7.5mg/kg- treated SD rats) was not significantly different from the control saline-treated SD rats, because the reactive hypertrophy and death of cardiomyocytes may have been balanced by the continuous growth of myocytes to replace those lost. The preservation of myocardial contractility (FS) suggests that the hypertrophy was compensatory.

Cell death may have occurred earlier during doxorubicin (DOX) intravenous infusion, causing oxidative injuries and subsequent cell death, reactivating growth of the remaining cardiomyocytes. The two separate rats (n=2) treated with 7.5 mg/kg of DOX, developed left ventricular hypertrophy and a marked decline in myocardial contractility indicated by a FS lower than 30% around week 14. This suggests that adaptive hypertrophy was short-lived. The transition to maladaptive hypertrophy may have been the result of further increases in cardiomyocyte death surpassing the amount observed during the adaptive hypertrophy of the 7.5 mg/kg DOX-treated SD rats that were euthanized at week 10. This hypertrophic effect that occurred in week 10 in the 7.5mg/kg treated rats was adaptive and was associated with a preserved myocardial contractility with a fractional shortening of 66.49±6.89 which was not significantly different than the 70.92±1.45 in the control saline-treated SD group (Figure 7). The systolic function (FS) in the two other SD rats treated with same amount of DOX declined significantly 14 weeks after treatment suggesting that prolonged hypertrophy with lower dose of DOX will always lead to decompensation and to heart failure as the end stage stream.

FS in the DOX-treated F344 group of rats was 53.97±7.5, significantly ($p<0.001^{**}$) lower compared to 71.32±2.09 in the control saline-treated of the same strain (F344) of rats. This fractional shortening was observed to plateau between week 10 and about week

18, suggesting adaptation (data between 10 and 18 is not presented), whereas in the SD rats, systolic function of 37.1 ±11.17% was a result of much faster decline and worsening by week 10 (Figure 7).

Considering the significance ($p<0.001$**) of a 47.69% drop in FS between the 15 mg/kg of DOX-treated SD rats and the control saline-treated rats of the same strain, a much lower decrease of 15.62% between the DOX-treated and the control saline-treated F344 rats indicated that the SD DOX-treated rats were the most affected strain. In fact, the SD rats were more at risk of death with a FS≤40% than the F344 rats (Figure 1, 7).

Differences in body and organ weight, LVmass, blood BUN and RBC, and possibly oxygen consumption and metabolism, make the SD rats prone to DOX-induced hypertension, heart and kidney failure at a much earlier stage than the F344 rats in a time-dependent response.

The amount of cell death was not analyzed in the F344 rats treated with 15 mg/kg of DOX because the MAP, RWT and the LVmass of DOX vs. control saline F344 rats of the same strain were not significantly different, suggesting that there was less DOX-induced oxidative injuries and that the F344 rats may have been more resistant to 15 mg/kg of DOX at this same time point (week 10). On the other hand, the amount of cell death would be less significant than the 15 mg/kg of DOX-treated SD of different strain since myocardial contractility in this strain of rats was not as significant as the SD-treated rats.

Losartan therapy in combination with the 15 mg/kg of DOX (DOX+LOS), in this context, was associated with a 23.88% decline in heart weight, correlating to 5.5% in the regression of LVmass and the 61.29% drop in RWT compared to saline SD-treated of the

same strain rats (SD). The FS in this group (DOX+LOS) of rats was 59.84±4.5 compared to 70.92±1.45 in saline-treated SD rats, indicating a 15.62% and 38.12% increase in myocardial contractility compared to the saline and 15mg/kg DOX-treated SD rats, respectively. This could also mean that losartan may also be associated with less significant cell death than with the 15 mg/kg DOX-alone treated SD rats, since the LVmass, MAP, and FS seemed to be maintained when combined with 15 mg/kg of doxorubicin.

3.1.7.3. Diastolic function-Left ventricular hypertrophy and remodeling

The preservation of systolic function in the 7.5 mg/kg of DOX-treated SD rats at week 10 was observed to be associated with diastolic dysfunction demonstrated by prolonged isovolumetric relaxation time (IVRT) using tissue Doppler imaging (TDI). This correlated with an increase in fibrosis and smaller amount of cell death (Figure 9). However, the diastolic dysfunction observed with the 7.5 mg/kg treated SD rats, was reported visually. An example of this process is shown in Figure 9 that was detected in the 15 mg/kg treated SD rats during the adaptive remodeling stage. This rat is in an adaptive stage of hypertrophy probably because concentration of DOX in this rat may be lower than the aimed 15 mg/kg. Cardiac adaptation in this rat (Figure 9B) was demonstrated by a concentric hypertrophy, diastolic dysfunction, and preserved systolic function.

Figure 9 B shows an example of adaptive hypertrophy with increased wall thickness (IVSD and PWTED) and constricted left ventricle chamber, indicated by the reduction of LVEDD and LVESD compared to saline (top A) and the 15 mg/kg of DOX-treated SD in the Figure (top C). The preserved systolic function (smaller LVESD) and diastolic

dysfunction during the adaptive remodeling (B, E) are shown by M-mode (top B) and TDI (bottom E).

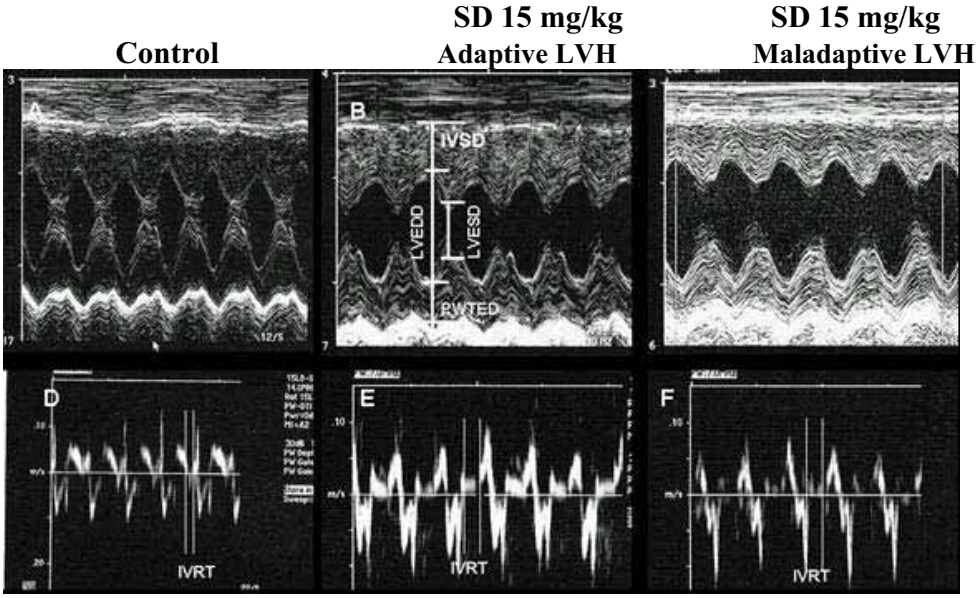

Figure 9 *M-mode A,B,C (top) and D,E,F (bottom) the corresponding tissue Doppler imaging (TDI) in conscious SD rats treated saline, 15 mg/kg of DOX at week 10(B, E and C, F). Saline-treated (A, D) show normal systolic (A) and diastolic function (D), 15mg/kg treated show concentric left ventricular hypertrophy with preserved systolic function (B) and diastolic dysfunction (E). Another 15 mg/kg treated SD rat shows dilated hypertrophy, with both systolic (C) and diastolic dysfunctions (F). Isovolumetric relaxation time (IVRT). n=3 DOX and n=2 saline. ANOVA one way analysis of variance P<0.001***

The TDI in the rats with adaptive hypertrophy showed a delayed IVRT (Figure 9E), indicating diastolic dysfunction with preserved FS of 57.14% (Figure 9B) that is higher than FS of 30.99% in the rat with maladaptive hypertrophy (top B). A preserved systolic function and diastolic dysfunction are characteristics of adaptive left hypertrophy and remodeling which could have been caused by a slightly higher amount of cardio-myocyte deaths than observed with the 7.5 mg/kg of DOX treatment in Figure 3A. The systolic

function in the rat (top B) with adaptive hypertrophy was significantly lower than the 7.5 mg/kg treated rats in the Figure 4B2 at week 10. FS ranging from 55-70% was considered within normal range in all the rats studied. The adaptive hypertrophy in Figure 9 B should correlate to more significant myocardial fibrosis accumulation and myocyte death than the 7.5 mg/kg DOX-treated rats because of the significantly higher wall thickness.

The M-mode of the SD rat treated with 15 mg/kg of DOX (Figure 9C) showed dilated left ventricular hypertrophy, with marked decline in myocardial contractility. The corresponding bottom tissue Doppler image (F) showed a prolonged IVRT, indicating diastolic dysfunction, while the systolic function (FS) by M-mode and the ejection time by TDI were also markedly reduced compared to control and DOX-treated in Figure 9,B,E. In fact, both systolic and diastolic function estimated by the Tei index and IVRT using the tissue Doppler echocardiography was 1.77±0.72 (Tei index) and 57±17.69 msec (IVRT) in the 15 mg/kg treated SD rats (n=3) (Figure 9F) than 0.75±0.07 (Tei index) and 26±1.41msec (IVRT) in the saline-treated rats (n=2) (Figure 9D). These results correlated to the significant decline in systolic function (FS) of 44.93±13.16% in the 15 mg/kg DOX-treated rats (Figure 9C) compared to 68.68±2.84% in the saline-treated rats (Figure 9A).

Both diastolic and systolic dysfunction are features of maladaptive hypertrophic remodeling which could be induced by a large amount of cardiomyocyte cell death, as observed in Figure 4A3.

The findings of this study suggest that diastolic function precedes systolic dysfunction. Evaluation of systolic function alone, therefore, could lead to irreversible damage to the myocardium as a long-term response to DOX toxicity. Diastolic function could be used

as an early diagnostic measure in the prevention of systolic dysfunction and may help in development of new therapeutic interventions. Prolonged IVRT with preserved systolic function was visually observed in the 7.5 mg/kg treated SD rats in the dose response study and correlated with a small amount of cardiomyocyte death and adaptive hypertrophy (Figure TDI). Diastolic dysfunction also correlates with mild to moderate kidney damage observed in the 7.5 mg/kg. This suggests that diastolic dysfunction could also be an early predictor of renal dysfunction and hypertension.

3.1.7.4. Gender differences and doxorubicin cardiac toxicity

A cumulative dose of either 2 to 3 mg/kg was associated with a mortality rate of 60% among male rats 20 to 50 weeks after treatment. FS in response to a cumulative dose of 2 mg/kg DOX in males was 51± 9, significantly ($p<0.001$**) lower than 69± 2 in 2 mg/kg DOX-treated female SD, 70%± 2 and 68.5±0.6 in control saline males and females, respectively at the age of 16 weeks (4 months). Mortality in the DOX-treated SD males correlated with a 30-40% decline in FS and the histological finding of DOX-induced cardiomyopathy (Figure 10).

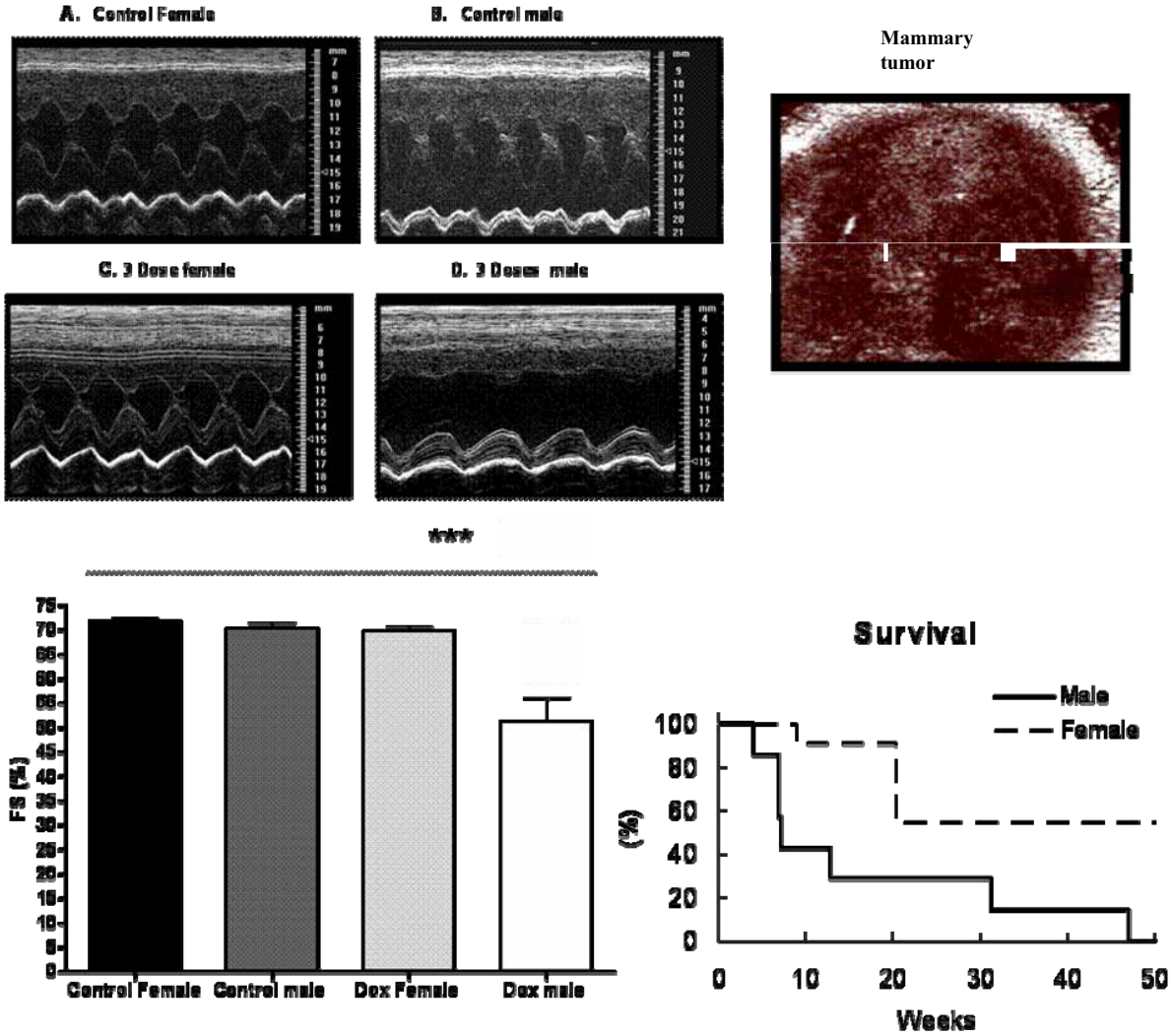

Figure 10 *M-mode echocardiogram of control females (A) and control males (B). M-mode echocardiogram in females treated with 3 dose (1mg/kg/week for 3weeks) shows normal myocardial contractility as demonstrated also by the fractional shortening in F (Dox female). The males M-mode echocardiogram shows left ventricular chamber dilatation and wall thinning with a significant (p<0.0001***) decline in the myocardial contractility as shown by the fractional shortening (FS) in Figure 1. DOX-induced cardiac toxicity resulted in about 60% of males 5-50 weeks after treatment (G). Females developed mammary tumors and lived more than 50 weeks longer than males. One-way analysis of variance showed a P<0.0001*** Dox female vs. Dox male.*

Males treated with 3 mg/kg of DOX died earlier than the 2 mg/kg treated males with FS≤40 (Figure 10), demonstrating a dose-response effect. The rapid decline in systolic function (FS %) in the males treated with 3 mg/kg DOX was unexpected. Females lived up to 10 months with systolic function ranging between 55 and 65%, slightly lower than normal control saline-treated rats of the same gender, and with a slight left ventricular hypertrophy, suggesting a partial cardio-protection against DOX toxicity. However, the majority of the females treated with either dose developed mammary tumors of which 85% were fibroadenomas and 15% were adenocarcinomas type. The female control did not developed tumor growth of any type at 12 month time-point but did later at 20 months as part of the aging process.

3.1.7.5. Autonomic regulation and cardiac toxicity

Heart rate in the saline (control) treated F344 rat was 4.06%, slightly higher (531.9±16.41) but not significantly different from the saline (control) treated SD strain of rat (510.3±1.45).

The F344 rats treated with 15 mg/kg of DOX showed a 9.82% decline in HR (479.7±27.2) compared to its control, saline-treated F344 rats (531.9±16.41), but was not as significant as the decline observed with the DOX+LOS and 15 mg/kg DOX treated SD rats.

Heart rate was 14.72% and 12.35% significantly (*p<0.001***) lower in the DOX+LOS and 15 mg/kg DOX - treated SD rats respectively, than the saline-treated SD rats (Table 1).

Heart rate was 5.90% slightly lower in 7.5mg/kg DOX treated SD rats (480±14.14) but not significantly different from the saline (control) treated SD rats.

There was no significant difference in heart rate between the DOX+LOS and the 7.5mg/kg DOX treated rats.

Changes in the heart rate appear to be secondary to the effect produced by losartan dose of 0.6g/liter which was administered in a drinking water after titration to reach comparable hemodynamic effects in vivo, including 15 to 20% decline in heart rate [273]. Whereas, changes in heart rate with DOX seem to be dose dependent responses. There was no phenotypic difference in heart rate between the SD and the F344 rats. Heart rate (HR) was consistent during the course of this study and showed less variability in both normal saline-treated F344 rats and normal saline-treated SD rats (Table 1). This suggested that these rats were studied during normal resting heart rate and that the rats were well adapted to the echocardiography procedure while in a conscious state.

3.1.7.6. In vivo non-invasive SPECT/CT and Tc-99m-HYNIC-Annexin V versus TUNEL staining and apoptosis analysis.

TUNEL staining of the 7.5 mg/kg DOX-treated rats showed a slightly significant ($p<0.001$**) increase in cardiomyocyte apoptosis (arrow head) of about 15±1.2 compared to a significantly ($p<0.0001$**) higher 30±6.7 increase in the 15 mg/kg DOX-treated rats and normal 5.7±0.3 in saline-treated rats (Figure 4A2).

The TUNEL (Figure 4A2) shows myofibers hypertrophy in the 7.5 mg/kg DOX-treated which are consistent with a significant left ventricular hypertrophy and preserved systolic function in response to a smaller amount of cell deaths observed in the M-mode (Figure 4B2) and RWT (Figure 8, Table 1). These results suggest there is balance between cardiomyocyte hypertrophy and cell death. In the 15 mg/kg DOX-treated SD rats, myofibers appear hypertrophied with extensive myocyte degeneration and disarray

consistent with the significant increase in cardiomyocytes death (Figure 4A3). The decline in RWT, the increase in the LVmass, and the decline in myocardial contractility suggest unbalanced cardiomyocyte hypertrophy and cell death. The transition to maladaptive hypertrophy may have been a result of more cell deaths than cardiomyocyte hypertrophy.

Sample pinhole SPECT or single photon emission computed tomography showed a significantly higher uptake of Tc-99m-hydrazionicotinamido (HYNIC)-Annexin (Tc-99m-HYNIC-Annexin V) in the rats treated with 15 mg/kg of DOX compared to saline-treated rats (Figure 11).

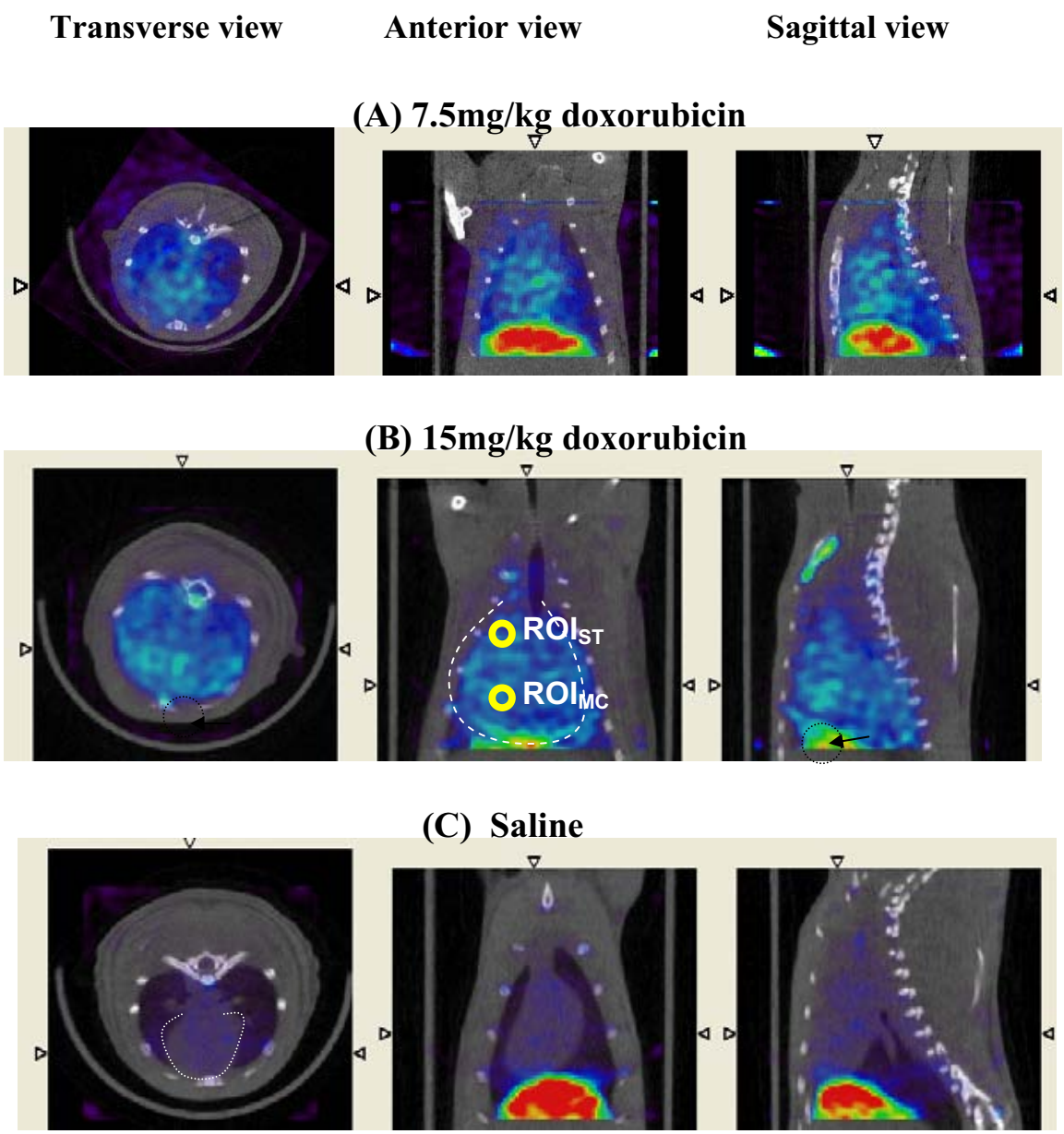

Figure 11 *Fused SPECT/CT images delineated the 3D distribution of Annexin V uptake in the heart. DOX shows a dose-response dependent Annexin V uptake in the heart (bright light blue patches as shown in the cycles and arrow heads (A, B)). 15 mg/kg DOX-treated rats (B) showed significantly highest uptake than (A) 7.5 mg/kg DOX-treated rats compared to (C) saline-treated rats. The heart is defined with dotted lines in transverse, anterior, and sagittal axis view. All images were displayed with the same color bar. Results were validated by the CUR calculated with chosen ROIs shown in (B).*

Both 7.5 mg/kg and 15 mg/kg of DOX exposure displayed a pathological uptake of Tc-^{99m}-HYNIC-Annexin V in all anatomic regions of the heart in a dose-dependent response as shown with bright white colors (Figure 11A, 11B). The heart of the 15 mg/kg DOX-treated rats, also appear larger than the normal control saline-treated rat when visualized in the SPECT/CT (Figure 11A, 11B). This enlargement coincides with the increase in LVmass (Figure 5) and the chamber dilation shown in the M-mode trace compared to saline-treated rats (Figure 4B3). The increase in LVmass, ventricular dilation, and decline in myocardial contractility correlated to the TUNEL (Figure 4A3) staining images showing myocytes hypertrophy, death, degeneration, and disarray characteristic of maladaptive hypertrophy and remodeling.

The semi-quantitative index of cardiac uptake ratio (CUR) for three groups of animals is shown in Figure 12.

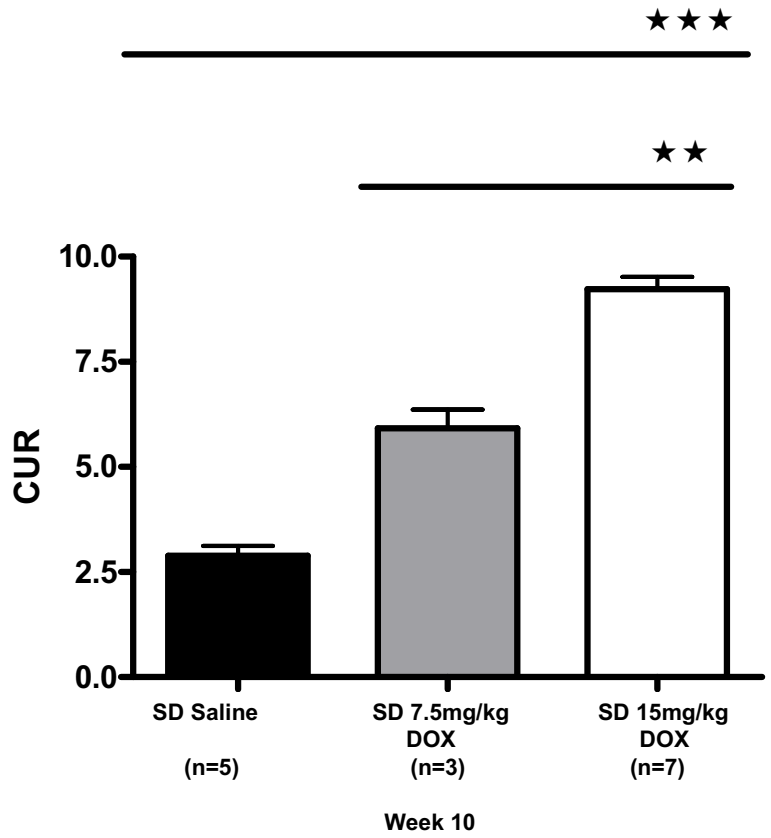

Figure 12 *Semi-quantitative index of cardiac uptake ratio (CUR) for 3 groups of animals. Results measured from in vivo SPECT imaging agreed with the spectral visualization showing the 15mg/kg doxorubicin treated rats had highest Annexin V uptake and the saline group showed the least uptake. Data expressed in mean±SD and $P < 0.01$; *, $P < 0.001$** was considered statistically significant.*

The results measured from in vivo SPECT imaging agreed with the spectral visualization, showing that the 15 mg/kg DOX-treated rats had highest Annexin V uptake and the saline group showed the least uptake.

The percent of injected dose of radio-labeled annexin V tracer per gram of tissue (%ID/g) was calculated from the left and right ventricle tissues and normalized with the %ID/g of radio-labeled annexin V tracer in the blood (Figure 13). The 15 mg/kg

showed a 60% uptake that was significantly ($p<0.001$) higher than the 7.5 mg/kg DOX and saline-treated rats (Figure 13).

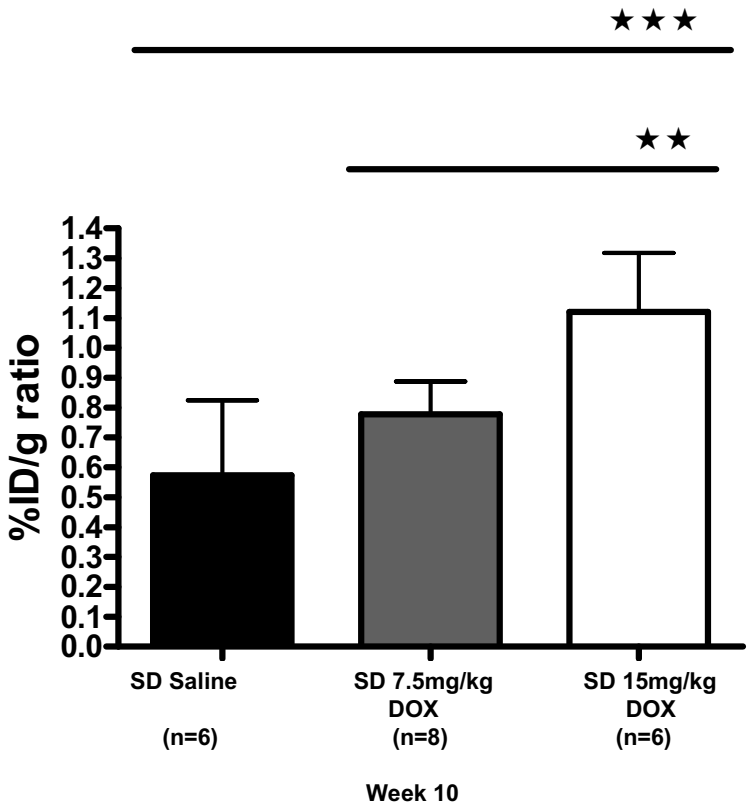

Figure 13 *In vitro biodistribution of radio-labeled Annexin V tracer localized in saline, 7.5mg/kg and 15mg/kg doxorubicin treated heart. This graph shows that doxorubicin-induced cardiac cell death was demonstrated by heart harvesting and blood collection after the bio-distribution study.*

3.1.8. Western blotting

ErbB2, NRG-1, Akt, mTOR, GSK3-β, heat shock 70 and 90, and TGFβ-1 (Figure 14-18) are expressed in graded response to 7.5 mg/kg and 15 mg/kg of DOX treatment in the SD rats, paralleling the increase in myocardial hypotrophy and cardiomyocytes death.

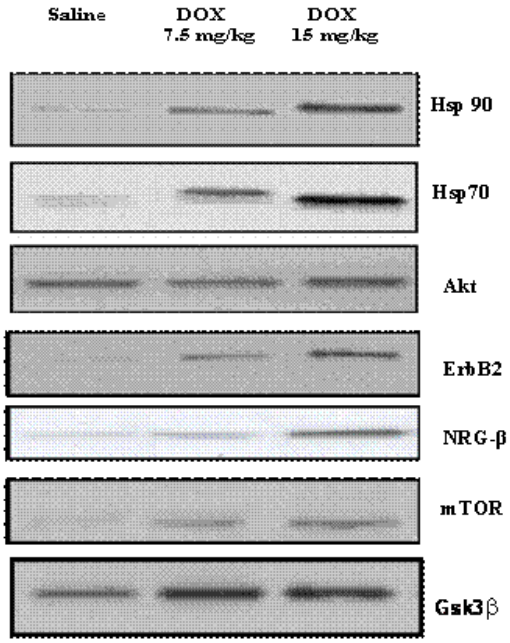

Figure 14 *Myocardial heat shock (Hsp) 90, Hsp 70, Akt, ErbB2, NRG-β, mTOR and Gsk3β expression in dose and time dependent response in Sprague-Dawley treated with 7.5mg/kg and 15mg/kg of doxorubicin (DOX 7.5mg/kg and DOX 15mg/kg) as compared to their control saline treated Sprague-Dawley rats at week 10 (n = 10 per group).*

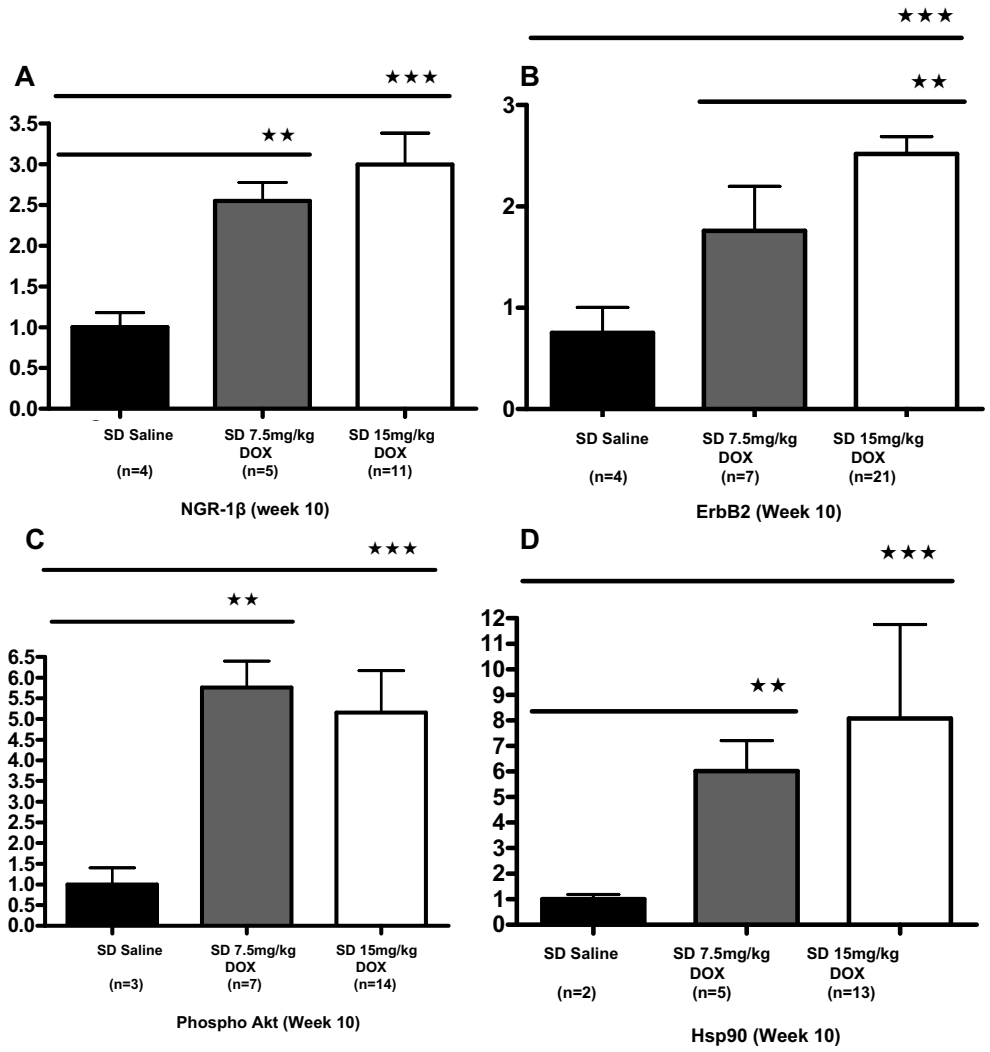

Figure 15 *Graphical representation of relative myocardial protein NRG-β (A), ErbB2(B), Akt (C), and (D) heat shock protein (Hsp 90) expression in graded response to 7.5mg/kg and 15mg/kg of doxorubicin (DOX) as compared to saline. Data expressed in mean±SD. P < 0.05*; P < 0.01**; P < 0.001***.*

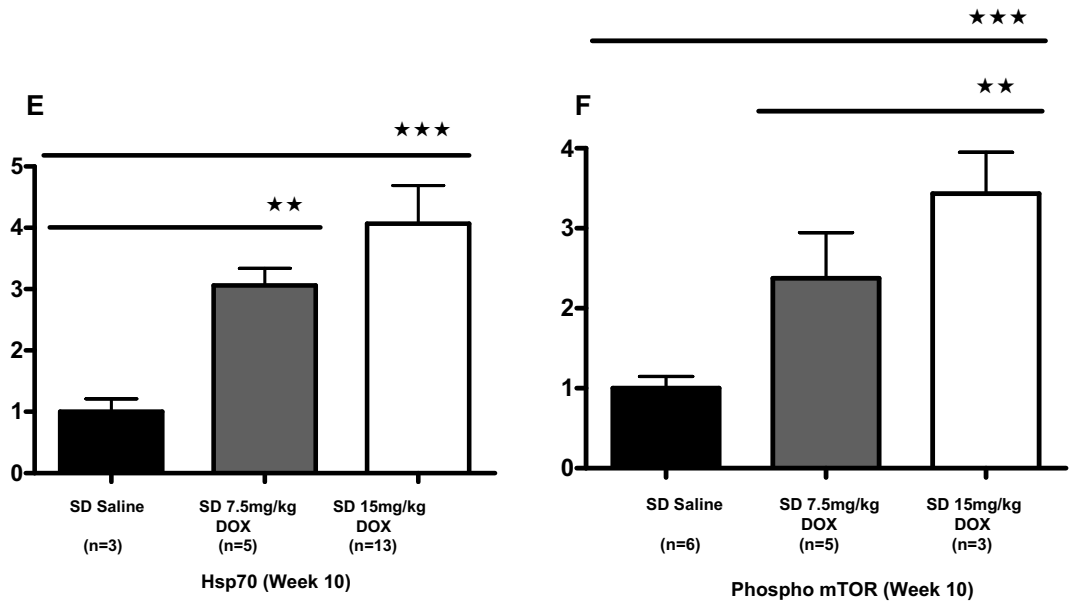

Figure 16 *Graphical representation of relative myocardial protein heat shock (Hsp) 70 (E), Hsp 70, ErbB2,and mTOR (F) expression in graded response to 7.5mg/kg and 15mg/kg of doxorubicin (DOX) as compared to saline. Data expressed in mean±SD. P < 0.05*; P<0.01**; P < 0.001***.*

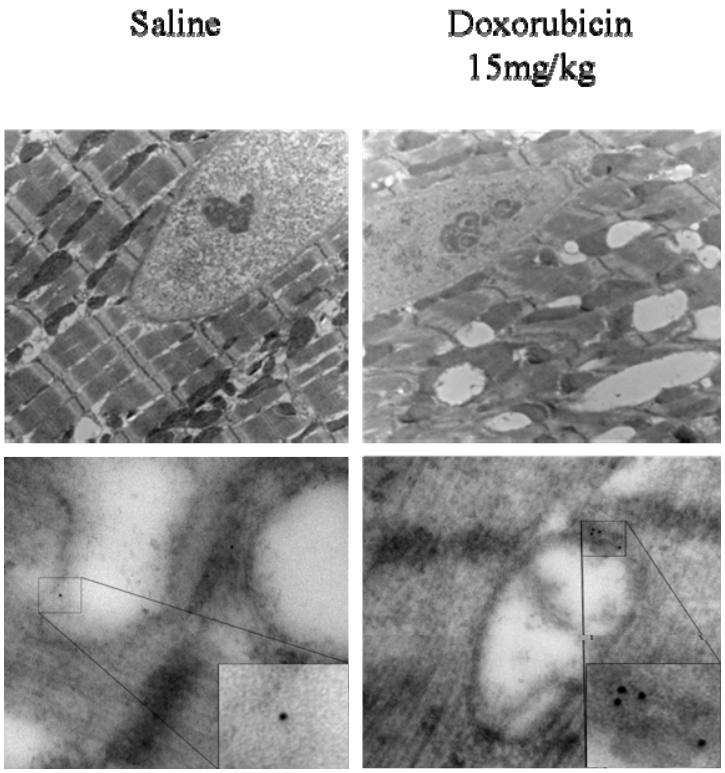

Figure 17 *Electron micrograph of hearts from a saline-treated rat (A and C) compared with a 15 mg/kg doxorubicin-treated rat (B and D). The vacuolization, rough sarcoplasmic reticulum and t-tubules dilation, abnormal Z-bands, and myofibrillar disarray are noted in the DOX-treated rats are dilated (B) compared to saline-treated rats (A). These changes are characteristics of cardiomyopathy. Magnification, X10.000 Bottom, immunoelectron micrographs of hearts from a saline-treated rat (C) and DOX-treated rat (D). Magnification, X200.000. Increased immunogold labeling of ErbB2 is observed with DOX treatment versus saline with subcellular localization of ErbB2 (arrow) to cardiomyocyte t-tubules adjacent to Z band (Figure C and D).*

A mild expression of these proteins was associated with a small amount of cardiomyocyte death in the 7.5 mg/kg DOX treatment, paralleling the mild increase in left ventricular hypertrophy (RWT), slight increase in MAP, and mild to moderate kidney damage. The left ventricular systolic function was preserved in this group of rats as a result of a compensatory mechanism of myocyte hypertrophy to replace the lost myocytes and in support of more cardiac output and oxygen consumption. Molecular signaling of hypertrophy and cardiomyocyte survival may have been mediated by ErbB2, NRG-1, Akt, mTOR, GSK3-β, heat shock 70 and 90 since they were expressed proportionally to cardiomyocyte hypertrophy and death in dose-dependent response, leading to the preservation of systolic function when they were mildly expressed and dysfunction when they were highly expressed. A persistent expression of these protein at significantly (*P<0.001**) higher rate with 15 mg/kg of DOX compared to 7.5 mg/kg of DOX and saline-treated SD rats paralleled the significant increase in LVmass, the significant increased amount of cardiomyocyte death, the significant increase in MAP, and marked decline in myocardial contractility. A parallel increase in pro-apototic pathways may have been induced as well since myocardial dysfunction was observed to be an inevitable process as demonstrated by the 7.5 mg/kg of DOX-treated rats that decompensated at week 14. These proteins are known to induce growth and cardio-protection and their down-regulation and/or deficiency with chemotherapeutic treatment has been suggested to lead to heart failure [234]. Myocardial contractility or the FS in this present study may have not been low enough for the down-regulation of these proteins. The continual expression of these proteins that may have lead to a persistent increase in pro-apototic pathways may be partly responsible for the dose-dependent increase in

RWT, LVmass, and the decline in myocardial contractility. Excess signaling of ErbB2, NRG-1, Akt, mTOR, GSK3-β, heat shock 70 and 90 and TGFβ-1(Figure 18), thus could be the contributing factor to the transition of adaptive to maladaptive hypertrophy and remodeling. Myocyte growth and survival by these proteins may have been dominated by the pro-apoptotic signaling pathways such as JNK and p38 MAPKs leading to heart failure.

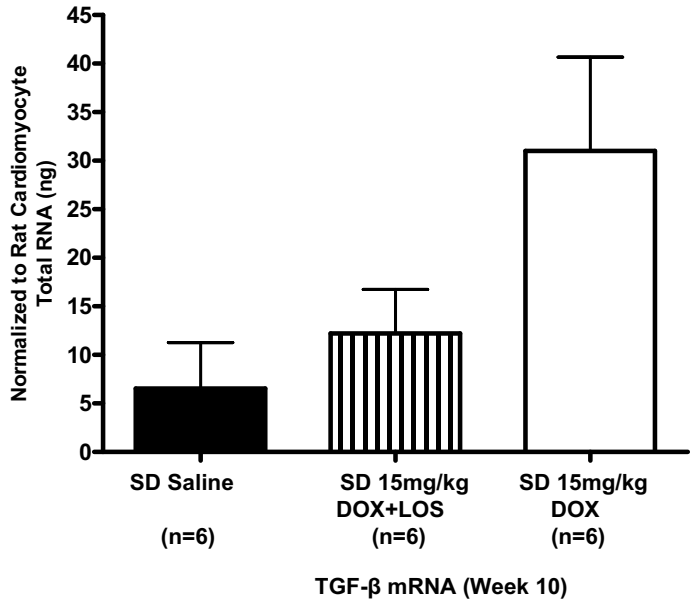

Figure 18 *Shows TGF-β mRNA expression in myocytes fraction of rats treated with 15mg/kg of doxorubicin, 15mg/kg of doxorubicin and losartan (DOX+LOS) combination and saline treatment in Sprague-Dawley rats only, 10 weeks after treatment (n=3), p>0.05 not statistical significance.*

Losartan supplement during 15 mg/kg DOX treatment in the SD rats resulted in the decline of TGFβ-1 signaling (Figure 17) paralleling the regression of myocardial hypertrophy, the improvement of myocardial contractility, and prevention of

hypertension. This suggests further that excess TGF-β-1 signaling (Figure 18) observed in the 15 mg/kg DOX alone treated SD rats may be pro-apoptotic and harmful to the heart since they were associated with significant increase in cardiomyocyte death and a marked decline in myocardial contractility. These findings suggest for the first time in vivo DOX – induces cardiac hypertrophy remodeling via the stimulation of AT1. This was demonstrated by the fact that hypertrophy was reversed by losartan which is an AT1 antagonist. The decreased hypertrophy may be secondary to decrease TGF-1 or equally, may be secondary to decreased AT1. The associated TGFβ-1 activation suggests AT1 as its activator and its influence to the growth and death of cardiomyocytes. AT1 may also have been responsible in the activation of other growth pathways such as ErbB2, NRG-1, Akt, mTOR, GSK3-β and probably apoptotic pathways such as p38 and JNK kinase. The inhibition of AT1 by losartan may have reduced the expression of ErbB2, NRG-1, Akt, mTOR, GSK3-β and lead to regression of hypertrophy and remodeling.

The decline inTGF-β-1 signaling using oral angiotensin type 1 receptor antagonist losartan may be used as a therapeutic agent for reversing or regressing left ventricular hypertrophy and remodeling that can be induced with chronic DOX treatment.

Nuclear pSMAD2 which are proteins effectors downstream to TGF-β signaling pathways are markedly increased in both the myocardium and the kidneys (representative positive brownish cell denoted by arrowhead) of the SD treated with 15 mg/kg of DOX compared to saline-treated and the F344 rats treated with the same dose of DOX at same point of time (Week 10) (Figure 19).

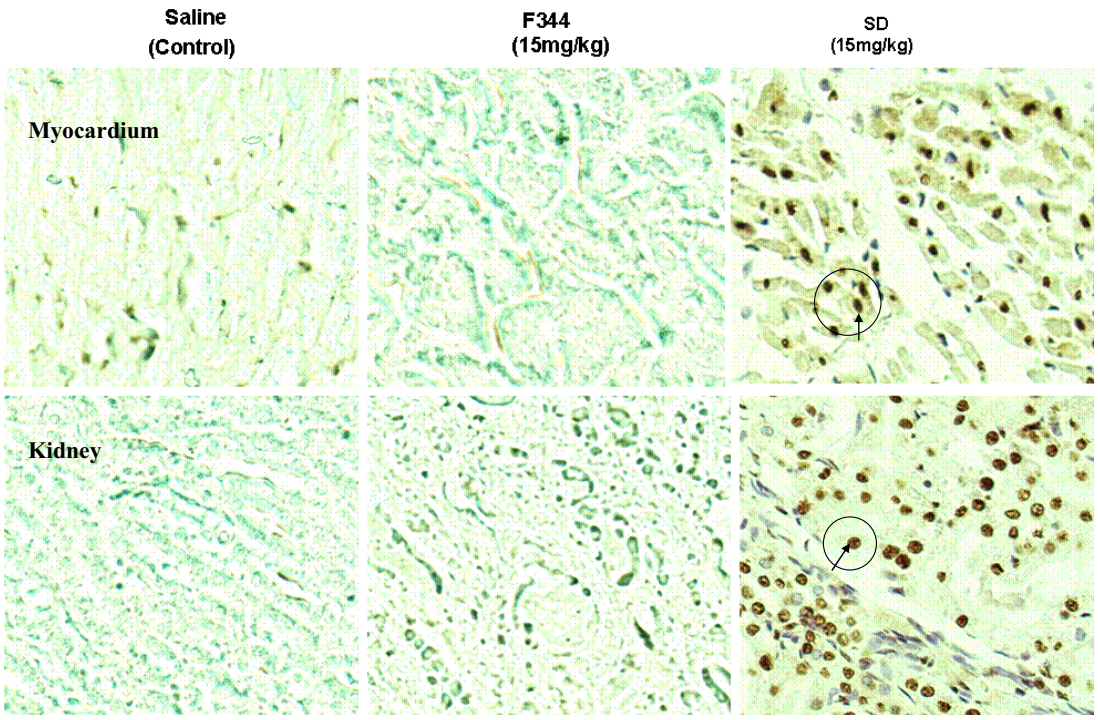

Figure 19 *Myocardial and kidney tissue showing nuclear pSMAD2 immunostaining of control saline, Fisher (F344) and Sprague-Dawley rats treated with 15mg/kg of doxorubicin at week 10. Positive nuclear pSMAD2 staining (brown cell shown by arrowhead in cycle) is significantly higher in the SD strain of rats treated with 15mg/k of doxorubicin as compared to control saline and F344 strain of rats treated with the same dose at the same point of time (Week 10). Scale bar X20μm.*

Increased nuclear pSMAD2 accumulation in the myocardium paralleled the significant increase in TGF-β expression shown by westerns and qPCR in isolated cardiomyocyte studies of the SD strain of rats treated with 15mg/kg of DOX compared to saline and 7.5mg/kg treated SD rats. Their excessive expression in the heart was associated with increased fibrosis (Figure 20C3), cardiomyocytes deaths, ventricular wall thinning, chamber dilation and systolic, and diastolic dysfunction.

The marked increase in pSMAD in the 15 mg/kg DOX-treated SD rats was also associated with a prominent interstitial fibrosis accumulation, extensive tubular dilation, and glomerunephropathy (Figure 20A3) compared to intact glomerular and tubular morphology in the saline-treated rats (Figure 20A1), indicating moderate to severe kidney damage. In the heart, the artery wall of the 15 mg/kg treated SD rats are thinner, with increased cross sectional area (Figure 20 B3) compared to the control (Figure 20 B1) and the 7.5 mg/kg treatment group (Figure 20 B2), indicating vasculopathy. The 7.5 mg/kg treated SD rats showed a mild interstitial fibrosis accumulation, mild tubular dilatation (Figure 20A2), and mild vascular wall thickening (Figure 20 B2) compared to the saline and the 15mg/kg DOX-treated SD rats, suggesting a mildly damaged kidney.

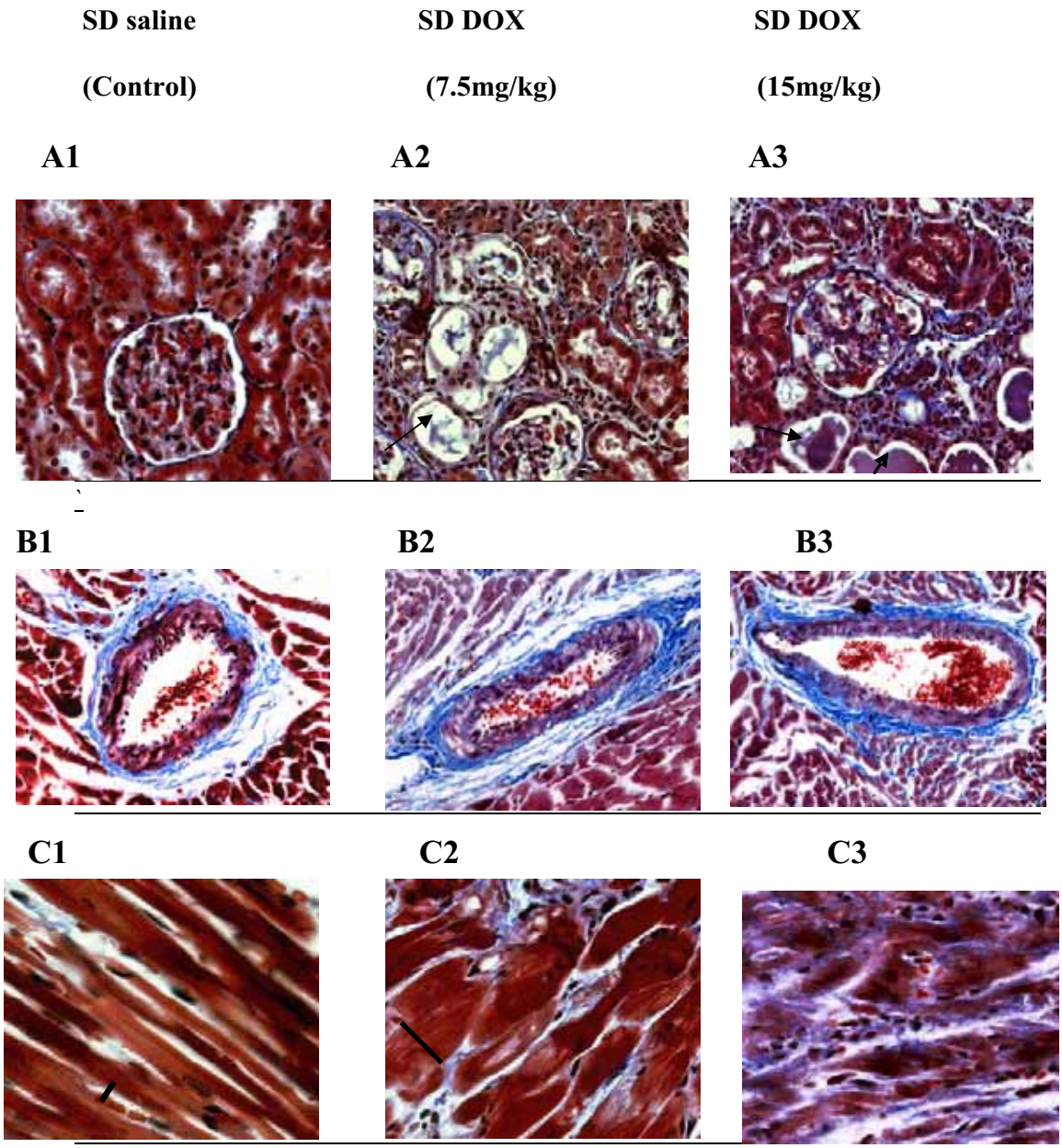

Figure 20 *Representative of photomicrograph of kidney (A), coronaries (B), and myocardium (C) histopathological sections showing, differences in trichrome staining for fibrosis in the 7.5mg/kg (2) and 15mg/kg (3) DOX treated Sprague- Dawley rats as compared to saline (Control)(1) at week 10. Note interstitial fibrosis accumulation (blue stain), tubular dilatation, glomerularnephritis (A2, A3), vasculopathy* (B2, B3), *myofiber hypertrophy (Dark Bar) (C2) and myofiber degeneration and disarray (C3) as compared to corresponding saline treated rats (A1, B1, C1). Photomicrograph reduced at X40 (A), X20 (B), and X40(C). n=10 of each group. Scale: small, mild, moderate, severe.*

The F344 rats treated with 15mg/kg of DOX showed no obvious nuclear pSMAD2 staining accumulation in the myocardium or the kidneys compared to the control. The saline-treated image with pSMAD2 staining of heart and kidney (Figure 19) is of F344 rat strain. The saline-treated SD rats were not stained and may be positive for pSMAD2 staining since they were the most susceptible to DOX toxicity. The DOX-treated F344 rats may be irresponsive to the amount of oxidative stress generated by the 15 mg/kg dose. The F344 rats may have higher level of antioxidant defense mechanism compared to the SD strain treated with the same dose, resulting in less significant amounts of pSMAD2 staining. This finding correlated with the histological findings of small to non-significant damage of the kidney in the F344 rats and moderate to severe in the kidneys of the SD rats (Figure 20B3) treated with the same dose of 15 mg/kg of DOX at the same point of time (week10). Cardiac hypertrophy and remodeling in the F344 rats were not as extensive as in the SD rats. Increasing the sample size of both saline and DOX-treated F344 and SD in the pSMAD2 study would help confirm the expression of pSMAD2 protein in response to DOX treatment and give better understanding of mechanism involved in strain differences, resistance, and susceptibility to DOX-induced renal and cardiovascular toxicity.

These findings show that TGF-β and pSMAD expression may be partly responsible for the stimulation of cardiomyocytes apoptosis and fibrosis and reactivation of hypertrophy. And when they are expressed in excess, the transition from adaptive hypertrophy to maladaptive hypertrophy is accelerated. The losartan supplement

findings suggest that AT1 mediates the activation of TGF-β and pSMAD expression in both the heart and the kidney of the SD rats after DOX treatment.

Nuclear pSMAD staining in the DOX+LOS-treated SD group was not performed and would lead to less fibrosis and less cell death accumulation, since hypertrophy, myocardial contractility, blood pressure, and kidney function were all normalized in the DOX-treated SD group.

The present study suggests phenotypic differences in RAAS response to doxorubicine treatment may exist and merit further investigation in both the F344 and the SD rats. The kidney and the heart share an important function in the regulation of blood pressure. In the normal physiological conditions, the increase in blood pressure lead to an increase in urinary output and decrease in blood volume and mean circulatory pressure [293]. This in turn, reduces the cardiac output **(Heart rate X stroke volume)** and the total peripheral resistance, and thereby normalizes the arterial pressure [293].

The rennin-angiotensin-aldosterone system (RAAS) as previously mentioned has been applicated as a major factor in both heart and kidney disease. Mechanism of RAAS in the kidney and cardiac injury are illustrated in the following figures (Figure 21A, 21B). In cardiac injury such as in myocardial infarction, RAAS activation helps maintain hemodynamic loading condition as cardiac output decline [289-292]. However overactivation of systemic and angiotensine were found to induce fibrosis, necrosis and hypertrophy of cardiomyocytes with fibroblast growth hormone factors, of which exacerbate remodeling [289-292]. In this present study, DOX-generated oxidative stress may have resulted in the activation of RAAS, activation of the

sympathetic nervous system, leading to endothelial injury, inflammation and impaired reactive oxygen, nitric oxide balance in the most susceptible rats (SD) [303], creating a vicious cycle stimulating cell death and remodeling in a biofeedback loop between the heart and the kidney. This process may have lead to a progressive decline in cardiovascular and renal function and may have resulted in both renal and heat failure as the end stage outcome.

A

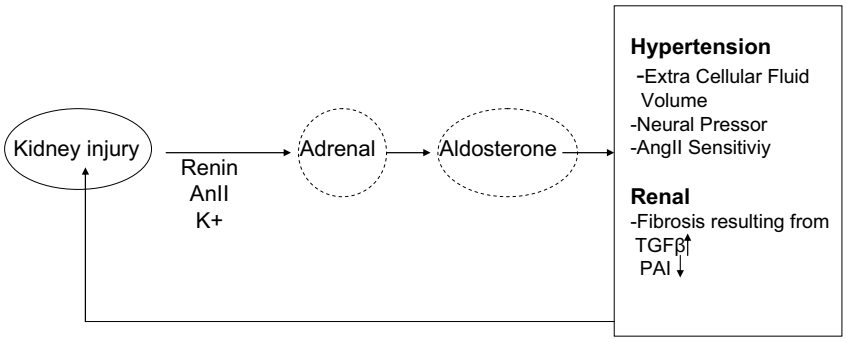

B

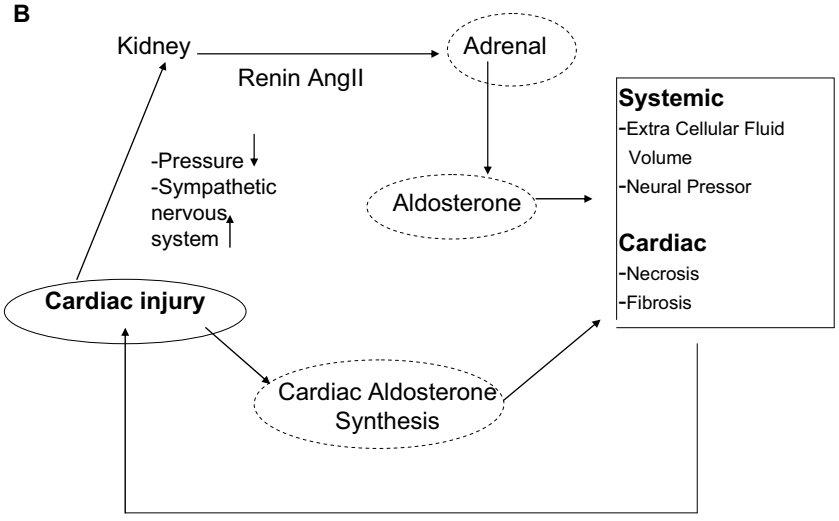

Figure 21 *Illustration of renal (A) and cardiac injury and their link to Renin-angiotensin-aldosterone system. Plasminogen activator inhibitor (PAI), angiotensin II (AngII), potasium (K+). Modified from Hosetter TH et al J Am Soc Nephrol 2003; 14:2395-2401 [293]*

In theory by bloking AT1 receptor, the angiotensine would not have an effect on cardiac fibrosis, and remodeling since there would be no AT1 receptor to bind to.with losartan treatment. However, the stimulation of aldosterone receptor present on cardioc myocytes and fibroblast has been shown to induce cardiac fibrosis and remodeling [289]. The inhibitory effect of RAAS by losartan may have synergic effect on reno-cardiovascular protection since normalization of blood pressure, regression of cardiac thickening, and decline in TGF-β expression was associated with an improvement of a cardiac function and decline or delay of mortality in the SD rats treated with DOX-LOS. This means that inhibition of AT1 not only protect the heart but also the kidney. On the other hand, blocking aldosterone as well, may also increase the effect of losartan on left ventricle remodeling and function in animal model [289, 294]

CHAPTER 4

DISCUSSION

4.1. Dose Response

4.1.1. Adaptive and maladaptive left ventricular hypertrophy- ΔLVmass vs. MAP and Δ LVmass vs. apopotosis

The findings of the present study suggest that a small amount of cell death and a slight increase in MAP result in significant increase in relative wall thickness (RWT) and preserved systolic function (Figure 4A), giving the characteristics of concentric hypertrophy with 7.5 mg/kg DOX treatment. At the same point of time (week 10), the 15 mg/kg DOX treatment caused a significant amount of cardiomyocyte death and a significant increase in MAP, leading to left ventricular chamber dilatation, a decline in RWT, wall thinning, increase in LVmass, and marked decline in myocardial contractility (FS). These features are characteristic of dilated hypertrophy developing from further pressure and volume overload. The significant increase in RWT in low dose 7.5 mg/kg DOX may have been induced by the small amount cardiomyocyte death as a result of a low level of oxidative stress. This lead to a reactive hypertrophy of myocytes to replace the lost myocytes that died during the oxidative stress process. This increase in RWT resulted in the preservation of systolic function in support of more cardiac output and in adaptation to increase workload. The high-dose 15 mg/kg of DOX induced a large amount of cardiomyocyte death. This process resulted in the decline of RWT and a marked decline in myocardial contractility due to the greater amount of myocyte death compared to the low amount observed in the 7.5 mg/kg DOX treatment. The increase in MAP and volume overload may have resulted from

graded damage to the kidneys, leading to ventricular and vascular hypertrophy. Sustained pressure and volume overload in 15 mg/kg DOX treatment from severely damaged kidneys and marked decline in glomerular filtration rate may have contributed to chamber dilation, wall flattening and thinning, leading to a significant increase in LVmass and giving rise to dilated hypertrophy in time-dependent response. Contrary to this, the slight increase in MAP and slight increase in LVmass in the 7.5 mg/kg DOX treatment at week 10 resulted in concentric hypertrophy, which in time lead to dilated hypertrophy.

The adaptative hypertrophy process observed with the 7.5 mg/kg DOX treatment at week 10 was also counterbalanced by these negative effects on cardiac decompensation seen around week 14 in two other rats treated with dose of 7.5 mg/kg of DOX that were kept for follow up cardiac hypertrophy and remodeling studies. These alterations were also characteristic of maladaptive response demonstrated by left ventricular chamber dilatation, wall thinning, and marked decline in myocardial contractility (FS), similar to the 15 mg/kg DOX-treated SD rats at week 10 (Figure 4C2, 4B3). Similar effects of increased myocytes apoptosis, volume, and pressure overload may have resulted from low-dose 7.5 mg/kg DOX over the 14 weeks after treatment, suggesting that chronic DOX induces left ventricular hypertrophy and remodeling in a dose- and time-dependent manner that will always lead to left ventricular decompensation.

The observed decline in renal function and vasculopathy may have been the contributing factors for the development of sustained hypertension and conversion of

adaptive hypertrophy to maladaptive hypertrophy, thus presenting a reno-cardiovascular connection in the development of hypertension and heart failure in DOX graded-dose response.

4.1.2. Reno-cardiovascular connection

This study shows that DOX-induced reno-cardiovascular damage might be partly responsible for the development of hypertension, left ventricular and vascular hypertrophy, and remodeling in dose- and time-dependent responses. Graded vascular damage and dysfunction may have occurred in this study. DOX redox cycling with oxygen, as previously discussed, generates reactive oxygen which may cause extensive tissue damage particularly when the antioxidant defense mechanism is declined or deficient and the renal detoxification mechanism by the renal tubule is impaired. Damage to the endothelial wall would lead to its inability to buffer the increase in pressure pulsations that accompanies ventricular pumping capacity [295, 296]. This increases cardiac workload and results in cardiac hypertrophy. A prolonged cardiac hypertrophy, as observed in the two rats treated with 7.5mg/kg at week 14, would lead to maladaptive hypertrophy and heart failure.

The DOX-induced oxidative stress may have resulted from the stimulation of hypertrophic and apoptotic responses at cellular and molecular levels. This may have involves the activation and reactivation of genetic and non-genetic factors, signals pathways that lead to a vicious patho-physiological cycle of cardiac and endothelial cell hypertrophy and death. The resultant hypertrophic response manifested by the rise in vascular pulse pressure which increases cardiac load can also damage the

vascular wall system supplying all the body tissues. Further increases in blood volume and blood pressure can result in damage to renal micro-vascularization, as observed in this present study and demonstrated by renal sclerosis, tubular dilation and fibrosis manifested with adverse cardiovascular outcome.

These finding show the reno-cardiovascular connection in the development of hypertension in response to DOX toxicity. The arterial and renal element relationship, referred to as the "cardio-aorto-renal ménage au trios" by Mitchell [295], have been examined extensively by Safar ME [296] and Guyton AC [297-299]. In that model, kidney, vascular system and the heart were shown to share an important function in the autoregulation of blood volume and pressure.

In normal physiological conditions, the increase in blood pressure lead to the increases in urinary output and the decrease in blood volume and mean circulatory pressure [300]. This, in turn, reduces the cardiac output and total peripheral resistance, and thereby normalizes the arterial pressure [300].

DOX side effects on the cardiovascular system can arise from inability of the kidneys to autoregulate blood volume and glomerular filtration rate and maintain normal arterial pressure. The kidneys therefore could be another primary target of toxicity since the blood filtration and DOX detoxification occur in the renal proximal tubules (Klaassen 2001). Toxicity at tubular level appears, also as strain-dependent since no significant damage were observed in the kidneys of the F344 rats treated with the same 15 mg/kg of DOX at week 10 compared to the control saline-treated SD rats.

Previous studies showed that, morphologically, the primary target for analgesic acetaminophen toxicity in the mouse kidneys are the S1 and S2 segments of the proximal tubules, whereas in the rats' kidneys, the S3 is the target for toxicity [301, 302]. The mechanism by which DOX or any other toxicant initiates proximal tubular cell death and eventually nephrotoxicity and heart failure has not been clearly defined.

The findings of this study suggest that DOX-induced oxidative stress generated by DOX could be partly responsible for tubular or glomerular damage in time- and dose-dependent responses. The kidneys of the SD rats were shown to be the primary target compared to the F344 rats strain. Damage to the kidneys in the DOX-treated SD rats was associated with an increased in blood volume and pressure, leading to increased cardiac workload and reno-cardiovascular damage in a biofeedback loop mode. Blood pressure and LVmass in the F344 rats were not significantly altered by DOX and showed no significant damage to the kidneys.

The result of this study shows that mild kidney damage in the 7.5 mg/kg DOX treatment was associated with a slight increase in MAP and left ventricular mass with a preserved systolic function and possible diastolic dysfunction; whereas, moderate to severe kidney damage was associated with sustained increase in MAP, a significant increase in LVmass, ventricular dilation, and marked myocardial dysfunction.

This shows DOX-induced hypertension and left ventricular hypertrophy in rats with associated kidney abnormalities; the inability of the kidneys to detoxify DOX and to regulate blood volume may have followed. Defects with the renal vascular and

tubules and depressed DOX clearance by the kidneys may be responsible for the sustained hypertension and early transition to heart failure in the SD rats compared to the F344 strain. Renal tubular defects and depressed salt clearance by the kidneys have been suggested to contribute to renal dysfunction and hypertension in spontaneously hypertensive rats (SHR) [303, 304]. The present study shows a relationship between the vascular and ventricular hypertrophy during adaptive and maladaptive remodeling and their connection to renal dysfunction and hypertension with DOX exposure.

4.1.3. Kidney failure

The 15 mg/kg treatment caused moderate to severe damage to the kidneys, consisting of tubulointerstitial inflammation, tubular necrosis, tubular hyperplasia, vacuolization, fibrosis, glomeronephritis, interlobular arterial wall thickening, sclerosis, and mineralization (Figure 20A3). These changes were moderate in the 7.5 mg/kg treated SD rats, to insignificant in the F344 rats strain also treated with 15 mg/kg of DOX at the same time point after treatment (week 10) (Figure 20A2). This suggests that genetic variation may exist in the SD rats, particularly, affecting the reno-vascular wall and its sensitivity to DOX.

4.1.4. Blood BUN and creatinine levels

Renal damage observed by H&E histological findings correlated to blood analysis of BUN and creatinine. The elevation of blood BUN and creatinine level at week 10 is significantly higher in the 15 mg/kg DOX-treated SD rats than the 7.5mg/kg treated SD group of rats, suggesting a marked impairment in glomerular filtration rate (GFR)

and marked kidney dysfunction. A correlation between mild kidney damage and cardiac adaptation in the 7.5 mg/kg treated SD rats and severe kidney damage and cardiac decompensation in the 15mg/kg treated SD rats was observed. These effects demonstrate the harmful effect of DOX on the reno-cardiovascular system.

4.1.5. Ascites and fluid accumulation

Fluid accumulation in the peritoneal, pleural, or pericardial cavity was observed to be more consistent with significant reno-cardiovascular damage than the 7.5 mg/kg treatment and the F344 treated rat.

Ascites formation is not well understood and was reported to result from alterations in the splanchnic circulation and functional renal abnormalities that support sodium and water retention [305]. Nitric oxide imbalance, low levels of antioxidant defense mechanisms, arterial vasodilatation, and vascular wall damage and stiffening have also been considered as primary factors in ascites formation [305]. This process may have also been partly responsible for the development of ascites, portal hypertension, and reno-cardiovascular damage with high doses of DOX (15 mg/kg).

The kidneys or renal medulla are known to play a vital role in long-term regulation of arterial pressure, extracellular fluid volume, sodium, and water homeostasis [306, 307]. A small alteration in medullary blood flow can have a major negative effect on the re-absorption of sodium and water [308] by the alteration in renal perfusion pressure [306]. This fact is identified as the pressure natriuresis [306]. Chronically, this process would lead to the development of hypertension that gradually leads to further organ damage, organ failure, and death [309].

DOX can accumulate in the proximal tubules, especially when detoxification by the proximal tubules is impaired, initially during the acute stage of the treatment and when DOX is chronically administered.

DOX–generated oxidative stress may results in the activation of the renin-aldosterone system, activation of the sympathetic nervous system, leading to endothelial dysfunction, inflammation, and impaired reactive oxygen nitric oxide balance, as reported previously in other experimental studies [310], creating a vicious cycle stimulating cell death and remodeling, accelerating decline in cardiovascular and renal function.

This study suggests that DOX-induced myocardial remodeling and hypertrophy may be linked to disturbed vascular and renal function in this SD strain of rats than the F344 strain because of possible genetic defects. The harmful side effects of DOX on the reno-cardiovascular connection are demonstrated by the mechanism of blood pressure autoregulation and homeostasis.

Chronic low doses of DOX treatment (7.5 mg/kg) lead to chronic decline in GFR and blood volume autoregulation with initial damage to the kidney. This would increase cardiac pressure and volume overload (as in hypertension), inducing myocardial and vascular wall thickening as a compensatory mechanism. Increased dose and frequency of DOX treatment, in time, can accelerate the decline in GFR. This would cause further increases in cardiac pressure and volume overload, leading to an earlier cardiac maladaptive remodeling and heart failure subsequent to severe renal damage in the SD strain than the F344 rats. The F344 rats did not show significant kidney

damage. Cardiac hypertrophy and remodeling in this group of rats seem to plateau up to 18 week.

In both of these circumstances, the increased blood pressure and volume with time leads to increase intraglomerular pressure, creating a cycle that will eventually induce irreversible functional and morphological damage in both the heart and kidneys in a negative biofeedback loop, leading to more advanced cardiac and renal damage [311, 312].

All together, this study shows that DOX toxicity affects the reno-cardiovascular system in most susceptible strains of rats (SD) and that this system should be considered for the prevention of DOX-induced damage to the heart, kidneys, and vascular system.

4.1.6. Vascular wall toxicity

DOX-induced oxidative stress may have occurred acutely during the course of its intravenous infusion (Injection). The vascular walls would be the first to be exposed to DOX since, by all means; the drug has to come into contact with the vascular wall before reaching its target, the heart, kidneys, and other organs. Thus, it is possible that chronic DOX-induced hypertension and left ventricular hypertrophy in this dose-response study may have resulted from lipid peroxidation of endothelial membranes and plasma protein, leading to vascular wall thickening, increased blood viscosity, endothelial and renal dysfunction in a time- and dose-dependent manner (Figure 20 B).

There was an increased wall thickness and smaller cross-sectional areas with the 7.5 mg/kg of DOX-treated rats at week 10, compared to a decline in vascular wall thickness and increased cross-sectional areas in the 15 mg/kg treatment and normal saline (control) treated rats. These observations were observed with 2D echocardiography (Data not available) during the course of the study and confirmed by histology. This orchestrates similar patterns of adaptive left ventricular hypertrophy in the 7.5 mg/kg treatment and decompensation with the 15 mg/kg treatments at week 10.

A graded increase in MAP and vascular wall changes suggest DOX-induced chronic thickening, remodeling, and lipid oxidation, destruction of endothelium-derived relaxing factors, inflammation, and endothelial damage as occurred with myocardial cells.

4.1.7. Hyperlipidemia

The 15 mg/kg DOX-treated rats exhibited a significantly higher level of lipids in the blood including cholesterol and triglycerides (Table 1). The combination of hypertension and hyperlipidemia was reported to induce vascular oxidative injury mediated by oxidant stress, inflammatory cell infiltration and matrix remodeling, and result in loss of tissue elasticity [313, 314]. This cycle was demonstrated to bring about chronic vascular wall dilatation and increase the pulse pressure required for the left ventricle to eject blood [315], thus adding more workload that lead to progressive increases LVmass and RWT (Laplacian law) that eventually lead to left ventricular decompensation in the DOX-treated SD rats 10 to 14 weeks after treatment.

The effect of doxorubicin-induced vascular wall thickening and/or stiffening in this study can be explain by previous studies using non-invasive methods of Pulse Wave Velocity (PWV), which is defined as arterial pulse's velocity of moving along vessel walls [316] (O'Rourke 1992). This method which was used in the assessment of arterial stiffening was shown to correlate with the degree of increased fibrosis concentration, arterial wall stiffening, and high systolic blood pressure as observed in this present study. This was shown to represent a major risk for cardiovascular morbidity and mortality in hypertension, diabetes, and end-stage renal failure [317].

Death among the 15 mg/kg DOX-treated rats (Figure 1) was associated with extensive renal damage (Figure 20A3) and marked myocardial (Figure 1, 4B3) and vascular fibrosis and dysfunction (Figure 20B3) which could have been the result of hypertension-induced earlier deaths in the 15 mg/kg treated compared to 7.5mg/kg treated SD rats.

The increase in wall thickness and stiffening were reported to induce a faster transmission of pressure as measured by the PWV along the arterial tress [317, 318]. This, in turn, was shown to increase systolic pressure and pulse pressure and contribute to the increase in cardiovascular complications in aged populations affected with hypertension [317, 319] (O'Rourke 1982, 1992, 1993).

In this context, chronic doxorubicin, which seems to be associated with myocardial and vascular wall thickening, fibrosis accumulation, may be the causal factor in the

development of hypertension. DOX treatment would thus be a risk in aged populations.

4.2. Blood profile

4.2.1. Blood Platelets, lipids, and thromboembolism

Thrombosis was often observed by echocardiography and confirmed by histology in the 15 mg/kg DOX-treated SD rats. The F344 rats treated with the same DOX regime did not develop thrombosis at the same point of time as the SD rats, suggesting genetic differences between the two strains of rats. Differences in polymorphisms and the predisposition to thrombosis formation has been reported but are still unclear [320]. The SD strain of rats may serve as a model for further understanding the mechanism of thrombogenesis and their susceptibility to this drug.

The decline in blood platelets in the 15 mg/kg DOX dose compared to high platelet levels with the 7.5 mg/kg DOX treatment may have aggregated into clots and thrombus due to higher level of oxidative stress.

The fact that cholesterol levels were significantly higher among the 7.5 mg/kg and 15 mg/kg treated rats suggests a significant increase in low density lipoproteins (LDL). LDL is oxidized in vascular endothelial cells and may have an association with endothelial thickening and dysfunction, and thrombus formation in a time- and in dose-dependent responses. LDL oxidation in the endothelial cells results in the inactivation of nitric oxide (NO) and further generation of free radicals [321]. This effect was suggested to increase platelet adhesion, stimulate plasminogen activator

inhibitor, cause inhibition of plasminogen activator, induce procoagulant tissue factor mRNA, inhibit mRNA transcription of thrombomodulin, and finally cause the stereochemical changes in heparan sulfate proteoglycan [322].

These changes were reported to impair antiplatelet and anticoagulant properties of the endothelium and to trigger thrombus formation [323]. A graded increase in LDL and oxidative stress in response to DOX may be the contributing factor to continuous damage to the endothelium, plasma protein and tissues, particularly when the detoxification of the DOX by the kidneys is impaired.

4.2.2. Anemia

The decline in RBC with the 15 mg/kg of DOX-treated rats was significantly higher than the 7.5 mg/kg treated SD and control group, suggesting anemia. This implies that DOX may have induced plasma protein hypoxia, death, leading to the decline of oxygen consumption and organ dysfunction in dose- and time-dependent responses. The kidneys are a major source of erythropoietin production [324] and severe kidney damage, as in the 15mg/kg DOX SD treated group, would lead to anemia. Erythropoietin is known to regulate production of erythrocytes or RBC by allowing erythroid progenitor cells to conclude their terminal differentiation [324]. It is possible that low levels of RBC may have resulted from erythroid progenitor cell deficiency and/or related genetic defects in the kidneys of the SD strain of rats. The control RBC level in this strain of rats was observed to be slightly lower than the control RBC level in the F344 strain. This would make the SD strain more susceptible to oxidative stress generated by DOX.

Anemia, in turn, could be the result of DOX-induced gastrointestinal infection leading to food malabsorption, iron and vitamin deficiency. This in turn may have lead to abnormal nutrient metabolism, deficiency in energy consumption and expenditure. Gastrointestinal mucosal injury was evidenced by the common occurrence of diarrhea observed especially with 15 mg/kg of DOX treatment. Bone degeneration was also evident during physical examination in the 15 mg/kg DOX-treated SD rat, suggesting also that anemia may have resulted from bone marrow deficiency in production of RBC.

4.2.3. Physical inactivity

Physical inactivity and lack of food intake was observed to be significantly poor in the 15 mg/kg SD rats compared to the DOX-treated F344 rats, supporting further the possibility of marked decline in oxygen consumption, deficiency in iron and other vitamins like folic acid [324].

The reno-cardiovascular connection and association with anemia syndrome are not clearly understood. The present study shows SD rats as the susceptible strain model for DOX-induced unfavorable reno-cardiovascular toxicity and anemia.

This study, also demonstrate that in humans, inter-individual susceptibility to DOX may exist. The SD strain of rats should serve as a model for understanding the mechanism of reno-cardiovascular toxicity at pathophysiological, molecular, and genetic levels. This in turn would help in the development of novel therapeutic strategies in prevention of toxicity.

4.3. Technical recommendations

4.3.1. Transthoracic tissue Doppler echocardiography

Transthoracic tissue Doppler imaging (TDI) is a novel validated method of quantifying global left ventricular function, including myocardial relaxation and contraction velocities. TDI is becoming a popular experimental method for studying cardiovascular disease in sedated rodents including rats and mice. The TDI as well as the M-mode results of this study are shown for the first time in conscious rats. This method is the gold standard (Figure 9) because it avoids the depressive effect of anesthesia on heart rate, systolic and diastolic function, and especially on the control of these parameters by the autonomic nervous system [325-327]. Previous studies using isoflurane, an anesthetic inhalation, were reported to depress cardiac output, stroke volume, and ejection fraction, resulting in both systolic [328] and diastolic dysfunction [329]. The success of this study is further evidenced by Baumwart et al. [330] showing that the Tei index was within normal range in normal conscious dogs, but increased with isoflurane anesthesia [331]. Delayed or increase in Tei index parameter, in this present study, were an indication of both systolic and diastolic dysfunction and decompensation in DOX-treated SD rats. A prolonged IVRT alone was also observed to be associated with diastolic dysfunction, while systolic was preserved during the adaptive stage of hypertrophy in the 7.5 mg/kg at week 10. The Tei index was demonstrated to increase with dilated cardiomyopathy, acute myocardial infarction, and congestive heart failure [331].

The changes in TDI were associated with moderate renal damage and a slight increase in MAP, reflecting their influence on abnormal myocardial relaxation and a preserved systolic function in the 7.5 mg/kg treated rats by week 10. Contrary to this, the 15 mg/kg dose of DOX showed a combination of diastolic and systolic dysfunction associated with severe renal damage and further increase in MAP (Hypertension) at week 10.

The method of tissue Doppler analysis and diastolic dysfunction have been reported as markers for the presence of myocardial fibrosis during the hypertrophic remodeling process [332]. The presences of apoptotic accumulation in the myocardium and its link to diastolic dysfunction have not been defined in conscious rats, particularly with chronic DOX treatment. Renal damage and its connection to left ventricular diastolic dysfunction and hypertrophic remodeling were also not clearly linked. The TDI findings demonstrate also for the first time that renal toxicity may precede cardiac toxicity and could be partly responsible for the transition of adaptive to maladaptive hypertrophy.

This study shows that the associated small amount of myocyte, increase in RWT, and mild to moderate renal damage with the 7.5 mg/kg treatment in the SD rats present a positive correlation with diastolic dysfunction and preserved systolic function. The large amount of cell death, decline in RWT, and moderate to severe renal damage, anemia, and hypertension with the 15 mg/kg treatment also present a positive correlation with both systolic and diastolic dysfunction. Diastolic dysfunction predicted mortality in the SD rats treated with 15 mg/kg of DOX. Two other rats treated with 7.5 mg/kg developed dilated cardiomyopathy by week 14, with systolic function below the expected threshold. A preserved systolic function and diastolic

dysfunction may predict the evolution of subsequent hypertrophic remodeling and heart failure phenotype. This method allows early therapeutic intervention and prevention of irreversible damage resulting from systolic dysfunction.

Hypertrophy of myocytes and fibrosis of the interstitium have been suggested to represent the two key pathological processes in the development of left ventricular hypertrophy (Figure 20), and systolic and diastolic dysfunction [332]. In this study, myocyte death may be the third key in the pathological processes of hypertrophy and remodeling, a causal factor for diastolic dysfunction, and an early predictor for mortality risk. Mortality, among the 15 mg/kg SD rats was commonly observed around week 10.

4.4. Cellular and Molecular mechanisms in response to doxorubicin treatment

4.4.1. Apoptosis detectation

The mechanisms of cardiac hypertrophy and apoptosis have been researched for several years, mainly using in vitro cardiomyocyte isolation from patients with end-stage dilated and ischemic cardiomyopathy, myocarditis, and aortic stenosis [333]. In vivo methods of detecting apoptosis in patients affected by these diseases have not been successfully developed because of lack of appropriate technologies.

In this study we determined the following: (1) myocytes apoptosis as the associative factor involved in the transition of adaptive hypertrophy to maladaptive using newly developed follow-up methods of echocardiography in conscious rats, and (2) the feasibility of newly developed non-invasive methods of SPECT/CT (Figure 11) with

Tc-99m-HYNIC-Annexin V imaging in identifying apoptosis. Both SPECT/CT with Tc-99m-HYNIC-Annexin V and conscious rat echocardiography follow-up in the development of left ventricular hypertrophy and dysfunction correlates to in vitro blood and cardiac analysis of apoptosis using the biodistribution method and ex vitro TUNEL method of analyzing apoptosis. These methods suggest that persistent increase in apoptosis is partly responsible for reactivation of hypertrophy and its progression to decompensation in DOX concentration and time-dependent response. The feasibility of SPECT/CT imaging with Tc-99m-HYNIC-Annexin V is a promising in vivo technique for monitoring and quantifying apoptosis and cardiotoxicity in rats at an early stage. Echocardiocardiography was used prior to SPECT/CT study to determine morphological and functional changes of the heart, and as a guide to determine the time point of cardiac adaption and heart failure. The SPECT/CT with Tc-99m-HYNIC-Annexin V imaging and conscious echocardiography follow-up methods may provide better understanding of hypertrophy and remodeling mechanisms and their correlation to cardiac apoptosis formation in rats and mice. These methods may also allow the development of new therapeutic drugs in the prevention of DOX-cardiac toxicity in experimental and clinical settings, without the use of invasive diagnostic methods.

4.4.2. Molecular signaling of hypertrophy and apoptosis

4.4.2.1. Doxorubicin-induced oxidative stress and apoptosis

The exact molecular mechanism in myocytes hypertrophy stimulation, ROS production, and induction of apoptosis is not understood. This has been attempted

experimentally mainly using in vitro isolated cardiomyocytes affected by hypoxia and ischemia reperfusion. ROS generation was not measured in this study, based on their widely known role in the induction of cardiomyopathy due to an increase in superoxide generation and decreasing antioxidant reserve [334] and based on their implication in many apoptotic signaling pathways, particularly with the hypoxia, ischemia reperfusion. This study has demonstrated that DOX-induced reactive oxygen species may be the causal factor to stimulation of apoptosis and reactive myocardial hypertrophy and remodeling in a dose- and time-dependent response. These findings were demonstrated for the first time in vivo, using conscious non-invasive echocardiography and the non-invasive method of SPECT/CT imaging with Tc-99m-HYNIC-Annexin V methods which correlated to in vitro and TUNEL staining methods of detecting apoptosis. Previous studies by Pimentel et al. reported that a low level of ROS generation in response to low cardiomyocyte stretch correlates with fetal gene expression and hypertrophy, while high amplitude stretch levels induce high ROS production and apoptosis [335, 336]. Cardiomyocytes stretch in this study may have resulted from a slight increase in MAP and small amount of cardiomyocytes death resulting from the initial low DOX-induced oxidative stress (7.5 mg/kg). Higher amounts of stretch may have resulted from a sustained hypertension and higher amount of cell death resulting from higher DOX concentration (15mg/kg). Further DOX availability was suggested to further participate in reduction/oxidation cycles and generation of more superoxide [121]. Renal impairment would result in the decline of DOX detoxification and excretion, and increase its concentration and circulation in the blood and tissues. The significantly higher amount of myocardial damage in the 15 mg/kg than any other

DOX-treated SD and F344 rats may also have resulted after the formation of the DOX-iron complex. Doxorubicin-iron complex has been suggested to reduce oxygen to hydrogen peroxide and cleave the peroxide to yield a hydroxyl peroxide (OH), an oxidant that contributes to more lipid peroxidation [126-128]. This was supported by the fact that iron-chelating agent dexrazoxane, ICRF-187, significantly reduced the development of DOX-induced cardiomyopathy in a dog model [337].

4.4.4. ErbB2 and other signaling pathways

DOX-induced myocardial hypertrophy may have resulted from increases in contractile force generated by the surviving myocytes as the pressure and cardiac workload increased. This process was reported to re-activating embryonic growth factors believed to be activated only during the embryonic stages of heart development and not in adulthood [201]. These embryonic growth factors increase protein synthesis and increase myofibril size and mass [201].

In this study, erbB2 receptor tyrosine kinase that belongs to the epidermal growth factors receptors (EGFR) family of tyrosine kinase: namely, the erbB1, erbB2, erbB3, and erbB4 [234, 338], also known as HER2, was of interest. ErbB2 inhibition with combination of anti-erbB2 (i.e., trastuzumab) and DOX was reported to accelerate the process of tumor killing in breast cancer over-expressing erbB2 compared to when DOX is used alone. This combination of DOX and anti-erbB2 was reported to also accelerate the process of cardiomyopathy more than when DOX is used alone.
As previously mentioned, erbB2 has to heterodimerize with erbB4 after erbB4 bind to neuregulin-1 (NRG-1), promoting hypertrophic changes including changes in cell

morphology, increases in protein synthesis, and expression of embryonic genes [233]. In this study, both ErbB2 and NRG-1 are up-regulated in dose- and time-dependent responses paralleling the increase in myocardial hypertrophy and apoptosis. In postnatal and adult hearts, erbB2/NRG-1 was shown to play an essential part in the myocardial adaptation to physiological stress, suggesting a primary role in cardiac growth and the survival mechanism [234]. In fact, the 7.5 mg/kg treatment induced a mild erbB2 expression that was associated with adaptive hypertrophy; a higher dose of DOX (15 mg/kg) was associated with regression of left ventricular hypertrophy, partly due to an increase in a significantly higher amount of cardiomyocyte apoptosis and a marked decline in myocardial contractility. Even mTOR, Akt, and heat shock 70 and 90, which are also known to be anti-apoptotic and promote growth, were expressed in graded response to low and high doses of doxorubicin. The adaptive hypertrophy in the two other 7.5 mg/kg treated SD rats decompensated 14 weeks, suggesting that even with lower doses, excess signaling of erbB2, mTOR, GSK-β and heat shock proteins may be persistently and inevitably expressed until heart failure results.

This indicates that persistent increase signaling of these proteins may also be associated with continuous increase in apoptosis. Excess apoptosis may be the contributing factor to the decline in myocardial contractility even when protections by these proteins are high. Previous study reported that erbB2 and erbB4 were found to be expressed during the early stage of pressure volume overload, during the compensatory mechanism, and six weeks after aortic stenosis in rat models with age-matched controls [54]. These studies showed that these proteins were down-regulated about 22 weeks after and during the end stage of heart failure, which does not happen

in DOX-induced heart failure of this present study [54]. The down-regulation of erbB2 or heat shock proteins, mTOR, and Akt, and GSK-β in the 15 mg/kg DOX was not observed. The reason may be that fractional shortening (FS) ≤ 40% was not low enough to induce their down-regulation. These rats had to be euthanized due to the unpredicted risk of sudden death. Nearly all these rats treated with 15 mg/kg were observed to develop thrombosis up to 50% or more in size around week 10. It also may imply that excessive signaling parallels the increase in apoptosis and this process lead to decompensation. The protection provided with these proteins, such as erbB2 and others, seems to extend the survival time by inducing hypertrophy which inevitably leads to decompensation once re-activated in adult rat hearts.

This study also shows the importance of erbB2 signaling in myocytes and growth [55]. If these proteins were not present, cell deaths would be continuous and heart failure would be accelerated. In addition to its role in the development of hypertrophy and growth, conditional deletion of erbB2 in adult mice resulted in dilated cardiomyopathy, confirming the requirement for functional erbB2 in the differentiated myocardium and providing a mechanism for the principal side effects (cardiomyopathy and heart failure) observed in patients undergoing chemotherapy with anti-erbB2 therapy [55].

The newly developed (FDA approved) lapatinib, an oral receptor tyrosine kinase inhibitor similar to trastuzumab that targets both erbB2 and erbB4 receptors in over-expressed breast cancers should be studied, since long-term side effects on the heart have not been determined.

4.4.5. Angiotensin and hypertrophy

Little is known about the role of EGFR transactivation in angiotensin II (ATII) and ROS-mediated cardiomyocyte hypertrophy [338]. AII activation was suggested to cause G-protein coupled receptors of AT1 and AT2-mediated growth and proliferation were dependent upon EGRF trans-activation [338]. The results of this study showed that DOX induced the expression of erbB2, NRG-1, as well as Akt, mTOR and GSK-β persistently, paralleling the increase in LVmass and cardiomyocytes deaths. Losartan AT1 receptor antagonist showed a regression of left ventricular hypertrophy and lowered blood pressure, suggesting AT1 to be partly responsible for cardiac hypertrophy and remodeling.

Previous reports suggest that the chronic vasoconstrictive effects of AT1 lead to the activation of enzyme systems and second messengers, including the phospholipases, and redox-sensitive mitogen-activated protein kinases (MAPKs) which includes extracellular signal-regulated kinases (ERK1/2), the c-jun NH2-terminal/stress-activated protein kinases (JNK/SAPKs), and the p38 reactivating kinase (p38 MAPK) [152].

The ERK1/2, the phosphatidylinositol 3-kinase (PI3K)-dependent signaling kinase [339], Akt (or PKB), and mTOR/S6 kinase [227] were reported to have an anti-apoptotic role involving cell growth and survival process [335, 336, 340], whereas the c-jun NH2-terminal/stress-activated protein kinases (JNK/SAPKs), p38 reactivating kinase (p38 MAPK)[152] lead to apoptotic pathways [335, 336, 340]. It was also

shown that the activation of these kinases might be dependent to ROS concentration, leading either to myocyte hypertrophy or apoptosis [336].

The p38 MAPK and JNK kinases, which are pro-apoptotic pathways, may have increased early and persisted until heart failure, thus dominating the protective role of erbB2 and other protective signaling pathways involved in cell survival and growth. Blocking these pathways may help prevent the formation of apoptotic bodies and prevent heart failure.

4.5. Losartan

Weight loss associated with diarrhea, anorexia, and gastrointestinal damage has been reported to be one of the most toxic side effects of chemotherapy [341], including treatment with DOX [342].

The greater body weight of the 15 mg/kg DOX-treated rats compared with the combined DOX+LOS-treated rats may be explained by the significant fluid accumulation in the peritoneal (ascites), pleural or pericardial cavity in the former group. These findings were observed using 2-dimensional echocardiography and confirmed during necropsy when approximately 7 ml of excess pleural and abdominal fluid taken from the 15 mg/kg treated rats at week 10.

The decrease in body weight with losartan reflects the ability of losartan, AT1 inhibitor, to act by inhibiting the activation of angiotensin II type 1 receptor (AT1) [273]. AT1 induces vasoconstriction and retention of sodium whereas inhibition by losartan has been shown to normalize tubular function in patients with mild

congestive heart failure and normal plasma levels of rennin and aldosterone [343, 344].

In this study, DOX induced a dose-dependant increase in TGF-β pathway activation, coinciding with a significant decline in myocardial contractility, an increase in the LV mass, and increase in MAP (Figure 5, 6, 7). Excessive TGF-β pathway activation in the 15 mg/kg DOX-treated SD rats was associated with a significant increase in myocardial cell death, contrary to 7.5 mg/kg which showed less myocytes death and preserved systolic function.

Losartan was associated with the regression of LVH, a decline of blood pressure, and improved myocardial contractility back to normal levels compared to 15 mg/kg DOX alone treated rats. These responses coincided with a decline in TGF-β pathway activation, resulting in cardioprotection and prevention of heart failure in the combined losartan and 15 mg/kg DOX-treated rats. This suggests that there could be an association between TGF-β pathways and angiotensin type 1 which could be partly responsible for the induction of apoptosis and, thereby, the conversion of adaptive hypertrophy to maladaptive hypertrophy and heart failure when expressed in excess. The cellular distribution, mechanism of induction, and source of increased TGF-β pathway activation in response to hypertrophic stimuli are not known. This study shows that DOX-induced left ventricular hypertrophy is associated with an increase in TGF-β pathway activation compared to normal saline-treated rats (Figure 18). This increase in TGF-β pathway activation correlates to marked increase in pSMAD2 expression and parallels the marked decline in the myocardial contractility (Figure 1, 5, 7 18, 19), and the increase in cardiomyocytes death and fibrosis (Figures 4A3, 11,

20C3). This suggests that TGF-β may have a pro-apoptotic effect in a dose- and time-dependent response.

In contrast, the combination of losartan and DOX (DOX+LOS) treatment was associated with a decline in TGF-β pathway activation, coinciding with regression of left ventricular hypertrophy, decline in mean arterial pressure, and increase in myocardial contractility compared to rats treated with 15 mg/kg DOX alone. These improvements also suggest that less pSMAD2 and less apoptosis were generated with losartan.

ATII activation by ROS generation from DOX redox cycling is known to mediate G-protein-uncoupling (AT1 and AT2). AT1 plays a role in the regulation of blood pressure, fluid homeostasis and cell growth, activates membrane-bound vascular NAD(P)H oxidase, the formation of reactive oxygen (ROS), and apoptosis [345]. The cardiac hypertrophy in this study might be due in part to the imbalance between cell growth and death. As the heart adapts and grows, apoptosis of cardiomyocytes seem to increase in DOX dose- and time-dependent manner. This is observed with the inevitable left ventricular decompensation in the two rats treated with lower doses of DOX (7.5 mg/kg) at week 14 after adaption at week 10 in other group treated with the same dose of doxorubicin. Adaptive hypertrophy as it was observed was associated with a small amount of cardiomyocyte death. Greater amount of cardiomyocyte apoptosis was associated with left ventricular decompensation at week 10 in the 15 mg/kg treated SD rats. The regulation of cell death and cell growth is not well understood. Dietz et al. reported that cardiomyocyte apoptosis is reduced after prolonged inhibition of the angiotensin pathway during the established phase of hypertension in spontaneously hypertensive rats [346]. The fact that a significant

decline in myocardial contractility was associated with a significant amount of cell death when 15 mg/kg DOX was administered alone in this present study suggests that the improvement of myocardial contractility with losartan supplement may be associated with less cardiomyocyte death. This also substantiates the findings that AT1 is partly responsible for the development of left ventricular hypertrophy, hypertension, myocardial dysfunction, and increase in cell death.

The improvement of both systolic and diastolic function with losartan treatment of this present study may also involve decline in Ca^{2+} overload in addition to angiotensin receptor type 1 (AT1) blockade, as demonstrated previously in isolated cardiomyocytes exposed to ischemia reperfusion [347].

Furthermore, previous published studies [273] demonstrate that losartan prevents aortic aneurysm in the mouse model of Marfan syndrome (MFS) [273]. Excessive TGF-beta signaling may have played a causal role in progressive aortic root and left ventricular enlargement [273] in MFS and 15 mg/kg of DOX-treated rats. These characteristics of maladaptive vascular remodeling in humans and with MFS are directly proportional to the risk of life-threatening aortic dissection [348]. In chronic DOX treatment, left ventricular dilatation and dysfunction are leading causes of heart failure and death. Losartan prevented elastic fiber fragmentation, interstitial collagen deposition, and reduced TGF-beta signaling in aortic media of MFS [278]. This was evidenced by nuclear accumulation of pSmad2 and histopathology results [273]. Wall elasticity, diameter, and wall thickness were maintained compared to the normal wild type group [273]. Improved vascular and myocardial elasticity, normalization of blood pressure, and myocardial contractility were observed in this study with the

combined losartan and DOX therapy and in previously studies in animal models of chronic renal insufficiency and cardiomyopathy [349, 350].

The effect of losartan on lowering blood pressure and cardiac hypertrophy has been demonstrated in a variety of in vitro and in vivo studies and in models of hypertension, renal disease, and stroke [351-354]. Few studies show in vivo follow up of LVmass reduction, but not all show a successful reduction of left ventricular hypertrophy, especially since most of these studies are conducted under anesthesia which is cardio depressive. Also, little is known about in vivo DOX-induced left ventricular hypertrophy and the losartan effect on prevention of DOX-induced left ventricular hypertrophy.

The in vivo follow up of left ventricular hypertrophy and remodeling, using conscious non-invasive echocardiography in this present study, clearly indicates that losartan is able to reduce the LV hypertrophy, reduce the mean arterial pressure, increase myocardial contractility by blocking TGF-β signaling pathways and AT1 activation, and should be used as a therapeutic supplement with DOX treatment.

4.6. Strain differences

The SD rats treated with a 15 mg/kg dose of DOX showed a significant increase in MAP, significant increase in LVmass, and marked decline in systolic function coinciding with moderate to severe kidney damage compared to the F344 treated with the same dose and at the same time point (week 10). These changes have been reported in spontaneously hypertensive rats subject to chronic salt diet in previous studies [355, 356]. The F344 rats showed normal MAP, less significant changes in the morphology and function of the left ventricular hypertrophy, and small to mild kidney

damage in response to 15mg/kg of DOX. The development of renal damage in spontaneously hypertensive rats was suggested to occur as a result of impairment in regulation of renal oxygen consumption by nitric oxide in response to increased superoxide [357]. The decline in kidney weight, sodium and water retention in the DOX-LOS-treated SD rat strain of this study suggest that AT1 may be partly responsible for the NO/O_2^- balance in the kidneys. A significant increase in lipid peroxidation and hydroxyproline content of the kidneys was reported in response to such imbalance [358]. A significantly lower SOD-3 than the SOD-1 and the SOD-2 antioxidant level in the kidneys were suggested may be responsible for ROS-induced kidney damage in DOX-exposed SHR strain of rats [357]. Increased superoxide generation and decline in antioxidant balance in the kidneys of the DOX-treated SD rats may have played a part in early renal tubular damage. This may have lead to a vicious cycle resulting in more extensive and irreversible damage of kidneys and heart, since both are involved in the autoregulation of blood pressure and volume. The kidneys thus could be the first target or the most susceptible organ to DOX-induced oxidative injuries and the leading cause of early heart failure and mortality in the SD rats than the F344 rats.

Other phenotypic differences that predispose SD rats to reno-cardiovascular damage are the increase in body weight, HW/BW ratio and low level of RBC compared to the F344 rats. These phenotypic differences should be considered prior to DOX treatment in humans with inter-individual differences. Kidney function and abnormalities should be assessed in prevention of heart failure and mortality.

4.7. Gender differences and doxorubicin toxicity

Consequent to follow up systolic function based on fractional shortening with 2-3 mg/kg of DOX treatment in male and female neonates has lead to the development of systolic dysfunction that resulted in 60% of deaths among the male rats within 50 weeks after exposure (Figure 10). Female rats in this study developed mammary tumors but the heart failure did not occur. They were euthanized due to discomfort and for comparative study (Figure 10). Prior studies have shown that mammary tumors begin to develop in SD rats beyond the age of 18 months as part of the aging process, which may be related to persistent estrous cycle in this strain of rats [359-361]. Other studies showed that environmental toxicant exposure and pharmacological doses of dietary estrogen could trigger mammary growth while the estrous cycle is normal without the aging effect or ovarian failure [361]. These tumors were also demonstrated to develop 11 months after receiving whole-body radiation given as a single exposure in the SD rats at the age of 20 days while the control showed none [362]. This present study shows acceleration of mammary tumors with a small dose of DOX, while maintaining normal cardiac function. The control did not develop any tumors, suggesting that DOX is a mutagen and could induce cancer. While mechanisms of this process are not completely understood, estrogen function in cardioprotection and in mammary tumors growth has been proposed to play a part in pre-menopausal and post-menopausal stages [363]. Some toxicants have been suggested to induce growth of mammary tumors directly via estrogenic effects on breast epithelial cell proliferation [364], while others act indirectly by shifting the expression of genes responsible for estrogen synthesis and metabolism [365] or by direct effect of epidermal growth factors signaling pathways [366]. In this study, it

was observed that these tumors grew rapidly into larger size once they started to appear. A greater amount of vascular systems were also observed in these tumors, suggesting the possible role of estrogen in development of vascular collateral in the heart as well. These observations suggest that increased blood flow may have played a part in cardiac protection.

The binding of estrogen ligands to its receptors, ERα and ER^{β}, in the cell was reported to activate protein kinases-enzymes that initiate the phosphorylation of cellular proteins such as MAPKs, EGFR and PI3K/Akt signaling pathways which are important regulators of cell growth and survival mechanisms and the stimulation of eNOS to syntheses NO [363]. NO, a vasodilator, activates the soluble guanylate cyclases (sGC), increasing the cyclic guanosine monophosphate (cGMP) concentration and protein kinase G (PKG), which in turn, regulates vascular tone, myocyte function, growth and remodeling [363]. NO acts as antioxidant and maintains normal O_2^-/NO homeostasis by inhibiting the activation of xanthine oxidase (XO) and NAD(P)H oxidase [367, 368]. Estrogen thus may play a part in both tumor growth and cardioprotection in female SD rats.

Deficiency of this hormone in male rats may be partly responsible for the acceleration of heart failure. An increase in O_2^-/NO level and low level of NO in the heart and the vascular wall system may have lead to an increase in peroxynitrite levels, triggering cytotoxic processes that includes lipid peroxidation, protein oxidation, nitration [117], and the initiation of left ventricular and vascular wall remodeling and dysfunction [129, 369]

5. CONCLUSION

Strain, age, and gender may be the predisposing factors to chronic DOX-induced reno-cardiovascular oxidative damage.

Smaller body and organ weight, LVmass, higher red blood cell levels, and normal kidney physiology make the F344 more resistant to DOX toxicity than the SD rats.

The findings of losartan treatment suggests excessive AT1 and TGF-β pathways activation, played a part in the stimulation of apoptosis and remodeling in dose- and time-dependent response that lead to reno-cardiovascular failure in SD rats treated with 7.5 mg/kg and 15 mg/kg of doxorubicin.

Excessive ErbB2, mTOR, GSK-β, Akt, and heat shock proteins expression may have also contributed to the transition of adaptive hypertrophy to heart failure at week 10 in the SD rats treated with 15 mg/kg DOX, with AT1 as the source of their activation.

DOX treatment with either 7.5 mg/kg or 15 mg/kg induced left ventricular hypertrophy and remodeling is accelerated in the SD rats than the F344 rats strain. This change will inevitably lead to failure, with renal failure as the first possible target of toxicity in the SD than the F344 strain because the F344 rats strain did not show extensive damage to the kidney as the SD strain of rats treated with the same dose of DOX (15mg/kg) at the same time point of time (Week 10). The present study suggests that a possible phenotipic difference in the kidney morphology, RAAS and function between the 2 strains of rats (SD and F344) in response to chronic DOX treatment may exist and merit further investigation. TGF-β-1 inhibition using the oral angiotensin type 1 receptor antagonist, losartan, may be used as a therapeutic

supplement for reversing or regressing left ventricular hypertrophy, lowering blood pressure, and preventing heart failure with chronic DOX treatment.

The evaluation of cardiac toxicity and/or cardiomyopathy with use of systolic function (FS) method alone has lead to irreversible damage that was associated with cardiomyocytes death and marked decline in myocardial contractility. Additional use of tissue Doppler imaging (TDI) predicts early diastolic dysfunction because it precedes systolic dysfunction. It may also predict early renal dysfunction because it is associated with adaptive hypertrophy with preserved systolic function (FS). Using both the methods in assessing systolic (FS) and diastolic function (TDI) would help determine physiological and molecular mechanisms of protection and may lead to early therapeutic interventions and prevention of risks that may contribute to chemotherapeutic toxicity in the reno-cardiovascular system.

SPECT/CT is a novel and feasible method of determining apoptosis in in vivo animal models using a guided conscious echocardiography method in the evaluation of left ventricular hypertrophy and remodeling.

Future aims:

Investigate the mechanism of losartan treatment and regression of thrombogenesis.

Investigate elastin, collagen level in the vascular wall system of F344 and SD rats strain.

Investigate type and level of antioxidant defense mechanisms in the reno-cardiovascular tissue of F344 and SD rats.

Investigate the effect of exercise endurance on the cardio-pulmonary and vascular system in response to chronic DOX therapy in SD and F344 rats.

6. AKNOWLEDGEMENTS

This study was carried out at The Johns Hopkins University School of Medicine, Department of Molecular and Comparative Pathobiology, in collaboration with the University of New South Wales, Graduate School of Biomedical Engineering. I am grateful to Dr. Kathleen Gabrielson for introducing me to the present theme and for her support and supervision during these years of scientific research. I would like to thank our lab members who contributed to the study of the cellular and molecular mechanisms of cardiac toxicity, including: Dr. Yi Xu, Nicol Murator, Scutt Pin, Keryn Greve, Tsao A, as well as Watchman LM, and past student members who helped me with conducting the physiological response to chronic doxorubicin in this rat model. I thank Dr. Cory Brayton and Nadine Forbes for their help in conducting lipid and hematology profiles. I thank Jane Habashi and Professor Harry Dietz for their help with pSMAD2 analysis and understanding its association with TGF-β signaling in aortic aneurysm of Marfan mice.

I thank Sarah Poynton, PhD and Martin Blair for her help with editing the thesis. I thank Professor Albert Avolio, PhD, for his interest in my work. His expertise of the highest grade in the field of biomedical engineering and hypertension encouraged me in very important ways. I thank Professor Barry Gow for supporting my research work in post-dilation of the aorta-hemodynamic and the histopathology and my

education that began at the University of Sydney, Division of Cardiovascular Physiology.

Thanks to Professor Janice Clement for making it possible for us to develop this newly non-invasive echocardiographic method in conscious mice and to correlate the results to molecular, cellular, and histopathological disease processes and therapy, particularly cardiovascular and cancer growth.

Thanks to all the professors, physicians, nurses, technician, and athletes from all over the globe for making me part of their team and the wonderful time I had working with them.

I express my warmest gratitude for my mum and dad who believed that science and sports go together and have no border. They gave me the opportunity to learn, travel, and get to know this independently and in the best way. I dedicate this thesis to them and to my son.

Djahida Bedja,

January 2008.

7. REFERENCES

1. Vasquez-Vivar, J., et al., *Endothelial nitric oxide synthase-dependent superoxide generation from adriamycin.* Biochemistry, 1997. **36**(38): p. 11293-7.
2. Fogli, S., P. Nieri, and M.C. Breschi, *The role of nitric oxide in anthracycline toxicity and prospects for pharmacologic prevention of cardiac damage.* Faseb J, 2004. **18**(6): p. 664-75.
3. Takemura, G. and H. Fujiwara, *Doxorubicin-induced cardiomyopathy from the cardiotoxic mechanisms to management.* Prog Cardiovasc Dis, 2007. **49**(5): p. 330-52.
4. Thorburn, A. and A.E. Frankel, *Apoptosis and anthracycline cardiotoxicity.* Mol Cancer Ther, 2006. **5**(2): p. 197-9.
5. Binaschi, M., et al., *Anthracyclines: selected new developments.* Curr Med Chem Anticancer Agents, 2001. **1**(2): p. 113-30.
6. Carter, S.K., *Adriamycin-a review.* J Natl Cancer Inst, 1975. **55**(6): p. 1265-74.
7. Lefrak, E.A., et al., *A clinicopathologic analysis of adriamycin cardiotoxicity.* Cancer, 1973. **32**(2): p. 302-14.
8. Von Hoff, D.D., et al., *Risk factors for doxorubicin-induced congestive heart failure.* Ann Intern Med, 1979. **91**(5): p. 710-7.
9. Weiss, R.B., *The anthracyclines: will we ever find a better doxorubicin?* Semin Oncol, 1992. **19**(6): p. 670-86.
10. Singal, P.K. and N. Iliskovic, *Doxorubicin-induced cardiomyopathy.* N Engl J Med, 1998. **339**(13): p. 900-5.
11. Wojtacki, J., E. Lewicka-Nowak, and K. Lesniewski-Kmak, *Anthracycline-induced cardiotoxicity: clinical course, risk factors, pathogenesis, detection and prevention--review of the literature.* Med Sci Monit, 2000. **6**(2): p. 411-20.
12. Singal, P.K., et al., *Significance of adaptation mechanisms in adriamycin induced congestive heart failure.* Basic Res Cardiol, 1992. **87**(6): p. 512-8.
13. Minotti, G., et al., *Anthracyclines: molecular advances and pharmacologic developments in antitumor activity and cardiotoxicity.* Pharmacol Rev, 2004. **56**(2): p. 185-229.
14. Lenaz, L. and J.A. Page, *Cardiotoxicity of adriamycin and related anthracyclines.* Cancer Treat Rev, 1976. **3**(3): p. 111-20.
15. Lipshultz, S.E., et al., *Late cardiac effects of doxorubicin therapy for acute lymphoblastic leukemia in childhood.* N Engl J Med, 1991. **324**(12): p. 808-15.
16. Steinherz, L.J., et al., *Cardiac toxicity 4 to 20 years after completing anthracycline therapy.* Jama, 1991. **266**(12): p. 1672-7.
17. Baker, K.S., et al., *Late effects in survivors of chronic myeloid leukemia treated with hematopoietic cell transplantation: results from the Bone Marrow Transplant Survivor Study.* Blood, 2004. **104**(6): p. 1898-906.
18. Oeffinger, K.C., et al., *Health care of young adult survivors of childhood cancer: a report from the Childhood Cancer Survivor Study.* Ann Fam Med, 2004. **2**(1): p. 61-70.

19. Garre, M.L., et al., *Health status of long-term survivors after cancer in childhood. Results of an uniinstitutional study in Italy.* Am J Pediatr Hematol Oncol, 1994. **16**(2): p. 143-52.
20. Green, D.M., et al., *Severe hepatic toxicity after treatment with single-dose dactinomycin and vincristine. A report of the National Wilms' Tumor Study.* Cancer, 1988. **62**(2): p. 270-3.
21. Mertens, A.C., et al., *Late mortality experience in five-year survivors of childhood and adolescent cancer: the Childhood Cancer Survivor Study.* J Clin Oncol, 2001. **19**(13): p. 3163-72.
22. Hancock, S.L., M.A. Tucker, and R.T. Hoppe, *Breast cancer after treatment of Hodgkin's disease.* J Natl Cancer Inst, 1993. **85**(1): p. 25-31.
23. Bhatia, S., et al., *Breast cancer and other second neoplasms after childhood Hodgkin's disease.* N Engl J Med, 1996. **334**(12): p. 745-51.
24. Tucker, M.A., et al., *Therapeutic radiation at a young age is linked to secondary thyroid cancer. The Late Effects Study Group.* Cancer Res, 1991. **51**(11): p. 2885-8.
25. Black, P., A. Straaten, and P. Gutjahr, *Secondary thyroid carcinoma after treatment for childhood cancer.* Med Pediatr Oncol, 1998. **31**(2): p. 91-5.
26. Olsen, J.H., et al., *Second malignant neoplasms after cancer in childhood or adolescence. Nordic Society of Paediatric Haematology and Oncology Association of the Nordic Cancer Registries.* Bmj, 1993. **307**(6911): p. 1030-6.
27. Swerdlow, A.J., et al., *Second malignancy in patients with Hodgkin's disease treated at the Royal Marsden Hospital.* Br J Cancer, 1997. **75**(1): p. 116-23.
28. Hoorweg-Nijman, J.J., et al., *Bone mineral density and markers of bone turnover in young adult survivors of childhood lymphoblastic leukaemia.* Clin Endocrinol (Oxf), 1999. **50**(2): p. 237-44.
29. Vassilopoulou-Sellin, R., et al., *Osteopenia in young adult survivors of childhood cancer.* Med Pediatr Oncol, 1999. **32**(4): p. 272-8.
30. Talvensaari, K.K., et al., *Long-term survivors of childhood cancer have an increased risk of manifesting the metabolic syndrome.* J Clin Endocrinol Metab, 1996. **81**(8): p. 3051-5.
31. Benjamin, I.J. and E. Christians, *Exercise, estrogen, and ischemic cardioprotection by heat shock protein 70.* Circ Res, 2002. **90**(8): p. 833-5.
32. Oeffinger, K.C., et al., *Obesity in adult survivors of childhood acute lymphoblastic leukemia: a report from the Childhood Cancer Survivor Study.* J Clin Oncol, 2003. **21**(7): p. 1359-65.
33. Strickland, D.K., et al., *Hepatitis C infection among survivors of childhood cancer.* Blood, 2000. **95**(10): p. 3065-70.
34. Brennan, B.M., et al., *Growth hormone status in adults treated for acute lymphoblastic leukaemia in childhood.* Clin Endocrinol (Oxf), 1998. **48**(6): p. 777-83.
35. Sklar, C., et al., *Abnormalities of the thyroid in survivors of Hodgkin's disease: data from the Childhood Cancer Survivor Study.* J Clin Endocrinol Metab, 2000. **85**(9): p. 3227-32.
36. Johnson, W.W. and D.C. Meadows, *Urinary-bladder fibrosis and telangiectasia associated with long-term cyclophosphamide therapy.* N Engl J Med, 1971. **284**(6): p. 290-4.

37. Wellwood, J.M. and B.T. Jackson, *The intestinal complications of radiotherapy.* Br J Surg, 1973. **60**(10): p. 814-8.
38. Rhoden, W., P. Hasleton, and N. Brooks, *Anthracyclines and the heart.* Br Heart J, 1993. **70**(6): p. 499-502.
39. Larsen, R.L., et al., *Electrocardiographic changes and arrhythmias after cancer therapy in children and young adults.* Am J Cardiol, 1992. **70**(1): p. 73-7.
40. Steinherz, L.J., P.G. Steinherz, and C. Tan, *Cardiac failure and dysrhythmias 6-19 years after anthracycline therapy: a series of 15 patients.* Med Pediatr Oncol, 1995. **24**(6): p. 352-61.
41. Steinherz, L. and P. Steinherz, *Delayed cardiac toxicity from anthracycline therapy.* Pediatrician, 1991. **18**(1): p. 49-52.
42. Jain, K.K., et al., *A prospective randomized comparison of epirubicin and doxorubicin in patients with advanced breast cancer.* J Clin Oncol, 1985. **3**(6): p. 818-26.
43. Havsteen, H., et al., *Prospective evaluation of chronic cardiotoxicity due to high-dose epirubicin or combination chemotherapy with cyclophosphamide, methotrexate, and 5-fluorouracil.* Cancer Chemother Pharmacol, 1989. **23**(2): p. 101-4.
44. Watts, R.G., *Severe and fatal anthracycline cardiotoxicity at cumulative doses below 400 mg/m2: evidence for enhanced toxicity with multiagent chemotherapy.* Am J Hematol, 1991. **36**(3): p. 217-8.
45. Villani, F., et al., *Possible enhancement of the cardiotoxicity of doxorubicin when combined with mitomycin C.* Med Oncol Tumor Pharmacother, 1985. **2**(2): p. 93-7.
46. Seidman, A., et al., *Cardiac dysfunction in the trastuzumab clinical trials experience.* J Clin Oncol, 2002. **20**(5): p. 1215-21.
47. Ewer, M.S., et al., *Cardiotoxicity in patients receiving transtuzumab (Herceptin): primary toxicity, synergistic or sequential stress, or surveillance artifact?* Semin Oncol, 1999. **26**(4 Suppl 12): p. 96-101.
48. Lee, K.F., et al., *Requirement for neuregulin receptor erbB2 in neural and cardiac development.* Nature, 1995. **378**(6555): p. 394-8.
49. Pugatsch, T., et al., *Anti-erbB2 treatment induces cardiotoxicity by interfering with cell survival pathways.* Breast Cancer Res, 2006. **8**(4): p. R35.
50. Feldman, A.M., B.H. Lorell, and S.E. Reis, *Trastuzumab in the treatment of metastatic breast cancer: anticancer therapy versus cardiotoxicity.* Circulation, 2000. **102**(3): p. 272-4.
51. McNeil, C., *Herceptin raises its sights beyond advanced breast cancer.* J Natl Cancer Inst, 1998. **90**(12): p. 882-3.
52. Moy, B. and P.E. Goss, *Lapatinib-associated toxicity and practical management recommendations.* Oncologist, 2007. **12**(7): p. 756-65.
53. Moy, B. and P.E. Goss, *Lapatinib: current status and future directions in breast cancer.* Oncologist, 2006. **11**(10): p. 1047-57.
54. Rohrbach, S., et al., *Neuregulin in cardiac hypertrophy in rats with aortic stenosis. Differential expression of erbB2 and erbB4 receptors.* Circulation, 1999. **100**(4): p. 407-12.
55. Crone, S.A., et al., *ErbB2 is essential in the prevention of dilated cardiomyopathy.* Nat Med, 2002. **8**(5): p. 459-65.
56. Chicco, A.J., C.M. Schneider, and R. Hayward, *Voluntary exercise protects against acute doxorubicin cardiotoxicity in the isolated perfused rat heart.* Am J Physiol Regul Integr Comp Physiol, 2005. **289**(2): p. R424-R431.

57. Doroshow, J.H., *Doxorubicin-induced cardiac toxicity.* N Engl J Med, 1991. **324**(12): p. 843-5.
58. Schwartz, R.G., et al., *Congestive heart failure and left ventricular dysfunction complicating doxorubicin therapy. Seven-year experience using serial radionuclide angiocardiography.* Am J Med, 1987. **82**(6): p. 1109-18.
59. Zucchi, R. and R. Danesi, *Cardiac toxicity of antineoplastic anthracyclines.* Curr Med Chem Anticancer Agents, 2003. **3**(2): p. 151-71.
60. Shan, K., A.M. Lincoff, and J.B. Young, *Anthracycline-induced cardiotoxicity.* Ann Intern Med, 1996. **125**(1): p. 47-58.
61. Wojnowski, L., et al., *NAD(P)H oxidase and multidrug resistance protein genetic polymorphisms are associated with doxorubicin-induced cardiotoxicity.* Circulation, 2005. **112**(24): p. 3754-62.
62. Henderson, I.C., et al., *Randomized clinical trial comparing mitoxantrone with doxorubicin in previously treated patients with metastatic breast cancer.* J Clin Oncol, 1989. **7**(5): p. 560-71.
63. Hayward, C.S., R.P. Kelly, and P. Collins, *The roles of gender, the menopause and hormone replacement on cardiovascular function.* Cardiovasc Res, 2000. **46**(1): p. 28-49.
64. Murphy, E. and C. Steenbergen, *Cardioprotection in females: a role for nitric oxide and altered gene expression.* Heart Fail Rev, 2007. **12**(3-4): p. 293-300.
65. Sterba, M., et al., *Early detection of anthracycline cardiotoxicity in a rabbit model: left ventricle filling pattern versus troponin T determination.* Physiol Res, 2006.
66. Sutton, D.C. and G.C. Sutton, *Needle biopsy of the human ventricular myocardium: review of 54 consecutive cases.* Am Heart J, 1960. **60**: p. 364-70.
67. Shirey, E.K., et al., *Percutaneous myocardial biopsy of the left ventricle. Experience in 198 patients.* Circulation, 1972. **46**(1): p. 112-22.
68. Sakakibara, S. and S. Konno, *Endomyocardial biopsy.* Jpn Heart J, 1962. **3**: p. 537-43.
69. Konno, S., M. Sekiguchi, and S. Sakakibara, *Catheter biopsy of the heart.* Radiol Clin North Am, 1971. **9**(3): p. 491-510.
70. Isner, J.M., et al., *Clinical and morphologic cardiac findings after anthracycline chemotherapy. Analysis of 64 patients studied at necropsy.* Am J Cardiol, 1983. **51**(7): p. 1167-74.
71. Steinherz, L.J., et al., *Guidelines for cardiac monitoring of children during and after anthracycline therapy: report of the Cardiology Committee of the Childrens Cancer Study Group.* Pediatrics, 1992. **89**(5 Pt 1): p. 942-9.
72. Panjrath, G.S. and D. Jain, *Monitoring chemotherapy-induced cardiotoxicity: role of cardiac nuclear imaging.* J Nucl Cardiol, 2006. **13**(3): p. 415-26.
73. Schlosshan, D., et al., *Implications of ejection fraction value for trastuzumab.* Bmj, 2006. **333**(7570): p. 704.
74. Suter, T.M. and B. Meier, *Detection of anthracycline-induced cardiotoxicity: is there light at the end of the tunnel?* Ann Oncol, 2002. **13**(5): p. 647-9.
75. Brockstein, B.E., et al., *Cardiac and pulmonary toxicity in patients undergoing high-dose chemotherapy for lymphoma and breast cancer: prognostic factors.* Bone Marrow Transplant, 2000. **25**(8): p. 885-94.
76. Sachdev, V., et al., *Diastolic dysfunction is an independent risk factor for death in patients with sickle cell disease.* J Am Coll Cardiol, 2007. **49**(4): p. 472-9.

77. Bu'Lock, F.A., et al., *Left ventricular diastolic function after anthracycline chemotherapy in childhood: relation with systolic function, symptoms, and pathophysiology.* Br Heart J, 1995. **73**(4): p. 340-50.
78. Deswal, A., *Diastolic dysfunction and diastolic heart failure: mechanisms and epidemiology.* Curr Cardiol Rep, 2005. **7**(3): p. 178-83.
79. Schirmer, H., P. Lunde, and K. Rasmussen, *Mitral flow derived Doppler indices of left ventricular diastolic function in a general population; the Tromso study.* Eur Heart J, 2000. **21**(16): p. 1376-86.
80. Nagueh, S.F., et al., *Doppler tissue imaging: a noninvasive technique for evaluation of left ventricular relaxation and estimation of filling pressures.* J Am Coll Cardiol, 1997. **30**(6): p. 1527-33.
81. Singal, P.K., C.M. Deally, and L.E. Weinberg, *Subcellular effects of adriamycin in the heart: a concise review.* J Mol Cell Cardiol, 1987. **19**(8): p. 817-28.
82. Doroshow, J.H., *Effect of anthracycline antibiotics on oxygen radical formation in rat heart.* Cancer Res, 1983. **43**(2): p. 460-72.
83. Kalyanaraman, B., E. Perez-Reyes, and R.P. Mason, *Spin-trapping and direct electron spin resonance investigations of the redox metabolism of quinone anticancer drugs.* Biochim Biophys Acta, 1980. **630**(1): p. 119-30.
84. Berthiaume, J.M. and K.B. Wallace, *Adriamycin-induced oxidative mitochondrial cardiotoxicity.* Cell Biol Toxicol, 2007. **23**(1): p. 15-25.
85. Singal, P.K., et al., *Changes in lysosomal morphology and enzyme activities during the development of adriamycin-induced cardiomyopathy.* Can J Cardiol, 1985. **1**(2): p. 139-47.
86. Myers, C.E., et al., *Adriamycin: the role of lipid peroxidation in cardiac toxicity and tumor response.* Science, 1977. **197**(4299): p. 165-7.
87. Revis, N.W. and N. Marusic, *Glutathione peroxidase activity and selenium concentration in the hearts of doxorubicin-treated rabbits.* J Mol Cell Cardiol, 1978. **10**(10): p. 945-51.
88. Siveski-Iliskovic, N., N. Kaul, and P.K. Singal, *Probucol promotes endogenous antioxidants and provides protection against adriamycin-induced cardiomyopathy in rats.* Circulation, 1994. **89**(6): p. 2829-35.
89. Bristow, M.R., et al., *Acute and chronic cardiovascular effects of doxorubicin in the dog: the cardiovascular pharmacology of drug-induced histamine release.* J Cardiovasc Pharmacol, 1980. **2**(5): p. 487-515.
90. Singal, P.K., et al., *Adriamycin-induced heart failure: mechanism and modulation.* Mol Cell Biochem, 2000. **207**(1-2): p. 77-86.
91. Bristow, M.R., et al., *Anthracycline-associated cardiac and renal damage in rabbits. Evidence for mediation by vasoactive substances.* Lab Invest, 1981. **45**(2): p. 157-68.
92. Bristow, M.R., et al., *Mediation of subacute anthracycline cardiotoxicity in rabbits by cardiac histamine release.* J Cardiovasc Pharmacol, 1983. **5**(6): p. 913-9.
93. Tong, J., P.K. Ganguly, and P.K. Singal, *Myocardial adrenergic changes at two stages of heart failure due to adriamycin treatment in rats.* Am J Physiol, 1991. **260**(3 Pt 2): p. H909-16.
94. Wakasugi, S., et al., *Detection of abnormal cardiac adrenergic neuron activity in adriamycin-induced cardiomyopathy with iodine-125-metaiodobenzylguanidine.* J Nucl Med, 1992. **33**(2): p. 208-14.

95. Dodd, D.A., et al., *Doxorubicin cardiomyopathy is associated with a decrease in calcium release channel of the sarcoplasmic reticulum in a chronic rabbit model.* J Clin Invest, 1993. **91**(4): p. 1697-705.
96. Singal, P.K. and V. Panagia, *Direct effects of adriamycin on the rat heart sarcolemma.* Res Commun Chem Pathol Pharmacol, 1984. **43**(1): p. 67-77.
97. Boucek, R.J., Jr., et al., *The major metabolite of doxorubicin is a potent inhibitor of membrane-associated ion pumps. A correlative study of cardiac muscle with isolated membrane fractions.* J Biol Chem, 1987. **262**(33): p. 15851-6.
98. Tokarska-Schlattner, M., T. Wallimann, and U. Schlattner, *Alterations in myocardial energy metabolism induced by the anti-cancer drug doxorubicin.* C R Biol, 2006. **329**(9): p. 657-68.
99. Zhang, J., et al., *Doxorubicin-induced apoptosis in spontaneously hypertensive rats: differential effects in heart, kidney and intestine, and inhibition by ICRF-187.* J Mol Cell Cardiol, 1996. **28**(9): p. 1931-43.
100. Rajagopalan, S., et al., *Adriamycin-induced free radical formation in the perfused rat heart: implications for cardiotoxicity.* Cancer Res, 1988. **48**(17): p. 4766-9.
101. Peterson, D.A., et al., *Reactive oxygen species may cause myocardial reperfusion injury.* Biochem Biophys Res Commun, 1985. **127**(1): p. 87-93.
102. Cave, A., et al., *NADPH oxidase-derived reactive oxygen species in cardiac pathophysiology.* Philos Trans R Soc Lond B Biol Sci, 2005. **360**(1464): p. 2327-34.
103. Bonomini, F., et al., *Atherosclerosis and oxidative stress.* Histol Histopathol, 2008. **23**(3): p. 381-90.
104. Narula, J., et al., *Mechanisms of disease: apoptosis in heart failure--seeing hope in death.* Nat Clin Pract Cardiovasc Med, 2006. **3**(12): p. 681-8.
105. Takimoto, E. and D.A. Kass, *Role of oxidative stress in cardiac hypertrophy and remodeling.* Hypertension, 2007. **49**(2): p. 241-8.
106. Bian, K., et al., *Proteomic modification by nitric oxide.* J Pharmacol Sci, 2006. **101**(4): p. 271-9.
107. Giordano, F.J., *Oxygen, oxidative stress, hypoxia, and heart failure.* J Clin Invest, 2005. **115**(3): p. 500-8.
108. Rhee, S.G., *Cell signaling. H2O2, a necessary evil for cell signaling.* Science, 2006. **312**(5782): p. 1882-3.
109. Touyz, R.M., *Reactive oxygen species and angiotensin II signaling in vascular cells -- implications in cardiovascular disease.* Braz J Med Biol Res, 2004. **37**(8): p. 1263-73.
110. Ignarro, L.J., G.M. Buga, and G. Chaudhuri, *EDRF generation and release from perfused bovine pulmonary artery and vein.* Eur J Pharmacol, 1988. **149**(1-2): p. 79-88.
111. Ignarro, L.J., et al., *Mechanisms of endothelium-dependent vascular smooth muscle relaxation elicited by bradykinin and VIP.* Am J Physiol, 1987. **253**(5 Pt 2): p. H1074-82.
112. Ignarro, L.J., et al., *Endothelium-derived relaxing factor and nitric oxide possess identical pharmacologic properties as relaxants of bovine arterial and venous smooth muscle.* J Pharmacol Exp Ther, 1988. **246**(1): p. 218-26.
113. Furchgott, R.F., *Role of endothelium in responses of vascular smooth muscle.* Circ Res, 1983. **53**(5): p. 557-73.

114. Pelc, L.R., G.J. Gross, and D.C. Warltier, *Mechanism of coronary vasodilation produced by bradykinin.* Circulation, 1991. **83**(6): p. 2048-56.
115. Kass, D.A., et al., *Phosphodiesterase regulation of nitric oxide signaling.* Cardiovasc Res, 2007. **75**(2): p. 303-14.
116. Pryor, W.A. and G.L. Squadrito, *The chemistry of peroxynitrite: a product from the reaction of nitric oxide with superoxide.* Am J Physiol, 1995. **268**(5 Pt 1): p. L699-722.
117. Katori, T., et al., *Peroxynitrite and myocardial contractility: in vivo versus in vitro effects.* Free Radic Biol Med, 2006. **41**(10): p. 1606-18.
118. Doroshow, J.H., G.Y. Locker, and C.E. Myers, *Enzymatic defenses of the mouse heart against reactive oxygen metabolites: alterations produced by doxorubicin.* J Clin Invest, 1980. **65**(1): p. 128-35.
119. Gajewski, E., et al., *Oxidative DNA base damage in MCF-10A breast epithelial cells at clinically achievable concentrations of doxorubicin.* Biochem Pharmacol, 2007. **73**(12): p. 1947-56.
120. Mordente, A., et al., *Anthracycline secondary alcohol metabolite formation in human or rabbit heart: biochemical aspects and pharmacologic implications.* Biochem Pharmacol, 2003. **66**(6): p. 989-98.
121. Davies, K.J. and J.H. Doroshow, *Redox cycling of anthracyclines by cardiac mitochondria. I. Anthracycline radical formation by NADH dehydrogenase.* J Biol Chem, 1986. **261**(7): p. 3060-7.
122. Thornalley, P.J. and N.J. Dodd, *Free radical production from normal and adriamycin-treated rat cardiac sarcosomes.* Biochem Pharmacol, 1985. **34**(5): p. 669-74.
123. Iliskovic, N., et al., *Mechanisms of beneficial effects of probucol in adriamycin cardiomyopathy.* Mol Cell Biochem, 1999. **196**(1-2): p. 43-9.
124. Thornalley, P.J., W.H. Bannister, and J.V. Bannister, *Reduction of oxygen by NADH/NADH dehydrogenase in the presence of adriamycin.* Free Radic Res Commun, 1986. **2**(3): p. 163-71.
125. Kalyanaraman, B. and J.E. Baker, *On the detection of paramagnetic species in the adriamycin-perfused rat heart: a reappraisal.* Biochem Biophys Res Commun, 1990. **169**(1): p. 30-8.
126. Gianni, L., et al., *Characterization of the cycle of iron-mediated electron transfer from Adriamycin to molecular oxygen.* J Biol Chem, 1985. **260**(11): p. 6820-6.
127. Sinha, B.K. and P.M. Politi, *Anthracyclines.* Cancer Chemother Biol Response Modif, 1990. **11**: p. 45-57.
128. Liu, Q.Y. and B.K. Tan, *Relationship between anti-oxidant activities and doxorubicin-induced lipid peroxidation in P388 tumour cells and heart and liver in mice.* Clin Exp Pharmacol Physiol, 2003. **30**(3): p. 185-8.
129. Turko, I.V. and F. Murad, *Protein nitration in cardiovascular diseases.* Pharmacol Rev, 2002. **54**(4): p. 619-34.
130. Palmer, H.J. and K.E. Paulson, *Reactive oxygen species and antioxidants in signal transduction and gene expression.* Nutr Rev, 1997. **55**(10): p. 353-61.
131. Finkel, T., *Oxygen radicals and signaling.* Curr Opin Cell Biol, 1998. **10**(2): p. 248-53.
132. Wei, S., et al., *Differential MAP kinase activation and Na(+)/H(+) exchanger phosphorylation by H(2)O(2) in rat cardiac myocytes.* Am J Physiol Cell Physiol, 2001. **281**(5): p. C1542-50.

133. Aikawa, R., et al., *Reactive oxygen species in mechanical stress-induced cardiac hypertrophy.* Biochem Biophys Res Commun, 2001. **289**(4): p. 901-7.
134. Tu, V.C., J.J. Bahl, and Q.M. Chen, *Signals of oxidant-induced cardiomyocyte hypertrophy: key activation of p70 S6 kinase-1 and phosphoinositide 3-kinase.* J Pharmacol Exp Ther, 2002. **300**(3): p. 1101-10.
135. Grieve, D.J. and A.M. Shah, *Oxidative stress in heart failure. More than just damage.* Eur Heart J, 2003. **24**(24): p. 2161-3.
136. Kwon, S.H., et al., *H(2)O(2) regulates cardiac myocyte phenotype via concentration-dependent activation of distinct kinase pathways.* J Mol Cell Cardiol, 2003. **35**(6): p. 615-21.
137. Griendling, K.K., D. Sorescu, and M. Ushio-Fukai, *NAD(P)H oxidase: role in cardiovascular biology and disease.* Circ Res, 2000. **86**(5): p. 494-501.
138. Kumar, D., H. Lou, and P.K. Singal, *Oxidative stress and apoptosis in heart dysfunction.* Herz, 2002. **27**(7): p. 662-8.
139. Kerr, J.F., *Shrinkage necrosis: a distinct mode of cellular death.* J Pathol, 1971. **105**(1): p. 13-20.
140. Kerr, J.F., A.H. Wyllie, and A.R. Currie, *Apoptosis: a basic biological phenomenon with wide-ranging implications in tissue kinetics.* Br J Cancer, 1972. **26**(4): p. 239-57.
141. Narula, J., et al., *Apoptosis in myocytes in end-stage heart failure.* N Engl J Med, 1996. **335**(16): p. 1182-9.
142. Wyllie, A.H., *Glucocorticoid-induced thymocyte apoptosis is associated with endogenous endonuclease activation.* Nature, 1980. **284**(5756): p. 555-6.
143. Cohen, J.J., *Programmed cell death in the immune system.* Adv Immunol, 1991. **50**: p. 55-85.
144. Valgimigli, M., et al., *Neurohormones, cytokines and programmed cell death in heart failure: a new paradigm for the remodeling heart.* Cardiovasc Drugs Ther, 2001. **15**(6): p. 529-37.
145. Arends, M.J. and A.H. Wyllie, *Apoptosis: mechanisms and roles in pathology.* Int Rev Exp Pathol, 1991. **32**: p. 223-54.
146. Suleiman, M.S., R.J. Singh, and C.E. Stewart, *Apoptosis and the cardiac action of insulin-like growth factor I.* Pharmacol Ther, 2007. **114**(3): p. 278-94.
147. Feuerstein, G.Z., *Apoptosis--new opportunities for novel therapeutics for heart diseases.* Cardiovasc Drugs Ther, 2001. **15**(6): p. 547-51.
148. Freude, B., et al., *Apoptosis is initiated by myocardial ischemia and executed during reperfusion.* J Mol Cell Cardiol, 2000. **32**(2): p. 197-208.
149. Guerra, S., et al., *Myocyte death in the failing human heart is gender dependent.* Circ Res, 1999. **85**(9): p. 856-66.
150. Sam, F., et al., *Progressive left ventricular remodeling and apoptosis late after myocardial infarction in mouse heart.* Am J Physiol Heart Circ Physiol, 2000. **279**(1): p. H422-8.
151. Zhou, Y.T., et al., *Lipotoxic heart disease in obese rats: implications for human obesity.* Proc Natl Acad Sci U S A, 2000. **97**(4): p. 1784-9.
152. Lou, H., I. Danelisen, and P.K. Singal, *Involvement of mitogen-activated protein kinases in adriamycin-induced cardiomyopathy.* Am J Physiol Heart Circ Physiol, 2005. **288**(4): p. H1925-30.

153. Sun, H.Y., et al., *Involvement of Na+/H+ exchanger in hypoxia/re-oxygenation-induced neonatal rat cardiomyocyte apoptosis.* Eur J Pharmacol, 2004. **486**(2): p. 121-31.
154. Tanaka, M., et al., *Hypoxia induces apoptosis with enhanced expression of Fas antigen messenger RNA in cultured neonatal rat cardiomyocytes.* Circ Res, 1994. **75**(3): p. 426-33.
155. Tatsumi, T., et al., *Intracellular ATP is required for mitochondrial apoptotic pathways in isolated hypoxic rat cardiac myocytes.* Cardiovasc Res, 2003. **59**(2): p. 428-40.
156. Stetka, D.G. and P.L. Webster, *Tritiated-thymidine induced changes in cell population kinetics in root meristems of Pisum sativum.* Radiat Res, 1975. **64**(3): p. 475-84.
157. Webster, K.A., et al., *Hypoxia-activated apoptosis of cardiac myocytes requires reoxygenation or a pH shift and is independent of p53.* J Clin Invest, 1999. **104**(3): p. 239-52.
158. Gill, C., R. Mestril, and A. Samali, *Losing heart: the role of apoptosis in heart disease--a novel therapeutic target?* Faseb J, 2002. **16**(2): p. 135-46.
159. Kajstura, J., et al., *Apoptotic and necrotic myocyte cell deaths are independent contributing variables of infarct size in rats.* Lab Invest, 1996. **74**(1): p. 86-107.
160. Gottlieb, R.A., et al., *Reperfusion injury induces apoptosis in rabbit cardiomyocytes.* J Clin Invest, 1994. **94**(4): p. 1621-8.
161. von Harsdorf, R., P.F. Li, and R. Dietz, *Signaling pathways in reactive oxygen species-induced cardiomyocyte apoptosis.* Circulation, 1999. **99**(22): p. 2934-41.
162. Bialik, S., et al., *The mitochondrial apoptotic pathway is activated by serum and glucose deprivation in cardiac myocytes.* Circ Res, 1999. **85**(5): p. 403-14.
163. Communal, C., et al., *Norepinephrine stimulates apoptosis in adult rat ventricular myocytes by activation of the beta-adrenergic pathway.* Circulation, 1998. **98**(13): p. 1329-34.
164. Kajstura, J., et al., *Angiotensin II induces apoptosis of adult ventricular myocytes in vitro.* J Mol Cell Cardiol, 1997. **29**(3): p. 859-70.
165. Itoh, G., et al., *DNA fragmentation of human infarcted myocardial cells demonstrated by the nick end labeling method and DNA agarose gel electrophoresis.* Am J Pathol, 1995. **146**(6): p. 1325-31.
166. Bishopric, N.H., et al., *Molecular mechanisms of apoptosis in the cardiac myocyte.* Curr Opin Pharmacol, 2001. **1**(2): p. 141-50.
167. MacLellan, W.R. and M.D. Schneider, *Death by design. Programmed cell death in cardiovascular biology and disease.* Circ Res, 1997. **81**(2): p. 137-44.
168. Regula, K.M. and L.A. Kirshenbaum, *Apoptosis of ventricular myocytes: a means to an end.* J Mol Cell Cardiol, 2005. **38**(1): p. 3-13.
169. Crow, M.T., et al., *The mitochondrial death pathway and cardiac myocyte apoptosis.* Circ Res, 2004. **95**(10): p. 957-70.
170. Zunino, F., et al., *Role of apoptotic response in cellular resistance to cytotoxic agents.* Pharmacol Ther, 1997. **76**(1-3): p. 177-85.
171. Shaw, J. and L.A. Kirshenbaum, *Prime time for JNK-mediated Akt reactivation in hypoxia-reoxygenation.* Circ Res, 2006. **98**(1): p. 7-9.
172. Gottlieb, R.A. and R.N. Kitsis, *Seeing death in the living.* Nat Med, 2001. **7**(12): p. 1277-8.
173. Reed, J.C., J.M. Jurgensmeier, and S. Matsuyama, *Bcl-2 family proteins and mitochondria.* Biochim Biophys Acta, 1998. **1366**(1-2): p. 127-37.

174. Chandler, J.M., et al., *Activation of CPP32 and Mch3 alpha in wild-type p53-induced apoptosis.* Biochem J, 1997. **322 (Pt 1)**: p. 19-23.
175. Green, D.R., *Apoptotic pathways: the roads to ruin.* Cell, 1998. **94**(6): p. 695-8.
176. Thornberry, N.A. and Y. Lazebnik, *Caspases: enemies within.* Science, 1998. **281**(5381): p. 1312-6.
177. Yue, T.L., et al., *Inhibition of extracellular signal-regulated kinase enhances Ischemia/Reoxygenation-induced apoptosis in cultured cardiac myocytes and exaggerates reperfusion injury in isolated perfused heart.* Circ Res, 2000. **86**(6): p. 692-9.
178. Robinson, M.J. and M.H. Cobb, *Mitogen-activated protein kinase pathways.* Curr Opin Cell Biol, 1997. **9**(2): p. 180-6.
179. Ip, Y.T. and R.J. Davis, *Signal transduction by the c-Jun N-terminal kinase (JNK)--from inflammation to development.* Curr Opin Cell Biol, 1998. **10**(2): p. 205-19.
180. Clerk, A., et al., *Stimulation of "stress-regulated" mitogen-activated protein kinases (stress-activated protein kinases/c-Jun N-terminal kinases and p38-mitogen-activated protein kinases) in perfused rat hearts by oxidative and other stresses.* J Biol Chem, 1998. **273**(13): p. 7228-34.
181. Clerk, A., A. Michael, and P.H. Sugden, *Stimulation of multiple mitogen-activated protein kinase sub-families by oxidative stress and phosphorylation of the small heat shock protein, HSP25/27, in neonatal ventricular myocytes.* Biochem J, 1998. **333 (Pt 3)**: p. 581-9.
182. Laderoute, K.R. and K.A. Webster, *Hypoxia/reoxygenation stimulates Jun kinase activity through redox signaling in cardiac myocytes.* Circ Res, 1997. **80**(3): p. 336-44.
183. Yaoita, H., et al., *Attenuation of ischemia/reperfusion injury in rats by a caspase inhibitor.* Circulation, 1998. **97**(3): p. 276-81.
184. Yue, T.L., et al., *Possible involvement of stress-activated protein kinase signaling pathway and Fas receptor expression in prevention of ischemia/reperfusion-induced cardiomyocyte apoptosis by carvedilol.* Circ Res, 1998. **82**(2): p. 166-74.
185. Katz, A.M., *Regression of left ventricular hypertrophy: new hope for dying hearts.* Circulation, 1998. **98**(7): p. 623-4.
186. Jerie, P., *[Milestones of cardiovascular therapy. III. Nitroglycerin].* Cas Lek Cesk, 2007. **146**(6): p. 533-7.
187. Wooley, C.F., *Osler, cardiac disease, and students of medicine--Columbus, OH: December 1899.* Am Heart Hosp J, 2006. **4**(4): p. 273-8.
188. Caplan, R.M., *Osler's legacies to dermatologists.* Int J Dermatol, 1998. **37**(1): p. 72-5.
189. Moran, M.E., S. Das, and S.A. Rosenberg, *Sir William Osler's perceptions of urolithiasis and the case of the indigo calculus.* J Endourol, 2005. **19**(10): p. 1157-60.
190. Katz, A.M., *Cardiomyopathy of overload. A major determinant of prognosis in congestive heart failure.* N Engl J Med, 1990. **322**(2): p. 100-10.
191. Wollert, K.C., et al., *Cardiotrophin-1 activates a distinct form of cardiac muscle cell hypertrophy. Assembly of sarcomeric units in series VIA gp130/leukemia inhibitory factor receptor-dependent pathways.* J Biol Chem, 1996. **271**(16): p. 9535-45.
192. Takimoto, E., et al., *Chronic inhibition of cyclic GMP phosphodiesterase 5A prevents and reverses cardiac hypertrophy.* Nat Med, 2005. **11**(2): p. 214-22.

193. Raju, S.V., et al., *Activation of the cardiac ciliary neurotrophic factor receptor reverses left ventricular hypertrophy in leptin-deficient and leptin-resistant obesity.* Proc Natl Acad Sci U S A, 2006. **103**(11): p. 4222-7.
194. Olson, L.E., et al., *Protection from doxorubicin-induced cardiac toxicity in mice with a null allele of carbonyl reductase 1.* Cancer Res, 2003. **63**(20): p. 6602-6.
195. Moens, A.L., et al., *Reversal of cardiac hypertrophy and fibrosis from pressure overload by tetrahydrobiopterin: efficacy of recoupling nitric oxide synthase as a therapeutic strategy.* Circulation, 2008. **117**(20): p. 2626-36.
196. Fatkin, D. and R.M. Graham, *Molecular mechanisms of inherited cardiomyopathies.* Physiol Rev, 2002. **82**(4): p. 945-80.
197. Kempf, T. and K.C. Wollert, *Nitric oxide and the enigma of cardiac hypertrophy.* Bioessays, 2004. **26**(6): p. 608-15.
198. Sugden, P.H., *Signaling in myocardial hypertrophy: life after calcineurin?* Circ Res, 1999. **84**(6): p. 633-46.
199. van Empel, V.P. and L.J. De Windt, *Myocyte hypertrophy and apoptosis: a balancing act.* Cardiovasc Res, 2004. **63**(3): p. 487-99.
200. Chicurel, M.E., C.S. Chen, and D.E. Ingber, *Cellular control lies in the balance of forces.* Curr Opin Cell Biol, 1998. **10**(2): p. 232-9.
201. Frey, N. and E.N. Olson, *Cardiac hypertrophy: the good, the bad, and the ugly.* Annu Rev Physiol, 2003. **65**: p. 45-79.
202. Dorn, G.W., 2nd, *Physiologic growth and pathologic genes in cardiac development and cardiomyopathy.* Trends Cardiovasc Med, 2005. **15**(5): p. 185-9.
203. Grossman, W., D. Jones, and L.P. McLaurin, *Wall stress and patterns of hypertrophy in the human left ventricle.* J Clin Invest, 1975. **56**(1): p. 56-64.
204. Dorn, G.W., 2nd and T. Force, *Protein kinase cascades in the regulation of cardiac hypertrophy.* J Clin Invest, 2005. **115**(3): p. 527-37.
205. Scheuer, J., et al., *Physiologic cardiac hypertrophy corrects contractile protein abnormalities associated with pathologic hypertrophy in rats.* J Clin Invest, 1982. **70**(6): p. 1300-5.
206. Diez, J., et al., *Mechanisms of disease: pathologic structural remodeling is more than adaptive hypertrophy in hypertensive heart disease.* Nat Clin Pract Cardiovasc Med, 2005. **2**(4): p. 209-16.
207. Chen, B., et al., *Molecular and cellular mechanisms of anthracycline cardiotoxicity.* Cardiovasc Toxicol, 2007. **7**(2): p. 114-21.
208. Sugden, P.H., *Ras, Akt, and mechanotransduction in the cardiac myocyte.* Circ Res, 2003. **93**(12): p. 1179-92.
209. Datta, S.R., et al., *Akt phosphorylation of BAD couples survival signals to the cell-intrinsic death machinery.* Cell, 1997. **91**(2): p. 231-41.
210. Cardone, M.H., et al., *Regulation of cell death protease caspase-9 by phosphorylation.* Science, 1998. **282**(5392): p. 1318-21.
211. Fulton, D., J.P. Gratton, and W.C. Sessa, *Post-translational control of endothelial nitric oxide synthase: why isn't calcium/calmodulin enough?* J Pharmacol Exp Ther, 2001. **299**(3): p. 818-24.
212. Brazil, D.P., Z.Z. Yang, and B.A. Hemmings, *Advances in protein kinase B signalling: AKTion on multiple fronts.* Trends Biochem Sci, 2004. **29**(5): p. 233-42.
213. Shiojima, I. and K. Walsh, *Regulation of cardiac growth and coronary angiogenesis by the Akt/PKB signaling pathway.* Genes Dev, 2006. **20**(24): p. 3347-65.

214. Mora, A., et al., *Deficiency of PDK1 in cardiac muscle results in heart failure and increased sensitivity to hypoxia.* Embo J, 2003. **22**(18): p. 4666-76.
215. McDevitt, T.C., M.A. Laflamme, and C.E. Murry, *Proliferation of cardiomyocytes derived from human embryonic stem cells is mediated via the IGF/PI 3-kinase/Akt signaling pathway.* J Mol Cell Cardiol, 2005. **39**(6): p. 865-73.
216. Shioi, T., et al., *The conserved phosphoinositide 3-kinase pathway determines heart size in mice.* Embo J, 2000. **19**(11): p. 2537-48.
217. Zhai, P., et al., *Glycogen synthase kinase-3alpha reduces cardiac growth and pressure overload-induced cardiac hypertrophy by inhibition of extracellular signal-regulated kinases.* J Biol Chem, 2007. **282**(45): p. 33181-91.
218. Rapacciuolo, A., et al., *G protein-coupled receptor signalling in in vivo cardiac overload.* Acta Physiol Scand, 2001. **173**(1): p. 51-7.
219. Minamino, T., et al., *MEKK1 is essential for cardiac hypertrophy and dysfunction induced by Gq.* Proc Natl Acad Sci U S A, 2002. **99**(6): p. 3866-71.
220. Hannan, K.M., et al., *mTOR-dependent regulation of ribosomal gene transcription requires S6K1 and is mediated by phosphorylation of the carboxy-terminal activation domain of the nucleolar transcription factor UBF.* Mol Cell Biol, 2003. **23**(23): p. 8862-77.
221. Proud, C.G., *Regulation of mammalian translation factors by nutrients.* Eur J Biochem, 2002. **269**(22): p. 5338-49.
222. Rohde, J., J. Heitman, and M.E. Cardenas, *The TOR kinases link nutrient sensing to cell growth.* J Biol Chem, 2001. **276**(13): p. 9583-6.
223. Thomas, G. and M.N. Hall, *TOR signalling and control of cell growth.* Curr Opin Cell Biol, 1997. **9**(6): p. 782-7.
224. Wang, L. and C.G. Proud, *Ras/Erk signaling is essential for activation of protein synthesis by Gq protein-coupled receptor agonists in adult cardiomyocytes.* Circ Res, 2002. **91**(9): p. 821-9.
225. Boluyt, M.O., et al., *Rapamycin inhibits alpha 1-adrenergic receptor-stimulated cardiac myocyte hypertrophy but not activation of hypertrophy-associated genes. Evidence for involvement of p70 S6 kinase.* Circ Res, 1997. **81**(2): p. 176-86.
226. Sadoshima, J. and S. Izumo, *Rapamycin selectively inhibits angiotensin II-induced increase in protein synthesis in cardiac myocytes in vitro. Potential role of 70-kD S6 kinase in angiotensin II-induced cardiac hypertrophy.* Circ Res, 1995. **77**(6): p. 1040-52.
227. McMullen, J.R., et al., *Inhibition of mTOR signaling with rapamycin regresses established cardiac hypertrophy induced by pressure overload.* Circulation, 2004. **109**(24): p. 3050-5.
228. Hirotani, S., et al., *Inhibition of glycogen synthase kinase 3beta during heart failure is protective.* Circ Res, 2007. **101**(11): p. 1164-74.
229. Michael, A., et al., *Glycogen synthase kinase-3beta regulates growth, calcium homeostasis, and diastolic function in the heart.* J Biol Chem, 2004. **279**(20): p. 21383-93.
230. Moasser, M.M., *The oncogene HER2: its signaling and transforming functions and its role in human cancer pathogenesis.* Oncogene, 2007. **26**(45): p. 6469-87.
231. Gabrielson, K., et al., *Heat shock protein 90 and ErbB2 in the cardiac response to doxorubicin injury.* Cancer Res, 2007. **67**(4): p. 1436-41.

232. Vollmer, C.M., Jr., et al., *Traumatic colonic hematoma.* J Trauma, 2000. **49**(6): p. 1155.
233. Zhao, Y.Y., et al., *Neuregulins promote survival and growth of cardiac myocytes. Persistence of ErbB2 and ErbB4 expression in neonatal and adult ventricular myocytes.* J Biol Chem, 1998. **273**(17): p. 10261-9.
234. Negro, A., B.K. Brar, and K.F. Lee, *Essential roles of Her2/erbB2 in cardiac development and function.* Recent Prog Horm Res, 2004. **59**: p. 1-12.
235. Erickson, S.L., et al., *ErbB3 is required for normal cerebellar and cardiac development: a comparison with ErbB2-and heregulin-deficient mice.* Development, 1997. **124**(24): p. 4999-5011.
236. Negro, A., et al., *erbB2 is required for G protein-coupled receptor signaling in the heart.* Proc Natl Acad Sci U S A, 2006. **103**(43): p. 15889-93.
237. Sadoshima, J., *Versatility of the angiotensin II type 1 receptor.* Circ Res, 1998. **82**(12): p. 1352-5.
238. Graus-Porta, D., et al., *ErbB-2, the preferred heterodimerization partner of all ErbB receptors, is a mediator of lateral signaling.* Embo J, 1997. **16**(7): p. 1647-55.
239. Oda, K., et al., *A comprehensive pathway map of epidermal growth factor receptor signaling.* Mol Syst Biol, 2005. **1**: p. 2005 0010.
240. Demirel, H.A., et al., *Exercise training reduces myocardial lipid peroxidation following short-term ischemia-reperfusion.* Med Sci Sports Exerc, 1998. **30**(8): p. 1211-6.
241. Powers, S.K., et al., *Exercise training improves myocardial tolerance to in vivo ischemia-reperfusion in the rat.* Am J Physiol, 1998. **275**(5 Pt 2): p. R1468-77.
242. Powers, S.K., L.A. M, and H.A. Demirel, *Exercise, heat shock proteins, and myocardial protection from I-R injury.* Med Sci Sports Exerc, 2001. **33**(3): p. 386-92.
243. Griffin, T.M., T.V. Valdez, and R. Mestril, *Radicicol activates heat shock protein expression and cardioprotection in neonatal rat cardiomyocytes.* Am J Physiol Heart Circ Physiol, 2004. **287**(3): p. H1081-8.
244. Barr, E., et al., *Efficient catheter-mediated gene transfer into the heart using replication-defective adenovirus.* Gene Ther, 1994. **1**(1): p. 51-8.
245. Kiang, J.G. and G.C. Tsokos, *Heat shock protein 70 kDa: molecular biology, biochemistry, and physiology.* Pharmacol Ther, 1998. **80**(2): p. 183-201.
246. Polla, B.S., et al., *Mitochondria are selective targets for the protective effects of heat shock against oxidative injury.* Proc Natl Acad Sci U S A, 1996. **93**(13): p. 6458-63.
247. Obermann, W.M., et al., *In vivo function of Hsp90 is dependent on ATP binding and ATP hydrolysis.* J Cell Biol, 1998. **143**(4): p. 901-10.
248. Stebbins, C.E., et al., *Crystal structure of an Hsp90-geldanamycin complex: targeting of a protein chaperone by an antitumor agent.* Cell, 1997. **89**(2): p. 239-50.
249. Morris, S.D., et al., *Specific induction of the 70-kD heat stress proteins by the tyrosine kinase inhibitor herbimycin-A protects rat neonatal cardiomyocytes. A new pharmacological route to stress protein expression?* J Clin Invest, 1996. **97**(3): p. 706-12.
250. Patel, H., A. Law, and S. Gouin, *Predictive factors for short-term symptom persistence in children after emergency department evaluation for constipation.* Arch Pediatr Adolesc Med, 2000. **154**(12): p. 1204-8.

251. Bueno, O.F. and J.D. Molkentin, *Involvement of extracellular signal-regulated kinases 1/2 in cardiac hypertrophy and cell death.* Circ Res, 2002. **91**(9): p. 776-81.
252. Takeishi, Y., et al., *Src and multiple MAP kinase activation in cardiac hypertrophy and congestive heart failure under chronic pressure-overload: comparison with acute mechanical stretch.* J Mol Cell Cardiol, 2001. **33**(9): p. 1637-48.
253. Zhai, P., et al., *An angiotensin II type 1 receptor mutant lacking epidermal growth factor receptor transactivation does not induce angiotensin II-mediated cardiac hypertrophy.* Circ Res, 2006. **99**(5): p. 528-36.
254. Rapacciuolo, A., et al., *Important role of endogenous norepinephrine and epinephrine in the development of in vivo pressure-overload cardiac hypertrophy.* J Am Coll Cardiol, 2001. **38**(3): p. 876-82.
255. Lin, W.Y., et al., *A decade of recurrent cystitis in a woman due to a giant vesical calculus.* Int Urogynecol J Pelvic Floor Dysfunct, 2006. **17**(6): p. 674-5.
256. Zhu, W., et al., *MAPK superfamily plays an important role in daunomycin-induced apoptosis of cardiac myocytes.* Circulation, 1999. **100**(20): p. 2100-7.
257. Bernstein, D., et al., *Differential cardioprotective/cardiotoxic effects mediated by beta-adrenergic receptor subtypes.* Am J Physiol Heart Circ Physiol, 2005. **289**(6): p. H2441-9.
258. Bueno, O.F., et al., *The MEK1-ERK1/2 signaling pathway promotes compensated cardiac hypertrophy in transgenic mice.* Embo J, 2000. **19**(23): p. 6341-50.
259. Sheng, Z., et al., *Cardiotrophin 1 (CT-1) inhibition of cardiac myocyte apoptosis via a mitogen-activated protein kinase-dependent pathway. Divergence from downstream CT-1 signals for myocardial cell hypertrophy.* J Biol Chem, 1997. **272**(9): p. 5783-91.
260. De Windt, L.J., et al., *Calcineurin-mediated hypertrophy protects cardiomyocytes from apoptosis in vitro and in vivo: An apoptosis-independent model of dilated heart failure.* Circ Res, 2000. **86**(3): p. 255-63.
261. Sporn, M.B. and A.B. Roberts, *Transforming growth factor-beta: recent progress and new challenges.* J Cell Biol, 1992. **119**(5): p. 1017-21.
262. Barnard, J.A., R.M. Lyons, and H.L. Moses, *The cell biology of transforming growth factor beta.* Biochim Biophys Acta, 1990. **1032**(1): p. 79-87.
263. MacLellan, W.R., T. Brand, and M.D. Schneider, *Transforming growth factor-beta in cardiac ontogeny and adaptation.* Circ Res, 1993. **73**(5): p. 783-91.
264. Shull, M.M., et al., *Targeted disruption of the mouse transforming growth factor-beta 1 gene results in multifocal inflammatory disease.* Nature, 1992. **359**(6397): p. 693-9.
265. Kulkarni, A.B., et al., *Transforming growth factor beta 1 null mutation in mice causes excessive inflammatory response and early death.* Proc Natl Acad Sci U S A, 1993. **90**(2): p. 770-4.
266. Diebold, R.J., et al., *Early-onset multifocal inflammation in the transforming growth factor beta 1-null mouse is lymphocyte mediated.* Proc Natl Acad Sci U S A, 1995. **92**(26): p. 12215-9.
267. Glick, A.B., et al., *Transforming growth factor beta 1 suppresses genomic instability independent of a G1 arrest, p53, and Rb.* Cancer Res, 1996. **56**(16): p. 3645-50.
268. Hoying, J.B., et al., *Transforming growth factor beta1 enhances platelet aggregation through a non-transcriptional effect on the fibrinogen receptor.* J Biol Chem, 1999. **274**(43): p. 31008-13.

269. Tang, B., et al., *Transforming growth factor-beta1 is a new form of tumor suppressor with true haploid insufficiency.* Nat Med, 1998. **4**(7): p. 802-7.
270. Glick, A.B., et al., *Targeted deletion of the TGF-beta 1 gene causes rapid progression to squamous cell carcinoma.* Genes Dev, 1994. **8**(20): p. 2429-40.
271. Engle, S.J., et al., *Transforming growth factor beta1 suppresses nonmetastatic colon cancer at an early stage of tumorigenesis.* Cancer Res, 1999. **59**(14): p. 3379-86.
272. Takahashi, N., et al., *Hypertrophic stimuli induce transforming growth factor-beta 1 expression in rat ventricular myocytes.* J Clin Invest, 1994. **94**(4): p. 1470-6.
273. Habashi, J.P., et al., *Losartan, an AT1 antagonist, prevents aortic aneurysm in a mouse model of Marfan syndrome.* Science, 2006. **312**(5770): p. 117-21.
274. Eghbali, M., et al., *Differential effects of transforming growth factor-beta 1 and phorbol myristate acetate on cardiac fibroblasts. Regulation of fibrillar collagen mRNAs and expression of early transcription factors.* Circ Res, 1991. **69**(2): p. 483-90.
275. Villarreal, F.J. and W.H. Dillmann, *Cardiac hypertrophy-induced changes in mRNA levels for TGF-beta 1, fibronectin, and collagen.* Am J Physiol, 1992. **262**(6 Pt 2): p. H1861-6.
276. Kupfahl, C., et al., *Angiotensin II directly increases transforming growth factor beta1 and osteopontin and indirectly affects collagen mRNA expression in the human heart.* Cardiovasc Res, 2000. **46**(3): p. 463-75.
277. Schultz Jel, J., et al., *TGF-beta1 mediates the hypertrophic cardiomyocyte growth induced by angiotensin II.* J Clin Invest, 2002. **109**(6): p. 787-96.
278. Qian, S.W., et al., *A second messenger RNA species of transforming growth factor beta 1 in infarcted rat heart.* Cell Regul, 1991. **2**(3): p. 241-9.
279. Sadoshima, J., et al., *The MEKK1-JNK pathway plays a protective role in pressure overload but does not mediate cardiac hypertrophy.* J Clin Invest, 2002. **110**(2): p. 271-9.
280. Bhambi, B. and M. Eghbali, *Effect of norepinephrine on myocardial collagen gene expression and response of cardiac fibroblasts after norepinephrine treatment.* Am J Pathol, 1991. **139**(5): p. 1131-42.
281. Yang, X.P., et al., *Echocardiographic assessment of cardiac function in conscious and anesthetized mice.* Am J Physiol, 1999. **277**(5 Pt 2): p. H1967-74.
282. Pollick, C., S.L. Hale, and R.A. Kloner, *Echocardiographic and cardiac Doppler assessment of mice.* J Am Soc Echocardiogr, 1995. **8**(5 Pt 1): p. 602-10.
283. Cui, W. and D.A. Roberson, *Left ventricular Tei index in children: comparison of tissue Doppler imaging, pulsed wave Doppler, and M-mode echocardiography normal values.* J Am Soc Echocardiogr, 2006. **19**(12): p. 1438-45.
284. Lutz, J.T., R. Giebler, and J. Peters, *The 'TEI-index' is preload dependent and can be measured by transoesophageal echocardiography during mechanical ventilation.* Eur J Anaesthesiol, 2003. **20**(11): p. 872-7.
285. Ahn, W. and Y.J. Lim, *Mean arterial blood pressure estimation and its limitation.* Can J Anaesth, 2005. **52**(9): p. 1000-1.
286. Safar, M.E., *Pulse pressure in essential hypertension: clinical and therapeutical implications.* J Hypertens, 1989. **7**(10): p. 769-76.
287. Benetos, A., et al., *Large artery stiffness in hypertension.* J Hypertens Suppl, 1997. **15**(2): p. S89-97.

288. Pinto, J.T., et al., *Adriamycin-induced increase in serum aldosterone levels: effects in riboflavin-sufficient and riboflavin-deficient rats.* Endocrinology, 1990. **127**(3): p. 1495-501.
289. Mudd, J.O. and D.A. Kass, *Reversing chronic remodeling in heart failure.* Expert Rev Cardiovasc Ther, 2007. **5**(3): p. 585-98.
290. Gray, M.O., et al., *Angiotensin II stimulates cardiac myocyte hypertrophy via paracrine release of TGF-beta 1 and endothelin-1 from fibroblasts.* Cardiovasc Res, 1998. **40**(2): p. 352-63.
291. Sun, Y., et al., *Cardiac angiotensin converting enzyme and myocardial fibrosis in the rat.* Cardiovasc Res, 1994. **28**(9): p. 1423-32.
292. Horiuchi, M., et al., *Angiotensin type 2 receptor dephosphorylates Bcl-2 by activating mitogen-activated protein kinase phosphatase-1 and induces apoptosis.* J Biol Chem, 1997. **272**(30): p. 19022-6.
293. Hostetter, T.H. and H.N. Ibrahim, *Aldosterone in chronic kidney and cardiac disease.* J Am Soc Nephrol, 2003. **14**(9): p. 2395-401.
294. Brilla, C.G. and H. Rupp, *Myocardial collagen matrix remodeling and congestive heart failure.* Cardiologia, 1994. **39**(12 Suppl 1): p. 389-93.
295. Mitchell, G.F., *Increased aortic stiffness: an unfavorable cardiorenal connection.* Hypertension, 2004. **43**(2): p. 151-3.
296. Safar, M.E., G.M. London, and G.E. Plante, *Arterial stiffness and kidney function.* Hypertension, 2004. **43**(2): p. 163-8.
297. Guyton, A.C. and T.G. Coleman, *Quantitative analysis of the pathophysiology of hypertension. 1969.* J Am Soc Nephrol, 1999. **10**(10): p. 2248-58.
298. Guyton, A.C., et al., *Arterial pressure regulation. Overriding dominance of the kidneys in long-term regulation and in hypertension.* Am J Med, 1972. **52**(5): p. 584-94.
299. Guyton, A.C. and J.W. Crowell, *Cardiac deterioration in shock: I. Its progressive nature. 1964.* Int Anesthesiol Clin, 1999. **37**(1): p. 119-28.
300. Safar, M.E., et al., *Altered blood volume regulation in sustained essential hypertension: a hemodynamic study.* Kidney Int, 1975. **8**(1): p. 42-7.
301. Hart, S.G., et al., *Acetaminophen nephrotoxicity in CD-1 mice. I. Evidence of a role for in situ activation in selective covalent binding and toxicity.* Toxicol Appl Pharmacol, 1994. **126**(2): p. 267-75.
302. Tarloff, J.B., et al., *Sex- and age-dependent acetaminophen hepato- and nephrotoxicity in Sprague-Dawley rats: role of tissue accumulation, nonprotein sulfhydryl depletion, and covalent binding.* Fundam Appl Toxicol, 1996. **30**(1): p. 13-22.
303. Welch, W.J., et al., *Renal oxygenation defects in the spontaneously hypertensive rat: role of AT1 receptors.* Kidney Int, 2003. **63**(1): p. 202-8.
304. Plante, G.E., et al., *Renal permeability alteration precedes hypertension and involves bradykinin in the spontaneously hypertensive rat.* J Clin Invest, 1992. **89**(6): p. 2030-2.
305. Cardenas, A., R. Bataller, and V. Arroyo, *Mechanisms of ascites formation.* Clin Liver Dis, 2000. **4**(2): p. 447-65.
306. Roman, R.J., *Pressure diuresis mechanism in the control of renal function and arterial pressure.* Fed Proc, 1986. **45**(13): p. 2878-84.

307. Granger, J.P., *Pressure natriuresis. Role of renal interstitial hydrostatic pressure.* Hypertension, 1992. **19**(1 Suppl): p. I9-17.
308. Cowley, A.W., Jr., *Role of the renal medulla in volume and arterial pressure regulation.* Am J Physiol, 1997. **273**(1 Pt 2): p. R1-15.
309. Dobrzynski, E., et al., *Adrenomedullin gene delivery attenuates hypertension, cardiac remodeling, and renal injury in deoxycorticosterone acetate-salt hypertensive rats.* Hypertension, 2000. **36**(6): p. 995-1001.
310. Matsubara, B.B., et al., *Left ventricular adaptation to chronic pressure overload induced by inhibition of nitric oxide synthase in rats.* Basic Res Cardiol, 1998. **93**(3): p. 173-81.
311. Bongartz, L.G., M.J. Cramer, and B. Braam, *The cardiorenal connection.* Hypertension, 2004. **43**(4): p. e14.
312. Bongartz, L.G., et al., *The severe cardiorenal syndrome: 'Guyton revisited'.* Eur Heart J, 2005. **26**(1): p. 11-7.
313. Ross, R., *Atherosclerosis--an inflammatory disease.* N Engl J Med, 1999. **340**(2): p. 115-26.
314. Heistad, D.D., *Oxidative stress and vascular disease: 2005 Duff lecture.* Arterioscler Thromb Vasc Biol, 2006. **26**(4): p. 689-95.
315. Weiss, R.M., *Lasting effects of lost vascular elasticity.* Circ Res, 2007. **100**(5): p. 604-6.
316. Laviades, C., et al., *Abnormalities of the extracellular degradation of collagen type I in essential hypertension.* Circulation, 1998. **98**(6): p. 535-40.
317. Skalska, A., et al., *The relationship between pulse wave velocity and indexes of collagen synthesis in hypertensive patients, according to the level of systolic blood pressure.* J Hum Hypertens, 2005. **19**(9): p. 731-5.
318. Karamanoglu, M., et al., *An analysis of the relationship between central aortic and peripheral upper limb pressure waves in man.* Eur Heart J, 1993. **14**(2): p. 160-7.
319. O'Rourke, M.F., *Arterial mechanics and wave reflection with antihypertensive therapy.* J Hypertens Suppl, 1992. **10**(5): p. S43-9.
320. Freedman, J.E., *Molecular regulation of platelet-dependent thrombosis.* Circulation, 2005. **112**(17): p. 2725-34.
321. Selwyn, A.P., et al., *Atherogenic lipids, vascular dysfunction, and clinical signs of ischemic heart disease.* Circulation, 1997. **95**(1): p. 5-7.
322. Cox, D.A. and M.L. Cohen, *Effects of oxidized low-density lipoprotein on vascular contraction and relaxation: clinical and pharmacological implications in atherosclerosis.* Pharmacol Rev, 1996. **48**(1): p. 3-19.
323. Holvoet, P. and D. Collen, *Oxidized lipoproteins in atherosclerosis and thrombosis.* Faseb J, 1994. **8**(15): p. 1279-84.
324. Erslev, A.J., *Erythropoietin.* N Engl J Med, 1991. **324**(19): p. 1339-44.
325. Vatner, S.F. and N.T. Smith, *Effects of halothane on left ventricular function and distribution of regional blood flow in dogs and primates.* Circ Res, 1974. **34**(2): p. 155-67.
326. Manders, W.T. and S.F. Vatner, *Effects of sodium pentobarbital anesthesia on left ventricular function and distribution of cardiac output in dogs, with particular reference to the mechanism for tachycardia.* Circ Res, 1976. **39**(4): p. 512-7.
327. Vatner, S.F., *Effects of anesthesia on cardiovascular control mechanisms.* Environ Health Perspect, 1978. **26**: p. 193-206.

328. Murray, D.J., R.B. Forbes, and L.T. Mahoney, *Comparative hemodynamic depression of halothane versus isoflurane in neonates and infants: an echocardiographic study.* Anesth Analg, 1992. **74**(3): p. 329-37.
329. Pagel, P.S., et al., *Alteration of left ventricular diastolic function by desflurane, isoflurane, and halothane in the chronically instrumented dog with autonomic nervous system blockade.* Anesthesiology, 1991. **74**(6): p. 1103-14.
330. Baumwart, R.D., K.M. Meurs, and J.D. Bonagura, *Tei index of myocardial performance applied to the right ventricle in normal dogs.* J Vet Intern Med, 2005. **19**(6): p. 828-32.
331. Sousa, M.G., et al., *Effects of isoflurane on Tei-index of myocardial performance in healthy dogs.* Can Vet J, 2007. **48**(3): p. 277-82.
332. Lindsay, M.M., P. Maxwell, and F.G. Dunn, *TIMP-1: a marker of left ventricular diastolic dysfunction and fibrosis in hypertension.* Hypertension, 2002. **40**(2): p. 136-41.
333. Engel, D., et al., *Cardiac myocyte apoptosis provokes adverse cardiac remodeling in transgenic mice with targeted TNF overexpression.* Am J Physiol Heart Circ Physiol, 2004. **287**(3): p. H1303-11.
334. Arola, O.J., et al., *Acute doxorubicin cardiotoxicity involves cardiomyocyte apoptosis.* Cancer Res, 2000. **60**(7): p. 1789-92.
335. Pimentel, D.R., et al., *Reactive oxygen species mediate amplitude-dependent hypertrophic and apoptotic responses to mechanical stretch in cardiac myocytes.* Circ Res, 2001. **89**(5): p. 453-60.
336. Fiorillo, C., et al., *Cardiac volume overload rapidly induces oxidative stress-mediated myocyte apoptosis and hypertrophy.* Biochim Biophys Acta, 2005. **1741**(1-2): p. 173-82.
337. Herman, E.H. and V.J. Ferrans, *Reduction of chronic doxorubicin cardiotoxicity in dogs by pretreatment with (+/-)-1,2-bis(3,5-dioxopiperazinyl-1-yl)propane (ICRF-187).* Cancer Res, 1981. **41**(9 Pt 1): p. 3436-40.
338. Smith, N.J., et al., *Hijacking epidermal growth factor receptors by angiotensin II: new possibilities for understanding and treating cardiac hypertrophy.* Cell Mol Life Sci, 2004. **61**(21): p. 2695-703.
339. Cantley, L.C., *The phosphoinositide 3-kinase pathway.* Science, 2002. **296**(5573): p. 1655-7.
340. Qin, F., J. Shite, and C.S. Liang, *Antioxidants attenuate myocyte apoptosis and improve cardiac function in CHF: association with changes in MAPK pathways.* Am J Physiol Heart Circ Physiol, 2003. **285**(2): p. H822-32.
341. Ohno, T., et al., *Incidence and temporal pattern of anorexia, diarrhea, weight loss, and leukopenia in patients with cervical cancer treated with concurrent radiation therapy and weekly cisplatin: comparison with radiation therapy alone.* Gynecol Oncol, 2006. **103**(1): p. 94-9.
342. Piontek, K.B., et al., *A functional floxed allele of Pkd1 that can be conditionally inactivated in vivo.* J Am Soc Nephrol, 2004. **15**(12): p. 3035-43.
343. Magri, P., et al., *Early impairment of renal hemodynamic reserve in patients with asymptomatic heart failure is restored by angiotensin II antagonism.* Circulation, 1998. **98**(25): p. 2849-54.

344. Volpe, M., et al., *Abnormalities of sodium handling and of cardiovascular adaptations during high salt diet in patients with mild heart failure.* Circulation, 1993. **88**(4 Pt 1): p. 1620-7.
345. Pacher, P., J.S. Beckman, and L. Liaudet, *Nitric oxide and peroxynitrite in health and disease.* Physiol Rev, 2007. **87**(1): p. 315-424.
346. Diez, J., et al., *Cardiomyocyte apoptosis and cardiac angiotensin-converting enzyme in spontaneously hypertensive rats.* Hypertension, 1997. **30**(5): p. 1029-34.
347. Cordeiro, J.M., S.E. Howlett, and G.R. Ferrier, *Simulated ischaemia and reperfusion in isolated guinea pig ventricular myocytes.* Cardiovasc Res, 1994. **28**(12): p. 1794-802.
348. Jones, K.B., et al., *Toward an understanding of dural ectasia: a light microscopy study in a murine model of Marfan syndrome.* Spine, 2005. **30**(3): p. 291-3.
349. Lavoie, P., et al., *Neutralization of transforming growth factor-beta attenuates hypertension and prevents renal injury in uremic rats.* J Hypertens, 2005. **23**(10): p. 1895-903.
350. Lim, D.S., et al., *Angiotensin II blockade reverses myocardial fibrosis in a transgenic mouse model of human hypertrophic cardiomyopathy.* Circulation, 2001. **103**(6): p. 789-91.
351. Eberhardt, R.T., et al., *Angiotensin II receptor blockade: an innovative approach to cardiovascular pharmacotherapy.* J Clin Pharmacol, 1993. **33**(11): p. 1023-38.
352. Goldberg, A.I., M.C. Dunlay, and C.S. Sweet, *Safety and tolerability of losartan potassium, an angiotensin II receptor antagonist, compared with hydrochlorothiazide, atenolol, felodipine ER, and angiotensin-converting enzyme inhibitors for the treatment of systemic hypertension.* Am J Cardiol, 1995. **75**(12): p. 793-5.
353. Goa, K.L. and A.J. Wagstaff, *Losartan potassium: a review of its pharmacology, clinical efficacy and tolerability in the management of hypertension.* Drugs, 1996. **51**(5): p. 820-45.
354. McIntyre, M., et al., *Losartan, an orally active angiotensin (AT1) receptor antagonist: a review of its efficacy and safety in essential hypertension.* Pharmacol Ther, 1997. **74**(2): p. 181-94.
355. Sterzel, R.B., et al., *Renal disease and the development of hypertension in salt-sensitive Dahl rats.* Kidney Int, 1988. **33**(6): p. 1119-29.
356. Johnson, R.J., et al., *Subtle acquired renal injury as a mechanism of salt-sensitive hypertension.* N Engl J Med, 2002. **346**(12): p. 913-23.
357. Adler, S. and H. Huang, *Oxidant stress in kidneys of spontaneously hypertensive rats involves both oxidase overexpression and loss of extracellular superoxide dismutase.* Am J Physiol Renal Physiol, 2004. **287**(5): p. F907-13.
358. Giri, S.N., et al., *Amelioration of doxorubicin-induced cardiac and renal toxicity by pirfenidone in rats.* Cancer Chemother Pharmacol, 2004. **53**(2): p. 141-50.
359. Benson, J., M. Lev, and C.G. Grand, *Enhancement of mammary fibroadenomas in the female rat by a high fat diet.* Cancer Res, 1956. **16**(2): p. 135-7.
360. Davis, R.K., G.T. Stevenson, and K.A. Busch, *Tumor incidence in normal Sprague-Dawley female rats.* Cancer Res, 1956. **16**(3): p. 194-7.
361. Eldridge, J.C., et al., *The mammary tumor response in triazine-treated female rats: a threshold-mediated interaction with strain and species-specific reproductive senescence.* Steroids, 1999. **64**(9): p. 672-8.

362. Shellabarger, C.J., et al., *The occurrence of mammary tumors in the rat after sublethal whole-body irradiation.* Radiat Res, 1957. **6**(4): p. 501-12.
363. Ballard, V.L. and J.M. Edelberg, *Harnessing hormonal signaling for cardioprotection.* Sci Aging Knowledge Environ, 2005. **2005**(51): p. re6.
364. Bradlow, H.L., et al., *Effects of pesticides on the ratio of 16 alpha/2-hydroxyestrone: a biologic marker of breast cancer risk.* Environ Health Perspect, 1995. **103 Suppl 7**: p. 147-50.
365. Coumoul, X., et al., *Differential regulation of cytochrome P450 1A1 and 1B1 by a combination of dioxin and pesticides in the breast tumor cell line MCF-7.* Cancer Res, 2001. **61**(10): p. 3942-8.
366. Tannheimer, S.L., et al., *Carcinogenic polycyclic aromatic hydrocarbons increase intracellular Ca2+ and cell proliferation in primary human mammary epithelial cells.* Carcinogenesis, 1997. **18**(6): p. 1177-82.
367. Feil, R., et al., *Cyclic GMP-dependent protein kinases and the cardiovascular system: insights from genetically modified mice.* Circ Res, 2003. **93**(10): p. 907-16.
368. Cote, C.G., et al., *Regulation of intracellular xanthine oxidase by endothelial-derived nitric oxide.* Am J Physiol, 1996. **271**(5 Pt 1): p. L869-74.
369. Pacher, P., et al., *Nitrosative stress and pharmacological modulation of heart failure.* Trends Pharmacol Sci, 2005. **26**(6): p. 302-10.

363. Miller et al, eds. SEER cancer statistics review 1973-1993. Bethesda, MD: National cancer institute; 1997.
364. O'Rourke MF. Arterial Function in Health and Disease. Edinburgh, UK: Churchill-Livingstone; 1982.
365. O'Rourke MF, Kelly RP, Avolio AP. The Arterial Pulse. Philadelphia, PA: Lea & Febiger; 1992:3-14
366. O'Rourke M, Safar ME, Dzau VJ, eds. Arterial Vasodilation: Mechanism and Therapy. London, UK: Edward Arnold; 1993:78-90.

ABBREVIATIONS:

AII: Angiotensin II

AT1: Angiotensin II receptor type 1

cGMP: Cyclic guanosine monophosphate

Ca^{2+}: Calcium

CHF: Congestive heart failure

CRFR: Corticotrophin-releasing factor receptor

CT-1 : Cardiotrophin-1

DOX: Doxorubicin

EGF: Epidermal growth factors

EGFR: Epidermal growth factor receptors

EDRF: Endothelial derived relaxing factor

eNOS: Endothelial nitric oxide synthase

EGF-1: Insulin like growth factor-1

ERK: Extracellular signal–regulated kinase

EF: Ejection fraction

ET-1: Endotholin-1

ET: Ejection time

F344: Fisher rat

FDA: Food and Drug Administration

FOXO: Forkhead box

FS: Fractional shortening

GSK-3: Glycogen synthase kinase-3

GPCRs: G protein-coupled receptors

H_2O_2: Hydrogen peroxide

IVCT: Isovolumetric contraction time

I/ R: Ischemia reperfusion

IVRT: Isovolumetric relaxation time

IVSD: Inter-ventricular septal thickness at end of diastole

KO (-/-): Knockout transgenic mice

JNK: Jun-nuclear kinase

LV : Left ventricle

LVEF: Left ventricle ejection fraction

LVEDD: Left ventricle chamber diameter at end of diastole

LVESD: Left ventricle chamber diameter at end of systole

LVH: Left ventricular hypertrophy

LVmass: Left ventricular

MAPKs: Mitogen-activated protein kinases

MAP: Mean arterial pressure

MI: Myocardial infarction

MMP: Matrix metalloproteinase

mTOR: Rapamycin

NAD(P)H: Nicotinamide-adenenine dinucleotide phosphate

NE : Norepinephrine

NRG-1: neuregulin- 1

NO: Nitric oxide:

NOS: Nitric oxide synthase

O_2^-: Superoxide

OH: Hydroxyl radical

$ONOO^-$: Peroxynitrite

PE: Phenylephrine

PI3K: Phosphatidylinositol-3 kinase

PWTED: Posterior wall thickness at end of diastole

PWV: Pulse wave velocity

ROS: Reactive oxygen species

RWT: Relative wall thickness

sCG: Soluble granulate cyclase

SD: Sprague-Dawley rat

SERCA: sarcoplasmic reticulum Ca2+-ATPase

SOD: Superoxide dismutase

SPECT/CT: Single-photon-emission computer tomography scanning

TGF-β: Transforming growth factors-β

TDI: Tissue Doppler imaging

XO: Xantine oxidase